Chem Soc Rev

REVIEW ARTICLE

View Article Online
View Journal | View Issue

Cite this: *Chem. Soc. Rev.*, 2018, **47**, 8263

Received 4th May 2018

DOI: 10.1039/c8cs00370j

rsc.li/chem-soc-rev

From 3D to 2D zeolite catalytic materials

J. Přech,[ab] P. Pizarro,[cd] D. P. Serrano [cd] and J. Čejka *[ae]

Research activities and recent developments in the area of three-dimensional zeolites and their two-dimensional analogues are reviewed. Zeolites are the most important industrial heterogeneous catalysts with numerous applications. However, they suffer from limited pore sizes not allowing penetration of sterically demanding molecules to their channel systems and to active sites. We briefly highlight here the synthesis, properties and catalytic potential of three-dimensional zeolites followed by a discussion of hierarchical zeolites combining micro- and mesoporosity. The final part is devoted to two-dimensional analogues developed recently. Novel bottom-up and top-down synthetic approaches for two-dimensional zeolites, their properties, and catalytic performances are thoroughly discussed in this review.

[a] *Department of Physical and Macromolecular Chemistry, Faculty of Science, Charles University, Hlavova 8, 128 43 Prague 2, Czech Republic*
[b] *Normandie Univ, ENSICAEN, UNICAEN, CNRS, Laboratoire Catalyse et Spectrochimie, 14000 Caen, France*
[c] *Thermochemical Processes Unit, IMDEA Energy Institute, 28935, Móstoles, Madrid, Spain*
[d] *Chemical and Environmental Engineering Group, ESCET, Rey Juan Carlos University, 28933, Móstoles, Madrid, Spain*
[e] *J. Heyrovský Institute of Physical Chemistry, Czech Academy of Sciences, Dolejškova 3, 182 23, Prague 8, Czech Republic. E-mail: jiri.cejka@jh-inst.cas.cz*

1. Introduction

Zeolites are widely used in petroleum and chemical industries due to their exceptional catalytic and selective adsorption properties in combination with thermal and chemical stability as well as environmental friendliness. At present, the dominant role of zeolites (as catalysts) is in crude oil upgrading. Most petrochemical processes employ zeolites, in particular for shape-selective reactions. Recently, a number of exciting examples of

J. Přech

Jan Přech obtained his bachelor's and master's (engineer's) degree from the University of Chemistry and Technology in Prague in 2012. For his PhD, he joined the group of Prof. Jiří Čejka at J. Heyrovský institute of physical chemistry of ASCR. He obtained PhD in physical chemistry in 2016 for a study on the synthesis and modifications of 2-dimensional titanosilicates in selective oxidation catalysis. Dr. Přech obtained the Jean-Marie Lehn prize in Chemistry 2016 for the best PhD thesis. Then Dr. Přech, joined the Laboratory of Catalysis and Spectrochemictry at Universite de Normandie in Caen (France) in the group of Dr. Valentin Valtchev working on the synthesis of metal–zeolite composite catalysts. Currently (2018) he is working on the CUCAM project at Charles University in Prague. His current research interests include synthesis, characterisation and application of Lewis acidic zeolite based catalysts, 2-dimensional zeolites and zeolite catalysed reactions in Fine Chemistry.

P. Pizarro

Patricia Pizarro is an Associate Professor of Chemical Engineering at Rey Juan Carlos University and a Senior Associate Researcher at IMDEA Energy Institute. She obtained her PhD from Rey Juan Carlos University (2005) and an Extraordinary Doctorate Award. She was a Visiting Researcher at Laboratoire d'application de la Chimie a L'environnement (France, 2003) and MPIK (Germany, 2006). Her research is mainly focused on the design of heterogeneous catalysts and materials for different chemical processes such as energy storage and biofuels generation. She has participated in 27 research projects, and is the co-author of 54 indexed publications (H-index = 23), 6 book chapters and of >90 congress communications as well as the supervisor of 2 PhD theses.

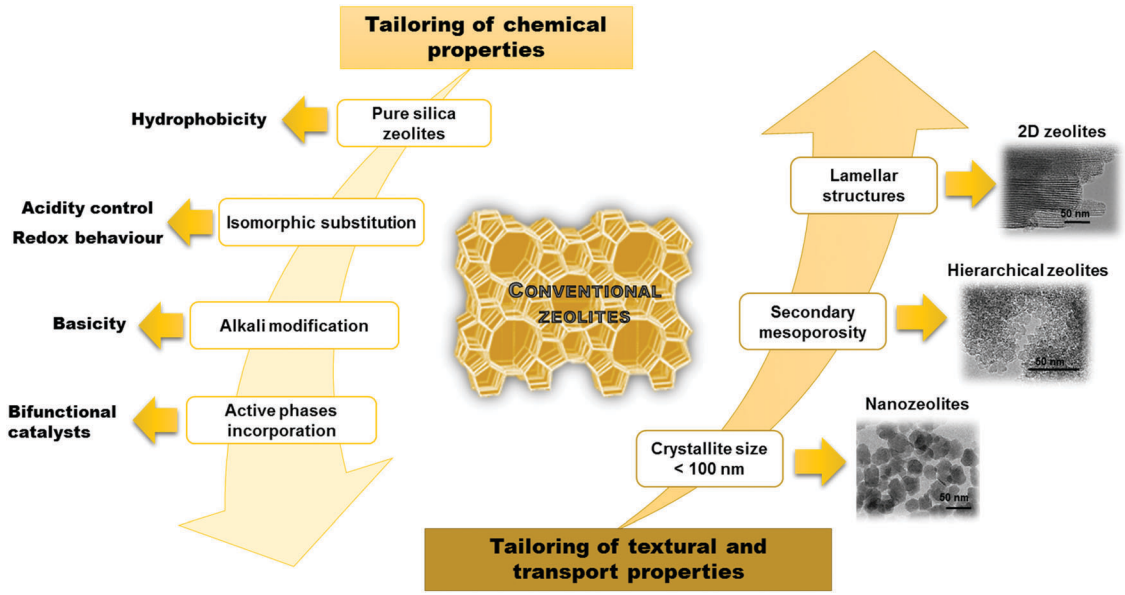

Fig. 1 Main strategies applied for tailoring the zeolite properties. TEM pictures adapted with permission from ref. 12–14.

highly active zeolites have been shown in selective synthesis of fine chemicals and environmental protection.[1–3]

The name zeolite, coined in 1756 and meaning 'boiling stone', refers to a diverse but uniform class of natural and synthetic crystalline aluminosilicates and related compositions with framework structures containing well-defined micropores, which are able to adsorb and discriminate molecules based on their size and shape. Zeolites crystallize under hydrothermal conditions from suitable synthesis mixtures. There is a continuous effort in numerous academic and industrial laboratories to discover new framework structures for particular processes and to gain a better fundamental understanding of synthetic mechanisms.

Despite a significant effort in the synthesis of zeolites, there are still limitations in increasing their pore sizes. While some zeolites have entrance windows consisting of up to 30 T-atoms (silicon or other atoms with tetraheral coordination in the framework),[4] the largest industrially relevant windows are formed by 12 T-atoms in the case of zeolite **FAU**. This strongly limits possibilities of using zeolites for transformation of larger (bulkier) substrates. As a result, several important approaches have been recently developed to overcome this limitation. All of them target at an increased accessibility of active sites in zeolites but in different ways. In the case of nanozeolites, size limitation of zeolite crystals to dozens of nanometers increases

D. P. Serrano

D. P. Serrano is a Full Professor of Chemical Engineering at Rey Juan Carlos University (since 2002) and the Director of the IMDEA Energy Institute (since 2007). He obtained his PhD from Complutense University of Madrid (1990). He was a Visiting Researcher in CALTECH (1991) and UCSB (2006). He was the Vice-rector for Research and Technological Innovation (2001–2002) and the Head of the Chemical and Environmental Technology Department (2002–2007) at Rey Juan Carlos University. He has participated in 60 research projects, and he is the author of >200 indexed publications (= 47) and of >300 congress communications as well as the supervisor of 21 PhD theses. He was the Coordinator of the FP7 EU CASCATBEL project (2013–2017) and the President of the Spanish Zeolite Group (since 2015).

J. Čejka

Prof. Jiří Čejka is currently employed at the J. Heyrovský Institute of Physical Chemistry and holds the position at the CUCAM project at the Faculty of Science, Charles University in Prague. In 2005 he chaired the 3rd FEZA Conference on Zeolites in Prague and is an organizer of Workshops on zeolites and catalysis, e.g. the EFCATS School on Catalysis in 2018. His research interests include synthesis of zeolites and nanoporous materials, sorption, and catalysis. Jiří Čejka is the co-author of 310 papers with more than 9200 citations, co-editor of 6 books, and has H-index = 52.

the external surface of zeolite crystals and decreases diffusion paths inside the crystals. In contrast, hierarchical zeolites consist of both micropores and mesopores facilitating diffusion of reactants and products.[5–7] Both bottom-up and top-down approaches have been described providing hierarchical zeolites with improved catalytic properties. While traditional zeolites have been conceptualized as 3D networks, a recent breakthrough revealed their formation as crystalline layered solids,[8–11] which can lead *e.g.* to creation of expanded architectures. Fig. 1 summarizes the major advances achieved in tailoring the properties of zeolites.

The aim of this review is to discuss the relationship among synthesis – properties – catalytic performance of three-dimensional (3D) zeolites including nanozeolites and hierarchical ones in comparison to the variety of forms with two-dimensional (2D) structures (Fig. 1). Similarities and differences in chemical and textural properties of different zeolites are highlighted based on different examples of catalytic performance including cracking reactions, biomass transformations, shape selective aromatic chemistry and fine chemical synthesis.

2. Classical three-dimensional zeolites

2.1. Synthesis

Although the first known zeolites were naturally occurring minerals, those having currently the most relevant applications are synthetic zeolites, which have been discovered and developed in laboratory research.[15] Synthetic zeolites are typically obtained by crystallization of gels containing water, silica and alumina sources (other metals) under hydrothermal conditions at basic pH, temperatures in the range 60–200 °C and autogenous pressure. The synthesis gel usually contains also basic agents and alkali cations, as well as organic compounds that may act as structure-directing agents.[16]

The Si/Al ratio is a key parameter of the synthesis as it may determine the type of zeolite structure being formed, its crystallinity, as well as the kinetics of the crystallization process. In general, the Si/Al ratio of the zeolite is lower than that of the gel. A variety of silica and alumina sources can be employed including polymeric and monomeric reagents.[17]

Due to the low solubility of silica and alumina in water, mineralization agents, like NaOH or KOH, must be added to the gel in order to solubilize the precursors and promote the formation of Si–O–Si and Si–O–Al bonds through condensation reactions. The alkali concentration is also a key parameter of the synthesis that must be conveniently balanced. Similarly, severe crystallization conditions, such as high temperature and long time, favour the formation of more thermodynamically stable phases.

Stirring also has a strong influence on zeolite crystallization. It may be accomplished in different ways, such as using mechanical agitators placed internally or by rotating the crystallization vessel. Many zeolite syntheses carried out in the laboratory proceed under static conditions, which may lead to a non-uniform composition of the gel and contamination. In general, stirring causes the crystallization to take place with a more favourable kinetics, leading to the formation of smaller crystals with a narrower size distribution.[17]

The crystallization mechanism of zeolites is usually described by a classical combination of nucleation and crystal growth steps.[18,19] An amorphous solid phase (hydrogel) is often formed at the beginning of the crystallization. In the solution-mediated mechanism, both nucleation and crystal growth are assumed to proceed just with the participation of soluble species, whereas any amorphous solid phase, that could be present, acts as a reservoir of nutrients. In contrast, in the hydrogel-mediated mechanism the zeolite crystallization is considered to occur by the reorganization of the amorphous solid phase formed during the early stages of the hydrothermal treatment. An intermediate scheme, which tries to reconcile the previous ones, proposes nucleation to occur within the hydrogel, whereas the crystal growth would take place by incorporation of soluble species. Taking into account the great diversity of gel compositions, synthesis conditions and zeolite structures, it is a majority opinion that a general zeolite crystallization mechanism does not exist.

Incorporation of organic compounds into the synthesis gel has been instrumental in the discovery of new zeolite structures (mainly with high silica compositions) over the past few decades revealing their role as structure-directing agents.[2,17] They influence the crystallization process *via* modification of the gel chemistry, as pore filling agents or templates. In the last case, a very high specificity exists between the organic template and the zeolite structure. This is, for instance, the case of tetrapropylammonium cation and the **MFI** zeolitic structure due to the almost perfect fitting of the organic molecule and the zeolite microporosity.[16]

Seeding has been widely applied in zeolite synthesis to accelerate the crystallization process as it provides an external source of nuclei, thus reducing the induction period associated with the nucleation step. Seeding is also effective for the organotemplate-free synthesis of zeolites, which has important advantages in terms of reagent cost reduction and avoiding the zeolite calcination treatment for removal of organics.[20,21]

The presence of water is necessary for zeolite crystallization as it makes possible the solubilisation of the Si and Al precursors and is deeply involved in the gel chemistry. However, an excess of water may have also undesired effects, such as a decrease in the zeolite yield and generation of aqueous waste streams. Accordingly, a number of methods have been developed to minimize the water content during the zeolite crystallization. These are dry-gel conversion, vapour-phase transport and steam-assisted synthesis.[22] Zeolite synthesis has also been conducted by hydrothermal treatment of wetness-impregnated xerogels.[23,24] These non-classical approaches have been reviewed together with contributions related to green routes for the synthesis of zeolites in a recent work.[25]

An alternative to hydroxide based syntheses is the use of fluoride-containing media. It allows the crystallization of zeolites at neutral or even slightly acidic pH.[26–28] Under these conditions, fluoride anions replace hydroxide anions as mineralizers and the

solubility of silica increases significantly due to the formation of hexafluorosilicate species. Typically, zeolite synthesis in fluoride media leads to large crystals with a lower concentration of defects and highly hydrophobic properties.

Microwave heating has been employed for zeolite synthesis, dramatically reducing synthesis times compared to conventional heating.[25] Moreover, microwave heating has been very effective for the preparation of zeolite membranes, enabling the control of a number of properties of the membrane *i.e.* morphology, orientation and permeation characteristics.[29] Ultrasound application in zeolite synthesis has also resulted in shorter crystallization times, as it contributes to a reduction of the induction period. Moreover, ultrasonication influences the size and morphology of the crystals and improves the crystallinity of the zeolite.[30]

Recently, the ADOR (assembly–disassembly–organisation–reassembly) methodology has been developed for the preparation of novel zeolite structures that could not be obtained by conventional hydrothermal synthesis.[31] This approach is discussed in Section 5.3.

2.2. Zeolite structures and properties

According to the classical definition, zeolites are crystalline microporous aluminosilicates with the general formula $M_{2/n}O{\cdot}Al_2O_3{\cdot}ySiO_2$, where "*n*" represents the valence of the cation M. The structure of the zeolites is formed by a 3D arrangement of TO_4 tetrahedra (T corresponds to Si and Al atoms), connected by oxygen bridges, which generates an open framework with pores and cavities accessible to molecules having kinetic diameter small enough to penetrate into the zeolite channels.

Taking into account all the possible arrangements of the TO_4 units, a great number of zeolitic structures could be generated.[32] However, in practice, just a relatively small number of structures have been synthesised. Nevertheless, the number of known zeolites is increasing continuously and by April 2018, the International Zeolite Association (http://www.iza-online.org/) has recognized 235 known structures, represented by three-letter framework codes.

The pore sizes existing within zeolite structures are mostly below 1 nm, so they are clearly within the micropore range (<2 nm). The size of these channels is directly related to the number of T atoms present in the pore rings. They are usually classified as small-pore zeolites (8-rings), medium-pore zeolites (10-rings), large-pore zeolites (12-rings) and extra-large pore zeolites (>12-rings). Accordingly, the pore size is typically specified by its minimum and maximum dimensions. In the case of zeolites with multidimensional pore systems, the occurrence of intersections between the channels has a very positive effect on their catalytic behaviour as this attenuates significantly their deactivation by pore blockage when coke is deposited.

Classical aluminosilicate zeolites are known by their acidic and cation-exchange properties, which derive from the extra negative charge of the framework associated with the Al tetrahedra that needs to be balanced by external counter-cations. The counter-cations can be exchanged by contacting the zeolite with a solution of another cation until reaching the equilibrium between the zeolite and the liquid phase. Typically, zeolites are synthesized in sodium or potassium form (related to the mineralisation agent) that can be transformed into the protonic form by ion-exchange with ammonium salts followed by calcination to remove ammonia. Acidic zeolites, prepared in this way, are used in a wide variety of acid-catalysed reactions.[33,34] In principle, acidity in zeolites arises from the presence of Brønsted acid sites directly linked to Al atoms in tetrahedral framework positions (see Section 6.1.1); however, zeolites may also contain significant amounts of Lewis acid sites, formed by dehydration of the Brønsted sites or linked to extra-framework Al species which can be formed during the synthesis or calcination treatments. The ratio between Brønsted/Lewis acid sites typically decreases for low Si/Al ratios in the framework. Thus, whereas high silica zeolites exhibit mainly Brønsted type acidity, both Brønsted and Lewis acid sites are present in significant concentrations in zeolites with low Si/Al ratios. It is remarkable that, compared to amorphous aluminosilicates, the acid sites in zeolites are stronger and more uniform, which is a direct consequence of the crystalline nature of zeolites. Various theoretical methods and experimental techniques have been developed and applied for the characterization of the zeolite acid sites[35,36] (see Section 6.1).

Although quite less developed than the acidic features, zeolites may also present basic properties.[37,38] This is the case of zeolites ion-exchanged with alkali cations, as well as of zeolites containing occluded basic metals and metal oxides. Thus, reactions such as alkylation of toluene with methanol, cyclo-addition of carbon dioxide to ethylene oxide, isomerization of 1-butene, and alkylation of toluene with ethylene occur *e.g.* over basic X zeolites.

The size of the zeolite micropores is on the level of molecular dimensions of small organic molecules. As a result, they exhibit so-called shape selectivity and molecular sieving effects.[39–41] A zeolite may discriminate between molecules having just a small variation in their size or shape, so the larger molecule cannot penetrate the zeolite micropores or it diffuses very slowly through channels while the smaller one can diffuse substantially faster. As a result, great differences have been observed in the uptake and reactivity of compounds such as xylenes or *n- vs.* iso-alkanes. The concept of shape selectivity was introduced in the 1960s, being initially classified according to three types: reactant, product and transition state shape selectivity depending on which of the species the most important steric restriction is related to.[40,41] Subsequently, a number of terms have been coined closely related to shape selectivity effects, such as molecular traffic control, surface pocket catalysis, and pore-mouth selectivity.

2.3. Zeolite modification

While traditional zeolites were known as aluminosilicates, it was realized early on that there is a possibility of preparing some of the zeolitic structures in pure silica form. Resulting materials possess almost no acidity or ion-exchange capacity, but the objective was to use them as supports for other catalytically active phases or in separation and purification processes

taking advantage of their high hydrophobicity and molecular sieving effects.[42,43] However, the number of zeolitic structures, which have been prepared as pure silica zeolites, is relatively limited since the presence of Al species in the gel is essential in many cases for the synthesis of the desired zeolite with high crystallinity. Thus, for instance, the pure silica form of zeolite Beta was difficult to synthesize in alkaline media, which was achieved instead by the fluoride route.[44]

Increasing the Si/Al ratio has been commonly employed as a method for enhancing the zeolite stability. For low silica zeolites this is achieved by post-synthesis treatments that cause the extraction and removal of Al species. This is the case of the USY (ultrastable Y) zeolite, prepared usually by steam treatment to extract a great part of the Al from the structure followed by washing the extra-framework species with dilute acid.[45] USY is a remarkable catalyst used in the cracking of heavy oil fractions in the FCC process.[46]

A variety of metallosilicates with a zeolite structure have been prepared through direct synthesis by isomorphous substitution of the Al^{3+} atoms by other trivalent cations, such as Sb^{3+}, B^{3+}, Ga^{3+} and Fe^{3+}. These zeolitic materials contain Brønsted acid sites with a diversity of strengths, which have a remarkable effect on their catalytic properties in many reactions. Thus, antimonosilicate, borosilicate, ferrisilicate, and gallosilicate with a **MFI** structure have been found to exhibit much higher *para*-selectivity for the alkylation of ethylbenzene with ethanol than the HZSM-5 zeolite, since the weaker acid sites of the metallosilicates catalyse to a lesser extent the undesired isomerization of *p*-diethylbenzene.[47] Likewise, zeolites containing Ga^{3+} in the framework have shown excellent catalytic properties in alkane aromatization,[48] whereas zeolites with Fe^{3+} incorporated into them have exhibited a remarkable catalytic activity for NO_x decomposition.[49]

Replacement of Al by tetravalent cations has yielded materials with Lewis acidity, showing catalytic properties very different from those exhibited by the corresponding aluminosilicates. Thus, incorporation of Ti^{4+} into zeolitic frameworks opened the way for the development of materials, like titanium silicalite 1 (TS-1) zeolite, with redox properties and remarkable catalytic performance in partial oxidation reactions.[50,51] Moreover, zeolitic catalysts containing Sn, Zr, Hf or Nb atoms in the structure have shown remarkable properties in a number of biomass conversion reactions due to the unique Lewis acid character of the corresponding tetrahedral metal sites, which promotes the activation and conversion of oxygen-containing molecules.[52] Last but not least, isomorphous incorporation of Ge^{4+} opened a way towards a number of large and extra-large pore zeolites[53] and in addition some of these zeolites can be transformed into others *via* the ADOR mechanism (see Section 5.3).

Zeolites have also been employed as supports for a wide variety of active phases in order to modify and complement their properties.[54–59] These active phases include metals, metal oxides, metal salts and metal complexes, generating materials with multifunctional properties and applications in a great variety of reactions in various sectors such as oil refining, petrochemistry, fine chemicals, waste valorization, pollutant removal in gaseous and liquid streams, biofuel production, *etc.*

Finally, a huge research effort has been made aiming to tailor zeolite properties directly related to their porosity and accessibility of the active sites in order to improve their catalytic behaviour, mainly in reactions involving bulky substrates that are controlled by steric and diffusional limitations. Accordingly, a new type of zeolitic material showing enhanced accessibility and external/mesopore surface area has been developed, which includes nano-sized, hierarchical and 2-dimensional zeolites, as reviewed in the following sections.

3. Nanozeolites

The intrinsic microporosity of zeolites, with uniform pore shapes and narrow size distributions, provides excellent properties as molecular sieves and as shape-selective catalysts. However, it is their main weakness when zeolites need to process bulky compounds that cannot access the internal active sites. This limitation has motivated the worldwide intensive research attempting to develop zeolitic materials with enhanced accessibility.[60]

Decreasing the crystal size to the nanometer scale is an effective way to enlarge the external surface area and the ratio of external/internal active sites, with the consequent improvement of their accessibility to bulky molecules. Besides, the diffusion path lengths are shortened enhancing the mass transport of reactants/products. According to these modifications, the catalytic applications of zeolites can be expanded to those reactions involving large molecules. Other benefits reported include an increased lifetime and a higher tolerance to coke than conventional zeolites.[60,61]

Among the different crystal sizes obtainable within the category of nanozeolites, there is a special interest on reaching values below 100 nm due to the unique properties they provide.[60] Below this size, nanozeolites can be obtained in the form of stable colloidal suspensions with narrow particle size distributions, which are excellent precursors for the preparation of either membranes, films, composites or hierarchical structures, with potential applications in a variety of fields such as heterogeneous catalysis, molecular separation, ion exchange, chemical sensors and medicine.[12] There are several reviews presenting the latest advances in the study of synthesis strategies, mechanisms of formation, properties, applications and types of zeolites prepared as nanocrystals.[12,60–64] Traditional synthesis methods to obtain zeolite nanocrystals use clear solutions or gels containing zeolite precursors. Clear solutions are recommended when stable suspensions with smaller and narrow particle size distribution are desired. The synthesis conditions must be carefully controlled in order to promote nucleation over crystal growth. For instance, it is preferable to work at low synthesis temperatures, since the activation energy of nucleation is generally lower than that of crystal growth.[12,65,66] In order to avoid aggregation of zeolite nanocrystals, large concentrations of organic structure-directing agents (OSDA) are employed, whereas the alkali cation content is reduced as such

cations neutralize the negatively charged (alumino)silicate sub-colloidal particles. Moreover, if the objective is to attain a colloidal suspension of nanocrystals, the as-synthesized suspension must be subjected several times to the sequence of high-speed centrifugation–redispersion in a liquid (using an ultrasonic device).

It can be inferred that traditional synthesis strategies of nanozeolites present serious difficulties to reach the industrial viability due to the large amounts of OSDA employed, together with the long synthesis times and low mass zeolite yields. Likewise, removal of the organic templates from as-synthesized nanozeolites is done by calcination at relatively high temperatures, which may cause aggregation of nanocrystals with some loss of size homogeneity and external surface area, or even destruction of the zeolite structure.[63] For these reasons, template-free strategies have been explored. The generation of small and homogeneous nanocrystals is more successful under mild synthesis conditions, vigorous stirring, and crystallizations in several steps. One of the first zeolites successfully prepared in the absence of an organic template was **FAU**-type, in particular Y and X zeolites.[67–69] Control of both the amount of water in the initial gel and temperature of crystallization, carried out in 2 or 3 stages, allowed obtaining individual particles as small as 30 nm.[67,68] Quite recently, the low-cost synthesis of NaX nanozeolites by the hydrothermal method without organic template addition and using agricultural wastes, in particular stem seep ash (SSA), as silica source has been reported.[70,71] Aggregates of nanoparticles with a mean size below 70 nm were attained from a clear solution hydrothermally treated at 60 °C and containing sodium aluminate, sodium hydroxide, water and silica extracted from SSA. Rice husk ash (RHA) has been also used as a low-cost source of silica by Ng *et al.*[72] to synthesize **EMT**-type nanocrystals by an organic-free hydrothermal route. Highly crystalline **EMT**-type nanocrystals with a mean size of 15 nm, narrow particle size distributions and relatively high yields based on silica (75 wt%) were obtained after 28 h of hydrothermal crystallization at 28 °C under strongly basic conditions.

The use of organic structure-directing agents can also be avoided by seeding the initial synthesis gel with small amounts of zeolite seeds, as is the case reported for Mordenite,[73] Beta[74] and ZSM-5 zeolites.[75,76] Together with the synthesis conditions, the amount of seeds introduced influences the final crystallite sizes. For instance, when the seeding was applied to prepare nanosized ZSM-5, it was observed that lower synthesis temperatures and higher seed concentrations led to smaller nanoparticles, with values ranging from 140 and 230 nm depending on the conditions.[76] Moreover, the solid yields were significantly higher (80%) than the typical values corresponding to the traditional synthesis routes. More examples regarding the use of seeds on the preparation of nanozeolites can be found in the review literature.[61]

Many other approaches have been proposed for the preparation of nanosized zeolites in the absence of organic templates.[60,61] Some of them are modifications of the traditional synthesis procedures, such as replacing conventional heating with microwave-irradiation,[29,77,78] fluid microreactors[79,80] or inert solid matrixes as templates (confined-space synthesis).[81–83] Top-down strategies have also been reported, as is the case of milling the primary zeolites with micro-meter sizes, usually followed by recrystallization.[84–86] Nevertheless, top-down routes are characterized by broader particle size distributions.

After appropriate post-synthesis treatments (intensive washing and pH neutralization), nanosized zeolites are usually very stable in different solvents. This allows their further processing to final shapes or macroscopic structures depending on their application (Fig. 2). For sorption and catalytic applications, nanosized zeolites are usually moulded as extrudates with different shapes (spheres, cylinders) with the aid of binders (silica or alumina). For optical devices and chemical sensors, thin-to-thick layers of nanozeolites can be created by different routes, including screen-printing, sol–gel techniques, dip- or spin-coating and direct growth of the substrates. Zeolites are also usually employed to fabricate membranes for gas–vapour and liquid–liquid separation processes.[64]

At present, there exist around 20 types of zeolites synthesized at the nanoscale (including **SOD**, **LTA**, **MTW**, **MEL**, **FAU**, **EMT**, **MFI**, **BEA**, **MOR**),[64] but it is presumable that this number

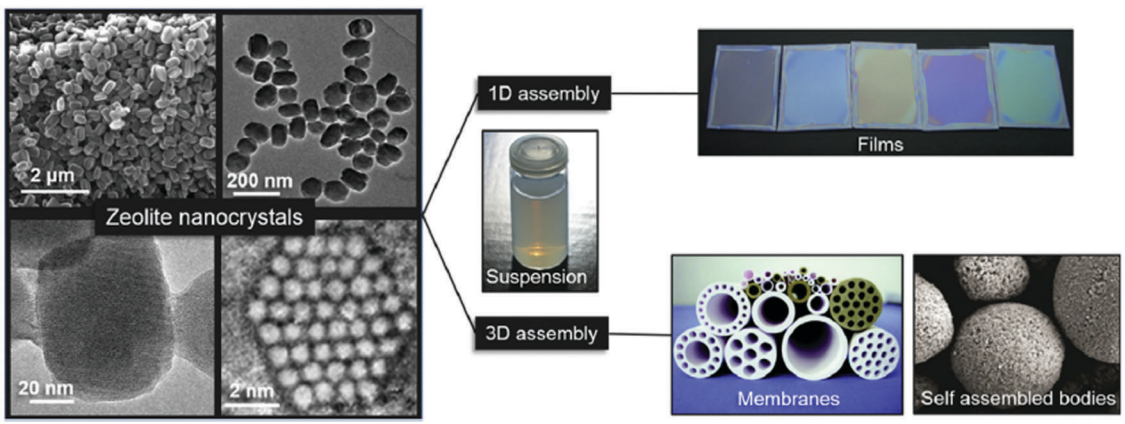

Fig. 2 Zeolite nanocrystals with diverse morphologies and sizes in colloidal suspensions and examples of processed forms as self-supported shapes, porous membranes, and optical quality films. Reproduced from ref. 64 S. Mintova, J. Grand and V. Valtchev, *C. R. Chim.*, 2016, **19**, 183–191. Copyright (c) 2016, published by Elsevier Masson SAS. All rights reserved.

will increase progressively. The challenge is to develop efficient strategies to stabilize the nanocrystals into small (<100 nm), discrete and homogeneous particles as well as to improve the control of their physico-chemical properties. The success on these targets will allow their expansion into new applications in different industrial fields, including food, cosmetics, medicine and nanotechnology.

4. Hierarchical zeolites

The term ''hierarchical zeolite'' was first applied at the beginning of the XXI century to zeolitic materials possessing a bimodal pore size distribution,[87–89] consisting of zeolitic micropores and a secondary porosity (usually in the range of mesopores). This mesoporosity can be generated by a variety of top-down or bottom-up synthesis strategies.[5] Some authors also call these materials as ''mesoporous zeolite'',[90,91] which can be somewhat misleading as it may suggest the presence of only mesopores, while in reality they still contain a great proportion of micropores. Accordingly, the term ''hierarchical zeolites'' seems to be more convenient.

Hierarchical zeolites exhibit enhanced accessibility of the active sites, faster mass transport of molecules and they are usually more resistant against coke deactivation. Therefore, they often show a higher catalytic activity than conventional zeolites, in particular in those reactions suffering from steric and/or diffusional limitations. Moreover, the secondary porosity provides an ideal space for the incorporation and grafting of other components and phases, opening a great diversity of routes for the preparation of multifunctional materials.

In the past 15 years, a large number of original papers have been published on the synthesis, properties and catalytic applications of hierarchical zeolites, which are now briefly reviewed. It must be noted that several review articles have also been published on this emerging and relevant topic.[60,92–98]

4.1. Synthesis strategies for the preparation of hierarchical zeolites

The methods reported for the preparation of hierarchical zeolites were classified as bottom-up and top-down approaches, depending on whether the creation of the secondary porosity is induced during or after the zeolite crystallization.[5] However, this classification is rather simplistic taking into account the great diversity of synthesis strategies that have been developed in the past few years, such as dealumination, desilication and degermanation treatments, fluoride etching, zeolitization of preformed solids, assembly of zeolite nanocrystals, hard-templating by carbon materials, use of organosilanes, templating by polymers and addition of surfactants to the synthesis gel. Those routes that have been more widely applied in the literature are briefly commented below.

Dealumination is a classical treatment of low silica zeolites that very often provokes the development of mesoporosity, being carried out by steaming at elevated temperatures and acid leaching.[99] This treatment has been traditionally applied to zeolite Y to remove a part of the aluminium in the zeolite framework, thus increasing its hydrothermal stability aimed to improve its performance when used as a catalyst in fluid catalytic cracking (FCC), which has also been noted to create some mesoporosity.

Degermanation is a method based on the liability of Ge–O bonds, which are usually located anisotropically in the framework of some microporous germanosilicates.[100–102] This method is discussed in more detail in Section 5.3 dedicated to the ADOR mechanism.[31]

Desilication is based on the treatment of zeolites with a base (usually sodium hydroxide), which causes creation of mesopores due to preferential removal of silica from the framework.[103] The alkali treatment can also be performed using organic bases (*e.g.* tetrapropylammonium hydroxide and tetrabutylammonium hydroxide) allowing mesopore volume to be optimized,[104] since these organic cations act as pore growth moderators. Desilication is a quite versatile method as it has been successfully applied to a large number of zeolite structures,[105] although a significant destruction/dissolution of the zeolite structure can happen.

Fluoride etching is somewhat similar to desilication; however, it is not selective to silicon or aluminium (or any other element). It starts from the boundaries of intergrown crystals or crystal domains, thus separating twins into single crystal parts.[106,107] Under certain conditions, the formation of uniform rectangular mesopores was observed yielding a material with an Emmental cheese-like morphology, but being fully crystalline and with the same acidic properties as the parent one.[108]

Hard-templating by carbon materials is another route widely employed for the synthesis of hierarchical zeolites. In this approach, the zeolite crystallizes around and/or within particles of a carbon matrix, which is removed by combustion after the formation of the zeolite crystals. Thus, mesopores are generated between or inside the zeolitic entities. A diversity of carbon sources have been employed, including active carbons (both micro- and mesoporous), colloid imprinted carbons, carbon nanoparticles, multi-walled carbon nanotubes (MWNT), carbon aerogels and ordered mesoporous carbons (CMK-3).[109–115] In the case of carbon nanoparticles, a substantial effect of microwave regime has been documented.[116]

Hierarchical zeolites have also been prepared starting from pre-formed solids, which are then subjected to crystallization into zeolites, preserving their initial shape and meso-/macroporosity. The crystallization is performed by the Vapour Phase Transport (VPT) method, in which a mixture of water and structure directing agents is vaporized and brought into contact with the dry gel. Alternatively, Steam-Assisted Conversion (SAC) can be applied for promoting the zeolitization process. In the SAC route only water is vaporized and the structure directing agents (non-volatile compounds) are already included in the solid gel. These approaches have been used for the preparation of hierarchical zeolites from different types of solid precursors, such as dry gels,[117] silica-based nanoparticles,[118] mesostructured solids,[119] or macroscopic hierarchical amorphous solids.[120,121]

Different types of polymers (cationic, amphiphilic and block polymers) have been added to the zeolite synthesis gel to act as porogens of the secondary porosity. Thus, mesoscale polydiallyldimethylammonium chloride has been used for the preparation of hierarchical Beta zeolites,[122] whereas polystyrene spheres have been employed for obtaining hierarchical zeolites with a microporous/macroporous pore structure.[123] Likewise, ZSM-5 single crystals with *b*-axis-aligned mesopores have been prepared using a designed cationic amphiphilic copolymer as a mesoscale template.[124] In the same way, hierarchical zeolite Y has been directly synthesized using a block copolymer (Pluronic F127) as the template, which guides the aluminosilicate gel to assemble into a zeolite with significant mesoporosity.[125]

Organosilane-based methods have also been reported as very effective strategies to develop mesoporosity in zeolites.[126] They are based on the addition of different types of organosilanes (simple organosilanes, silylated polymers or amphiphilic organosilanes) to the zeolite synthesis gel in order to perturb the crystallization process, causing the generation of secondary porosity.[127–132] Their effect is noticeable even when incorporating relatively small amounts of the organosilane. Amphiphilic organosilanes become linked to the aluminosilicate species in the gel, promoting their arrangement around the formed amphiphile micelles. In the case of using simple organosilanes or silylated polymers, these reagents are anchored on the external surface of protozeolitic nano-units, partially hindering their aggregation and, therefore, the growth of standard zeolite crystals (Fig. 3). In all cases, the removal of the organosilane generates the mesoporosity finally present in the hierarchical zeolite.

Hierarchical zeolites have also been prepared by surfactant-assisted crystal rearrangement of the zeolite framework.[134–137] Thus, dealuminated zeolite Y was treated with an NH_4OH/surfactant (cetyltrimethylammonium bromide) solution, followed by heating at 150 °C under autogenous pressure.[134] This treatment augmented the mesoporosity initially present in the sample, leading to a material showing a quite uniform mesopore size distribution. The authors proposed that a local rearrangement of the zeolite structure takes place around the micelles of the surfactant, which provokes the transformation of the initial mesoporosity into a more uniform one, so the final materials exhibit mesostructured features. Fig. 4 illustrates digital analyses of TEM micrographs of hierarchical USY samples obtained by this approach, as well as of the parent zeolite.

Other methods for the preparation of hierarchical zeolites have been envisaged by combining several of the above mentioned strategies in order to achieve a better control of the properties of the final zeolite, and in particular of its mesoporosity. In this way, the sequential combination of desilication/dealumination treatments has been explored for the synthesis of a number of zeolites, such as ferrierite, clinoptilolite and L zeolites.[139,140] The main challenge in the post-synthetic modification of these zeolites is their high Al content, requiring a tailored dealumination prior to the desilication step. On the other hand, a combination of seed silanization and surfactant-assisted crystal rearrangement strategies has been very effective for obtaining zeolites TS-1, **MFI** and ***BEA** with quite uniform mesopore size distribution.[141–143]

4.2. Properties of hierarchical zeolites

The presence of bimodal porosity in hierarchical zeolites causes sharp changes in many physicochemical properties of these materials compared to conventional zeolites. Thus, hierarchical zeolites typically exhibit enhanced accessibility, improved textural properties, faster intraparticle transport properties, changes in the acidity and better resistance against deactivation by coke formation compared with their conventional counterparts. In addition, as has been indicated earlier, hierarchical zeolites can be transformed into multifunctional materials by incorporation and/or grafting of other components taking advantage of their large share of mesopore volume and surface.

4.2.1. Accessibility and textural properties. While for conventional zeolites the textural properties are mainly determined by the zeolitic micropores, in hierarchical zeolites both micro- and mesopores contribute significantly to the BET area and pore volume. Thus, depending on the preparation method and type of zeolite, mesopores may account for up to 50% of the overall BET area.[144] This fact enables a high accessibility as the mesopore surface may interact and adsorb bulky

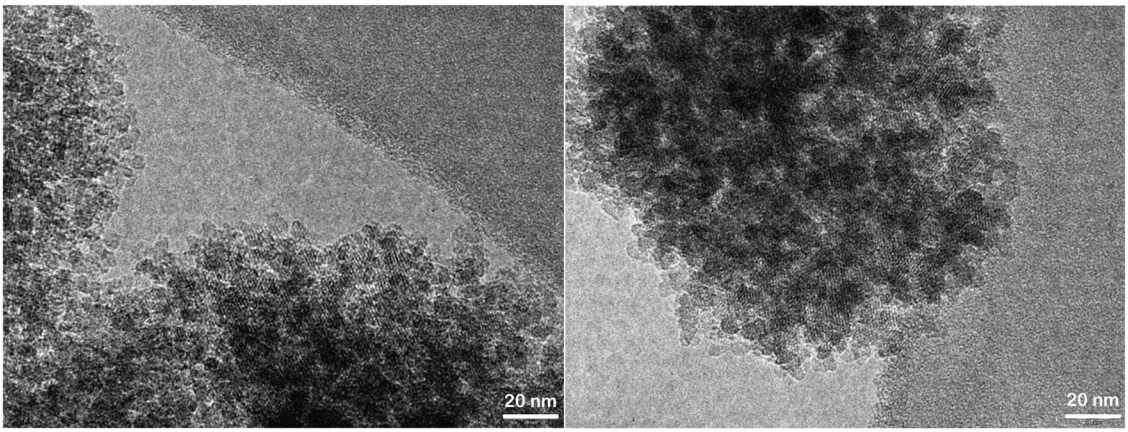

Fig. 3 TEM images of hierarchical ZSM-5 prepared using organosilanes in the synthesis gel.[133]

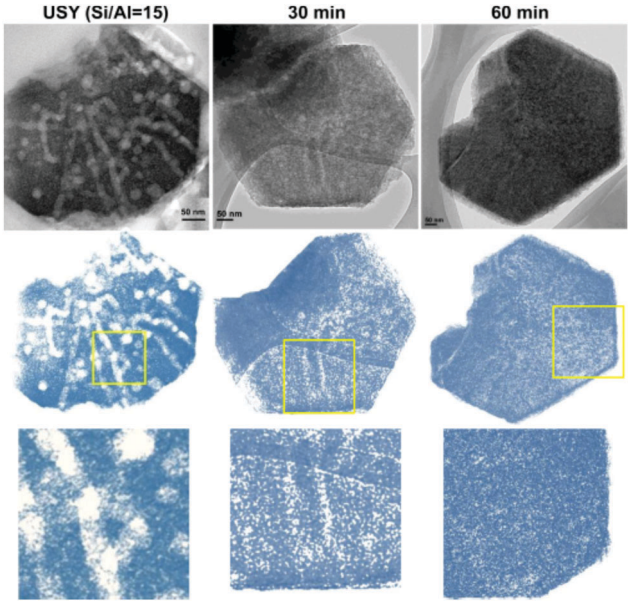

Fig. 4 TEM micrographs and digitally treated TEM micrographs of the parent USY zeolite (left) and *ex situ* surfactant-templated USY zeolites treated at 373 K for 30 min (center) and 60 min (right). Reprinted with permission from ref. 138.

compounds that, on the contrary, cannot penetrate into the zeolitic micropores.

The mesopores occurring in hierarchical zeolites, as well as their connectivity with the zeolitic micropores, have been visualized using transmission electron microscopy,[96,145,146] as well as by other techniques, such as hyperpolarized ^{129}Xe-NMR,[147] positron annihilation[148] and electron tomography.[149] A variety of 2D and 3D microscopic techniques have been demonstrated to probe the pore structure of hierarchical zeolites.[96] Thus, zeolite single crystals with intracrystalline mesopores incorporating metal oxide particles have been characterised by direct TEM stereo-imaging,[145] whereas polarized-light microscopy has been used to unravel the pore geometry of ZSM-5 crystals containing mesopores.[146] Likewise, one- and two-dimensional ^{129}Xe-NMR spectroscopy has been employed to study the porosity of hierarchical zeolites under the continuous flow of laser-hyperpolarized xenon gas, demonstrating that these hierarchical pores have connected networks that facilitate xenon diffusion and exchange.[147] On the other hand, the porosity of hierarchical zeolites has also been characterized by high-contrast electron tomography, the samples being supported with platinum.[149] The resultant tomograms showed disordered and interconnected networks of Pt nanowires and nanosheets, which corresponded to the shape of the surfactant-directed mesopores. It was proposed that the micropores and mesopores could be connected through apertures, in which the neck of the surfactant molecule had been located.

Hierarchical zeolites usually present enhanced BET areas in comparison with conventional ones. This fact is a result of the lower restrictions that exist for the adsorption of gases over the mesopore surface, as it occurs also on the external surface of zeolite nanocrystals.[150] Accordingly, a general trend is observed for hierarchical zeolites, showing an increase in the BET area due to the contribution of the secondary mesoporosity. In the case of hierarchical ZSM-5 zeolites, values of the BET area of up to 800 $m^2\ g^{-1}$ have been reported for samples prepared using organosilanes, which represents almost twice that of a conventional zeolite sample.[151] Regarding the assessment of the pore size distribution, the application of NLDFT models has made calculation of the individual contribution of the micro- and the mesoporosity to the overall zeolite textural properties possible, also providing a continuous pore size distribution curve extending from micro- to mesopores.[151] Fig. 5 shows the cumulative pore volume and pore size distribution curves obtained applying the NLDFT model to Ar adsorption isotherms (87 K) of a hierarchical Beta zeolite before and after being subjected to (above mentioned) mesopore narrowing treatment with a surfactant/ammonia solution.

4.2.2. Mass transport properties. The presence of mesopores in hierarchical zeolites leads to a faster diffusion of the reactants towards the active sites, which results in enhanced reaction rates for systems under diffusion control. Likewise, products formed within the zeolite micropores diffuse out more rapidly, limiting secondary reactions and bringing improved selectivity. When using conventional zeolites, the intracrystalline mass transport is strongly hindered due to the similarity between the kinetic diameters of reactants/products and the zeolite micropore diameter (configurational diffusion). In hierarchical zeolites, the major kinetic effect derived from the secondary porosity is the shortening of the effective length of the diffusional pathway what leads to an increase in the overall diffusion rate. Thus, the existence of an interconnected network of mesopores and micropores has been proposed to favour also the intracrystalline mass transport in hierarchical zeolites.[152]

Different literature studies investigated experimentally the expected enhancement of the mass transport rates in hierarchical zeolites. Two-order of magnitude improvement in the diffusion rate of neopentane within desilicated ZSM-5 has been observed, due to both shorter diffusion path length and the presence of an accessible network of mesopores.[153] Similarly, water diffusion is favoured in Na^+ zeolites in which, in addition to the micropores, the crystals are traversed by a network of mesopores.[154] For instance, for zeolite ***BEA**, an increase in water diffusion rate by a factor of 3 was observed. The effect of mesopores on the adsorption and diffusion properties of **MFI** zeolites was studied for *n*-heptane and toluene using the zero length column (ZLC) method.[155] The effective diffusion coefficients of these hydrocarbons increased greatly in the presence of mesopores, while the corresponding activation energy decreased. Expectably (having in mind size and shape of the two molecules), a higher enhancement was observed for toluene relative to that for *n*-heptane.

The increase in the mass transport rate is preserved even when the hierarchical zeolites are shaped into technical forms using binders. The influence of shaping on the adsorption and diffusion properties of hierarchical ZSM-5 has been assessed by studying gravimetric uptake of 2,2-dimethylbutane over

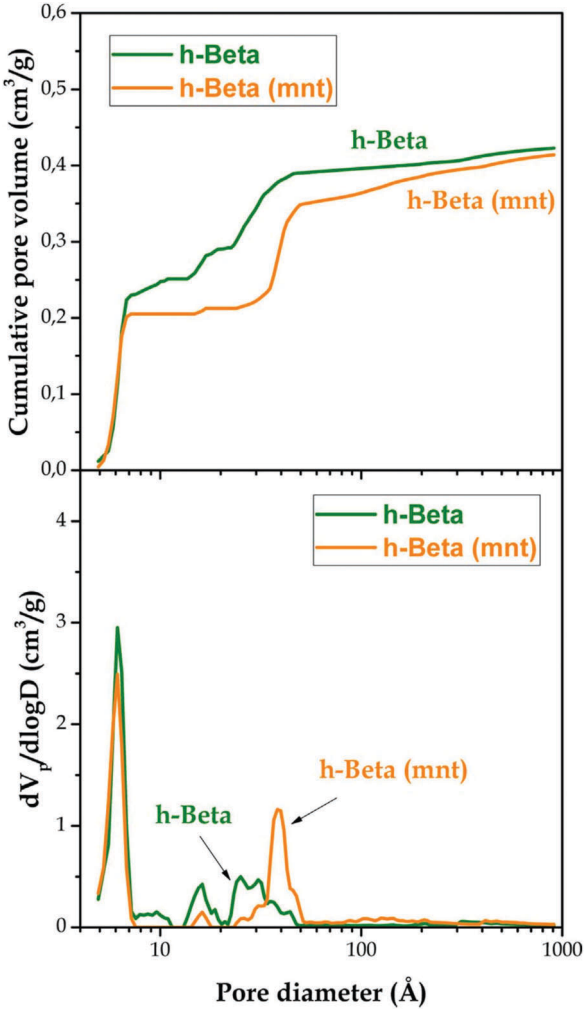

Fig. 5 Cumulative pore volume curves (upper graph) and pore size distribution curves (lower graph) of the h-Beta and h-Beta (mnt) samples obtained using the NLDFT method to analyse Ar adsorption–desorption isotherms measured at 87 K. Reprinted with permission from ref. 143.

powders and millimeter-sized bodies.[7] Improved intracrystalline diffusivity (due to the presence of interconnected mesopores) was observed in powder as well as in the macroscopic bodies, independently of the shaping method or binder applied.

4.2.3. Acidity. Despite the fact that many of the reactions, in which zeolites are used as catalysts, occur over acid sites, the effect that the secondary porosity has on the zeolite acidity has been relatively less investigated than other factors in the literature; in some cases with contradictory conclusions, in particular about the strength and nature of the acid sites located on the mesopore surface.

For hierarchical zeolites prepared by desilication, it has been concluded that the acid strength of the Brønsted sites of zeolites does not change significantly after the generation of mesopores.[156] For mesoporous ZSM-5 prepared using amphiphilic organosilane, a lower concentration of Brønsted acid sites compared to conventional ZSM-5 was assessed by infrared-mass spectroscopy/temperature-programmed desorption (IRMS-TPD) of ammonia.[157] Characterization by FTIR/pyridine of hierarchical ZSM-5 zeolites, prepared using organosilanes, has shown that they contain a higher proportion of Lewis acid sites compared to conventional samples, which arise probably from the larger concentration of extra-framework Al species in the former.[158]

The formation of Lewis acid sites in hierarchical ZSM-5 samples during a typical air calcination has been investigated,[159] showing that it occurs to a higher extent than for conventional ZSM-5, due to lower stability of the Al atoms located on the mesopores. However, when a two-step (nitrogen/air) calcination treatment was applied, the so obtained hierarchical ZSM-5 preserved most of the Al atoms in tetrahedral coordination having the acid sites mainly of Brønsted type. This result noted the possibility of limiting the formation of extra-framework Al species, as well as of the associated Lewis acid sites, providing a convenient calcination treatment.

To describe in detail acid sites in hierarchical ZSM-5 materials, the so-called "accessibility index" has been determined from the FTIR spectra obtained after adsorbing substituted alkylpyridines with different molecular size: pyridine (0.57 nm), 2,6-lutidine (0.67 nm) and 2,4,6-collidine (0.74 nm).[160] The accessibility index is defined as the ratio between the number of Brønsted acid sites probed by the employed alkylpyridine and the total amount of Brønsted acid sites determined from pyridine adsorption. While 2,6-lutidine has access to roughly 50% of the ZSM-5 acid sites, collidine only probes the acid sites present on the external/mesopore surface.

Accessibility studies of acid sites in hierarchical ZSM-5 zeolites have also been carried out by IR measurements after adsorption of pivalonitrile, determining the corresponding accessibility factor (AF) referenced to pyridine.[161] The main advantage of this probe molecule is that it can interact and, therefore, assess both Brønsted and Lewis acid sites. This technique was applied to desilicated ZSM-5 zeolites, observing that the accessibility of Lewis acid sites in the desilicated samples is even more enhanced than that of Brønsted sites. The authors proposed that in desilicated zeolites the majority of Lewis sites originate from dehydroxylation of the Si–OH–Al groups, previously formed by the reinsertion of Al extracted from zeolite during alkaline treatment. Accordingly, newly formed Lewis sites are expected to be located mainly on the mesopore surfaces, which facilitates the accessibility of bulky molecules like pivalonitrile.

4.2.4. Retardation of deactivation effects. Hierarchical zeolite catalysts exhibit in many reactions increased lifetime due to their higher resistance to coke deactivation in comparison with conventional zeolites. Interestingly, in many cases this is not caused by a lower formation of coke. The deactivating effect of the coke deposits is attenuated in hierarchical zeolites thanks to the connectivity between micro- and mesopores existing in these materials which lowers the extension of pore blockage phenomena when coke is deposited. In addition, coke precursors formed in the micropores can diffuse out more easily in hierarchical zeolites, avoiding their transformation into coke.

Retardation of deactivation has been observed in a number of reactions over ZSM-5 zeolites,[162] such as isomerisation of

1,2,4-trimethylbenzene, cumene cracking and esterification of benzyl alcohol with hexanoic acid. In all cases, the hierarchical ZSM-5 showed a lower deactivation rates than conventional ZSM-5. In the methanol-to-hydrocarbon reaction,[163] the catalyst lifetime was more than three times prolonged using the hierarchical ZSM-5 in comparison with a conventional ZSM-5. The impact of the textural properties of both hierarchical and nanocrystalline ZSM-5 zeolites has been investigated in conversion of ethanol to hydrocarbons.[164] The lifetime of the catalysts is not correlated with the coking rate but with the number of pore mouths. Thus, the longest catalyst lifetime (>100 h) was observed with a hierarchical nanosized zeolite even though most of its acid sites were poisoned.

Extension of the catalyst lifetime has also been reported for other types of hierarchical zeolites. Thus, isomerization and cracking of *n*-hexadecane have been investigated over ZSM-12 zeolites containing mesopores, showing significantly improved resistance to poisoning by coke formation.[165] Similarly, hierarchical zeolite Y has been found to exhibit remarkably higher resistance to deactivation in the aldol condensation of benzaldehyde with *n*-butyl alcohol than a commercial zeolite Y, which is attributed to its highly mesoporous structure minimizing the diffusion length of coke precursors out of the zeolite matrix.[166]

4.2.5. Multifunctional features. The secondary porosity present in hierarchical zeolites is an ideal space for incorporation of other active phases, opening new routes for the preparation of multifunctional materials. This fact has been reflected in numerous recent papers using hierarchical zeolites as supports for a variety of catalytically active phases.

Different metals, such as Pt, Pd, Ni, Co and Cu, have been added to hierarchical zeolites by impregnation of the precursors.[167–171] These metals are present usually in the form of nanoparticles located mainly in the mesopores in close contact with the support and with an improved dispersion compared with the use of conventional zeolites. These findings have been related to the existence of a significant mesoporosity in hierarchical zeolites, as well as to the occurrence of a high concentration of structural defect sites, which act as preferred deposition points for dispersion of metal phases.[172] Such materials exhibit bifunctional properties, being applied in hydrogenation, hydroisomerization, Fischer–Tropsch synthesis, and hydrocarbon abatement.

Metal oxides, sulphides and phosphides have also been supported over hierarchical zeolites in order to expand their catalytic applications in reactions such as aromatization, alkylation, desulphurization and hydrodeoxygenation.[173–176] Thus, ZnO-containing **MFI** zeolite catalysts with bimodal and trimodal hierarchical pore structures have been studied for the conversion of methanol to aromatics. The presence of highly dispersed ZnO clusters enhanced the selectivity for aromatics.[173] Interestingly, a catalyst with basic properties has been synthesized by supporting of MgO over hierarchical silicalite-1, showing an improved catalytic activity for the side chain alkylation of toluene with methanol compared to bulk MgO.[174] On the other hand, mesoporous ZSM-5 modified with metal sulfides (NiMoS/ZSM-5 and CoMoS/ZSM-5) was active in deep hydrogenation of phenanthrene.[175] Ni_2P has been supported over hierarchical ZSM-5 zeolites, showing an enhanced activity in hydrodeoxygenation reactions of bio-oil model compounds.[176]

In addition to metals, metal oxides and salts, hierarchical zeolites have been used as supports for other catalysts: encapsulation of Fe–Schiff bases and Ti–salen complexes, incorporation of heteropolyacids and enzymes, and functionalization by grafting of sulfonic groups.[177–181]

5. Zeolites with 2-dimensional forms

A zeolite is considered 2-dimensional when one of the dimensions of its crystals is less than several nanometres, corresponding to about one or two unit cells. In such a case, the well accessible external surface per mass/volume unit is highly increased (in comparison with 3D (conventional) zeolites) and a number of post-synthesis modifications (*e.g.* swelling, pillaring, exfoliation *etc.*), characteristic of layered materials, become possible.[9,182]

From the synthesis point of view, 2D zeolites have been reviewed recently. Reviews by Roth and coworkers[9,183] and Eliášová and coworkers[31] are recommended for more details.

In principle, there exist 3 general approaches to the synthesis of 2D zeolites. (I) Some zeolites (**FER**, **MWW**, **NSI**, **SOD**, and several others) can be directly prepared as lamellar precursors (which can be processed or modified in a way that their 2D character is preserved). (II) 2D zeolites can be obtained *via* a restricted crystal growth mechanism using a specially designed (surfactant) structure directing agent which blocks crystal growth in one of the crystallographic directions forming sheet-like single crystals. (III) Top-down post-synthesis modification of zeolites with anisotropic structures (namely germanosilicates).

5.1. Hydrothermal synthesis

3D zeolites traditionally crystallize under hydrothermal conditions from appropriate synthesis gels or from clear solutions. Some of them, however, form lamellar precursors, which are intercalated with the structure directing agent (SDA). The molecules of the SDA, *inter alia*, keep the layers organised in a way that opposite silanol groups on the surface of two neighbouring layers can condense into oxygen bridges thus forming a fully 4-connected zeolite upon calcination. In some cases the condensation does not produce the 3D framework (EU-19, RUB-20, RUB-40).[184]

The first zeolite, for which the formation of a layered precursor was observed (and so far the most studied of the 2D zeolites), is the **MWW**. In its 3D form (reported independently as PSH-3,[185,186] SSZ-25,[187] MCM-22,[188] ERB-1[189]), it is a medium pore zeolite with two independent 2-dimensional channel systems of 10-ring pores. One of the pore systems contains 7.1×18.1 Å supercages.[190] The layered character of the as-synthesised material was disclosed by the Mobil researchers in 1990s and confirmed by others.[189,191] Later on, synthesis routes yielding directly 3D **MWW** (MCM-49[192]), delaminated **MWW**

(MCM-56; material which does not condense into a 3D zeolite upon calcination even without any further modification[193]) and, recently, *in situ* swollen **MWW** (ECNU-7)[194] were also disclosed.

Ferrierite[195] (IZA code **FER**) is another important zeolite found to form a lamellar precursor (denoted as PREFER).[196] In fact, the PREFER layers do not condense only to form ferrierite but when prepared using a different procedure, they are shifted and condensed to form a **CDO** structure (CDS-1 zeolite), which is composed of the same layers but stacked in a different symmetry.[197,198] Similarly, RUB-36 (**CDO** lamellar precursor) can be either directly calcined to form the **CDO** zeolite, or swollen with cetyltrimethylammonium cations (see Section 5.4) and de-swollen with EtOH/HCl which results in a layer shift yielding PREFER and after calcination 3D **FER**.[199] In fact it is possible to switch between the CDO and FER arrangements by intercalation and pH adjustment.[200] Such pairing on 3D zeolites composed of same layers, where in one of them the layers are propagated by translation while in the other by mirror plane, is observed also for **NSI**/**CAS**, **RRO**/**HEU** and **FAU**/**EMT** structures[9] (for **FAU** and **EMT**, lamellar precursors were not disclosed yet). Rich chemistry of the lamellar zeolite precursors has been recently reviewed by Roth *et al.*[9] and Díaz *et al.*[201]

5.2. Surfactant templated synthesis

Until 2009, the only known lamellar zeolitic materials were those forming lamellar precursors during crystallization. These lamellar precursors can then condense into fully four-connected 3-dimensional zeolites upon calcination (*e.g.* **MWW**, **FER**; see previous chapter). The main role of the SDA in crystallization of these zeolites is the same as for those forming 3-dimensional network directly; that is to fill and stabilize void volumes in the structure of zeolites against dissolution or transformation into more stable (denser) phases.[202]

In 2009, the Ryoo group introduced the concept of surfactant structure directing agents enabling to prepare lamellar (or nanosponge; *vide infra*) forms of zeolites such as **MFI** (Fig. 6) or **MTW**, which were not yet known to form lamellar precursors directly.[203] Quaternary ammonium surfactants (*e.g.* cetyltrimethylammonium (CTMA)) were used before in the synthesis of mesoporous molecular sieves;[204,205] however, their templating effect was not strong enough to promote zeolite crystallization. Only very recently was a synthesis of hierarchical **MFI** using CTMA in combination with KOH reported.[206] Choi *et al.* augmented the structure directing effect designing a di-quaternary ammonium surfactant, where the ammonium groups in the hydrophilic part of the molecule are separated by an organic linker of an appropriate structure and size (*n*-C_6 for **MFI**).[203] In the pioneering work,[203] a surfactant $C_{22}H_{45}$–$N^+(-CH_3)_2$–C_6H_{12}–$N^+(-CH_3)_2$–C_6H_{13} (denoted as C_{22-6-6}) was used to form **MFI** in a form of nanosheets of about 2.5 nm thickness. The surfactant nature of the SDA is a key to form the layered structure. The hydrophilic end with two quaternary ammonium groups templates the zeolite crystallization while the long hydrophobic chain prevents the crystal growth in one of the crystallographic directions (*b*-axis for **MFI**). In addition, the hydrophobic chains support (under certain conditions) regular stacking of the formed (nanosheet) crystals. As a result, bigger aggregates of the nanosheets (not a colloidal suspension) are formed and these are easy to process. Note an important difference in comparison with zeolites forming lamellar precursors: the **MFI** nanosheets (and generally all materials prepared using surfactant SDAs) do not condense into a 3-dimensional zeolite upon calcination but the layers stack randomly one to another forming a material with slit-shaped mesopores because the nanosheets do not fit regularly one on another (Fig. 6). Condensation of surfactant templated nanosheets into a 3D structure is still a challenge and particularly in the case of **MFI** nanosheets it may lead to a new zeolite.

Deeper investigations of the surfactant templated syntheses[209] revealed that shorter hydrophobic chains (C_{18}, C_{16}) also provide the lamellar **MFI** phase and in some cases it is beneficial to use them to shorten the crystallization time (*e.g.* for layered titanium silicalite-1[210]). The minimum hydrophobic chain length to form lamellar **MFI** is about C_{10}[209] and the hydrophobic chain length enables to control the interlayer *d*-spacing.[211] Tailoring of the hydrophilic part of the SDA controls the thickness of the **MFI** nanosheet. Addition of third and fourth quaternary ammonium groups results in the formation of nanosheets composed of 5 resp. 7 pentasil layers instead of 3 for C_{22-6-6}.[209]

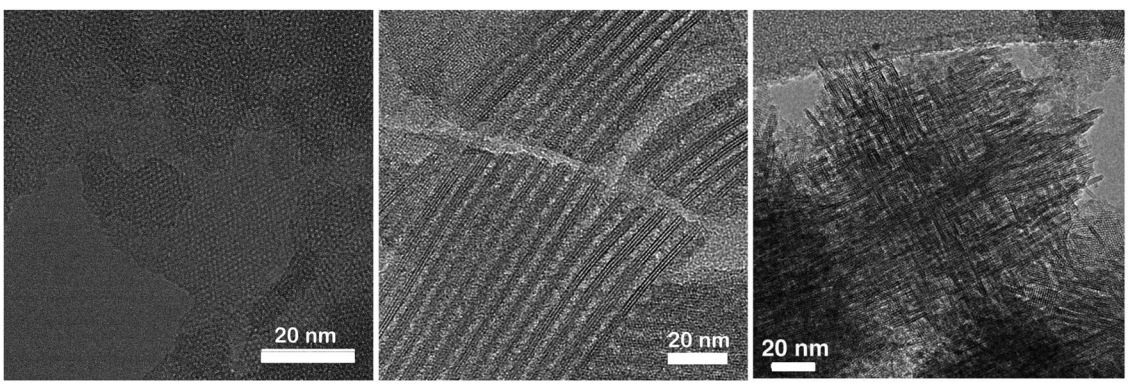

Fig. 6 TEM images of nanosheet **MFI** viewed along the *b*-axis (left), pillared nanosheet **MFI** viewed along the *a*–*c* plane (middle) and self-pillared-pentasil zeolite (right). Reprinted with permission from ref. 207 (left, middle) and ref. 208 (right).

On the other hand, the nanosheet thickness can be as low as 2 pentasil layers (**MFI** unit cell) when a surfactant with two hydrophobic tails and 3 quaternary ammonium groups is used [$C_{18}H_{35}$–$N^+(-CH_3)_2$–C_6H_{12}–$N^+(-CH_3)_2$–C_6H_{12}–$N^+(-CH_3)_2$–$C_{18}H_{35}$] (in short C_{18}–N_3–C_{18}).[212] Under certain conditions the C_{18}–N_3–C_{18} surfactant can also promote the formation of a hexagonally ordered mesoporous material with walls of crystalline **MFI** instead of lamellar (nanosheet) **MFI**[213] bridging the boundary between zeolites and mesoporous molecular sieves. This shows that the surfactant SDA is not the only driving parameter determining the properties of the resulting material but the gel composition, alkalinity and other parameters are also important. Choi *et al.* demonstrated that concentration of Na^+ ions influences the stacking of the formed nanosheets (forming a material denoted as multilamellar (ordered stacking) or unilamellar (disordered stacking))[203] and studies on the synthesis gel composition were conducted by Machoke *et al.*[214] and Wei *et al.*[215]

The concept of surfactant templating was applied also to other zeolites but the results were not so straightforward. Nanosheet **MTW** was reported together with **MFI**[203] using a –CH_2–(*p*-phenylene)–CH_2– spacer in addition to *n*-C_6. The same mechanism as for **MFI** restricted crystal growth has been proposed (*cf.* TEM images in the supplementary information of ref. 203); however, further studies on this material have not yet been reported.

Interestingly, the surfactants with phenylene spacers among ammonium groups can also be used for disordered mesoporous molecular sieves with walls of zeolite beta[213] and similar materials with ***MRE** and **MTW** structures.[216,217] Based on the TEM images,[213] it appears that the crystal growth is restricted by the template in all 3 crystallographic directions in this case. Nevertheless, these materials (later denoted as nanosponge zeolites) have a hierarchical sponge-like structure composed of intergrown zeolite nanocrystals with an intercrystalline system of mesopores. In contrast to the above (***BEA**, ***MRE** and **MTW**), nanosponge **MFI** is obtained when the synthesis mixture for nanosheet **MFI** is seeded with bulk **MFI** crystals[218,219] or a polymer (polystyrene) randomly grafted with –CH_2–$N^+(-CH_3)_2$–C_6H_{12}–$N^+(-CH_3)_2$–C_6H_{12}–$N^+(-CH_3)_2$–C_6H_{13} groups is used.[220] The nanosponge **MFI** keeps the lamellar morphology according to the TEM images although it is a 3-dimensionally intergrown material and post-synthesis layer manipulations applicable to 2-dimensional materials have not been reported (and most probably are not possible).

A similar sponge-like morphology of intergrown lamellar **MFI** and **MEL** crystals was prepared also by Zhang *et al.*[208] (referred to as self-pillared pentasil zeolite (SPP); Fig. 6 left) and Chen *et al.*[221] Interestingly, these materials were obtained using tetrabutylphosphonium and tetrabutyl ammonium hydroxide SDAs[208] and no surfactant was used to support the formation of lamellar or hierarchical architecture.

The nanosheet **MFI**, the SPP, and nanosponge **MFI** zeolites typically exhibit increased BET area (510–610 $m^2\ g^{-1}$) in comparison with conventional **MFI** (300–400 $m^2\ g^{-1}$) and almost an order of magnitude increased external surface area (270, 420, 360 $m^2\ g^{-1}$ respectively *vs.* 20–60 $m^2\ g^{-1}$), which is a direct consequence of their lamellar character.[207] Similarly, their total adsorption capacity (total pore volume) increases depending on their layer arrangement as follows: nanosheet **MFI** 0.36–0.65 cm^3 < nanosponge **MFI** 0.56–0.62 cm^3 < SPP 0.73–1.0 cm^3 *vs.* conventional **MFI** 0.16–0.25 $cm^3\ g^{-1}$.[207,208,215,222] The improvement of transport properties of the above **MFI** catalysts was nicely documented in etherification of benzyl alcohol in the presence of di-*tert*-butylpyridine (DTBP) over SPP, pillared nanosheet **MFI** (*vide infra*) and several conventional **MFI** catalysts.[208] DTBP was used to deactivate external acid sites thus allowing observation of the transport phenomena *via* the etherification occurring exclusively in micropores. Observed data are in perfect agreement with the plot of effectiveness factor *vs.* Thiele modulus (Fig. 7) documenting that commonly observed improvements of apparent reaction rates in 2D catalysts truly account for suppressing the diffusion limitations.

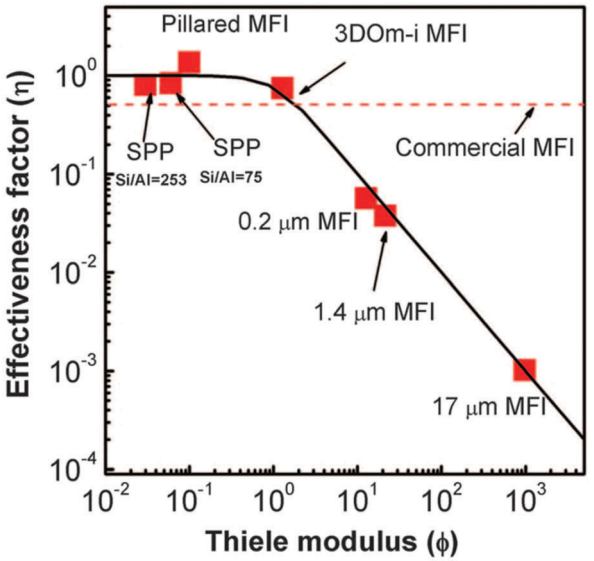

Fig. 7 Effectiveness factor *vs.* Thiele modulus plot and experimental data for etherification of benzyl alcohol over different **MFI** catalysts. Reprinted with permission from ref. 208.

Summarising the above discussed findings, it is clear that the surfactant templating is a useful and versatile tool for preparation of layered forms of zeolites, for which layered precursors have not yet been synthesized by hydrothermal synthesis; however, in some cases the nanocrystalline form rather than the layered one (nanosheet) can be obtained.

5.3. ADOR

Synthesis routes to 2D zeolites described *vide supra* discussed bottom-up approaches either with conventional or specially designed templates.[8,182] A top-down synthetic protocol is an opposite way, which is applicable for zeolites with anisotropic structures affording the possibility of chemically selective removal of some structural units. This is nicely documented for a series of germanosilicates, originally started with a **UTL** zeolite followed by **UOV** and SAZ-1.[31,223–225]

Introduction of Ge allowed synthesizing a number of new zeolites with large or extra-large pores. Simultaneously,

it resulted in the formation of relatively labile Ge–O bonds. Location of germanium in double-four-rings (d4r) is a characteristic feature of germanosilicate zeolites (sometimes even d3rs).[226,227] The d4r units form connecting pillars between individual layers (porous or non-porous depending on the zeolite structure) in the framework. It was observed that Ge–O bonds can be easily hydrolysed in aqueous solutions not depending on the pH.[31,228] This hydrolysis utilizes the chemical weakness of Ge–O bonds and leads to the removal of species from the destroyed d4r units leaving the rest of the zeolite structure (mostly siliceous zeolitic layers) unaffected. In the case of the **UTL** zeolite, a layered material called IPC-1P is formed.[100,229] Obtaining the layers of IPC-1P from the **UTL** zeolite opened new possibilities to manipulate with the layers in different ways. The most important is the use of IPC-1P and related layered zeolites prepared by the top-down approach for the preparation of new zeolites. Hydrolysis of the **UTL** zeolite results in the formation of 4 silanol groups at each layer instead of 4 connections to each original d4r. Thus, layers possess very high concentration of available silanol groups, which can be used either for condensation or for another interlayer chemistry.[230]

Roth *et al.* described the formation of IPC-1P layers from zeolite **UTL** when it was hydrolysed at ambient or increased temperatures.[100] Removal of the debris formed from d4r units from the interlayer space depends on the pH of the solution. While in diluted solutions practically all such species are removed to the aqueous phase, at higher concentrations these species remain partly in the interlayer space. As a result, calcination of layered materials formed under different pH leads to the different outcome. In the case of IPC-1P formed under diluted conditions, calcination provided a new zeolite **PCR** having the individual layers connected just by oxygen bridges (10–8-rings).[101] When part of original d4r remained in the interlayer space, calcination led to the **OKO** zeolite having single-4-rings (s4r) connecting layers.[231]

The mechanism leading to **PCR** or **OKO** zeolites has been named ADOR (A – assembly, D – disassembly, O – organization, R – reassembly), see Fig. 8.[31] This mechanism offers a variety of possible outcomes in particular due to the top-down preparation of layered precursors not available by direct synthesis. At present, zeolites **PCR**, **OKO**, IPC-6, and IPC-7 have been prepared by different condensation of IPC-1P layers. **OKO** has also been prepared using high pressure (about 1 GPa) at 200 °C, which means at a much lower temperature than that usually used for calcination (500–550 °C).[232] General applicability of the ADOR mechanism has been recently confirmed starting from the UOV zeolite and obtaining a new zeolite IPC-12[224] by substituting d4r units for s4r ones and recently from SAZ-1 creating IPC-15 and IPC-16.[225]

In addition, the individual IPC-1P layers can be connected with different organic or inorganic pillars making stable systems with larger layer distance. This achievement opens new possibilities in preparing porous hybrid materials being amenable to different post-synthesis modifications involving addition of functional groups with catalytic activity.[233]

Next and very interesting target for the ADOR mechanism was shifting of the individual layers prior to calcination,

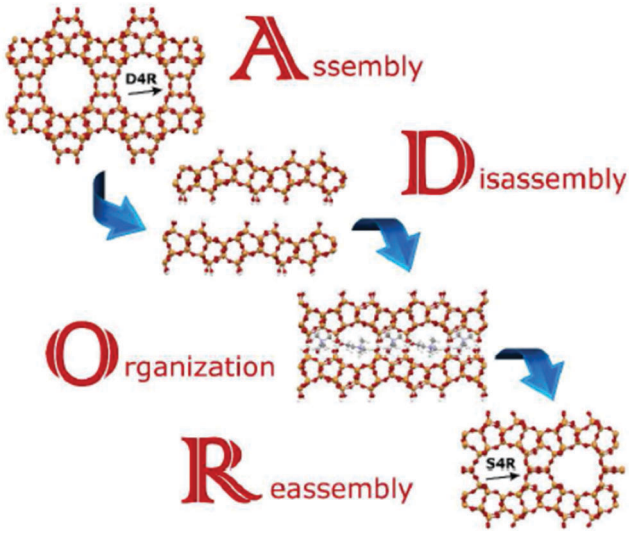

Fig. 8 Scheme of the ADOR process for transformation of the germanosilicate parent zeolites, Reproduced from ref. 232 with permission from the Royal Society of Chemistry, copyright 2017.

which could lead to new frameworks. In such a case, zeolites with odd number of channels and having relatively high energy on the energy/density plot proposed by Deem should be achieved.[32,234] Those zeolites were considered as "unfeasible". Mazur and coworkers succeeded in this by intercalation of choline chloride at a specific pH into the interlayer space, which induced shift of the layers.[228] The condensation resulted in a new zeolite IPC-9 having a 10–7-ring zeolite while addition of silica to the interlayer space followed by condensation produced zeolite IPC-10 (12–9-rings).[194] Structural features of novel zeolites are summarized in Table 1. These zeolites have not yet been synthesized by direct solvothermal synthesis.

To increase the stability of these zeolites the substitution of Ge for more stable Si was carried out. Tuel, Eliášová or Wu and their teams replaced substantial part of Ge with Si, which increased dramatically the stability of these zeolites. In addition, Si can also be replaced by Al introducing acid sites to the structure sites.[235] Opanasenko *et al.* evidenced for zeolites **ITH** and **IWW** that aluminium can be incorporated either directly into the synthesis mixture or *via* post-synthesis substitution

Table 1 List of zeolites prepared by the ADOR protocol

Parent zeolite	New zeolite	Channel structure
UTL	IPC-2 (**OKO**)	12 × 10
	IPC-4 (**PCR**)	10 × 8
	IPC-6	10 × 8 + 12 × 10
	IPC-7	12 × 10 + 14 × 12
	IPC-8	10 × 8 + 14 × 12
	IPC-9	10 × 7
	IPC-10	12 × 9
UOV	IPC-12	12–8 (1D)
CIT-13	IPC-13	12 × 8
SAZ-1	IPC-15	10
	IPC-16	12 × 8
IWR	IPC-17	12 × 8
IWW	IPC-18	12–8 × 8

of Ge with Al, thus introducing activity for acid-catalysed reactions.[236,237]

There is no doubt that the ADOR protocol represents a substantial breakthrough in the synthesis of new zeolites complementing the traditional synthesis approaches. Until now ADOR has been limited to germanosilicate zeolites, posing an important challenge for synthesis, namely how to extend ADOR applicability to zeolites without germanium.

5.4. Post-synthesis modifications

The great advantage of 2D zeolites lies in their structural flexibility and rich post-synthesis modification chemistry,[183] especially layer manipulations with increasing, decreasing or preserving the interlayer distance (Fig. 9). The present figure is based on the modifications of the **MWW** zeolite (a zeolite with hydrothermally synthesised lamellar precursor); however, it can be considered universal for all of the 2D zeolites. The variations for surfactant templated synthesis and ADOR mechanism are discussed below.

As shown in the scheme in Fig. 9, a 2D zeolite precursor consists of alternating crystalline siliceous layers and the SDA molecules in between the layers. In contrast to the 3D zeolites (where the structure is fully covalently bonded directly after the synthesis), there are no covalent bonds between the individual layers and the whole structure (crystalline layers and SDA molecules) is kept together only by interactions with SDA molecules and hydrogen bonds.[9]

In the case of ADOR transformation, the layered precursor is formed without the SDA (*e.g.* IPC-1(P)) but subsequent intercalation with an appropriate molecule (the organisation step in the ADOR mechanism) is the key to the layer manipulation and even lateral shift of the layers yielding "unfeasible" zeolites IPC-9 and IPC-10[31,100,101,228] (*vide supra*). The third approach – surfactant template synthesis yields a swollen 2D zeolite intrinsically.

The SDA molecules prevent full 3-dimensional covalent connection (during the hydrothermal synthesis) but keep the layers in regular orientation one to another (or intercalated molecules helps to orient the layers in the ADOR mechanism). Upon calcination, the SDA molecules are removed and subsequently a dehydration of two corresponding silanol groups occurs forming a covalent oxygen bridge connecting the discrete layers into a fully connected 3D framework (Fig. 9, "standard route").

In some cases, the SDA can be removed from the lamellar precursor not only by calcination, but also at low temperature (below 80 °C; Fig. 9 "detemplated"), under conditions when the silanol condensation into oxygen bridges does not occur. For instance, the template from MCM-22(P) can be removed by diluted HNO_3 solution (<2 M).[238] In the resulting material, called a MCM-56 analogue, the layers are randomly oriented one on another and the detemplated **MWW** material exhibits increased external surface area (150 *vs.* 117 $m^2\ g^{-1}$) and decreased micropore volume (0.13 *vs.* 0.17 $cm^3\ g^{-1}$) with respect to the 3D-**MWW**. Similarly, textural properties of IPC-1 (a partially disordered material formed by disassembly of **UTL**) exhibit lower micropore volume in comparison with corresponding reassembled **PCR** (0.095 $cm^3\ g^{-1}$ *vs.* 0.106 $cm^3\ g^{-1}$).[100,101] These collapsed materials were called sub-zeolites.[239]

Besides simple calcination, forming a fully connected 3D framework, also an additional bridging group (either additional silicon atom or *e.g.* organic bridge[240]) can be inserted in between the layers and connected to the silanol groups. As a result so-called interlayer expanded zeolites (IEZ) are obtained.[241] The process of interlayer expansion is sometimes referred to as stabilisation. The IEZ zeolites are characterised by larger interlayer pore openings in comparison with their parent structures. For instance IEZ-**MWW** has 12-ring pores and 2.7 nm basal *d*-spacing while conventional **MWW** has 10-ring pores and a basal *d*-spacing of 2.5 nm. Except for IPC-2 and IPC-10 materials,[101,228]

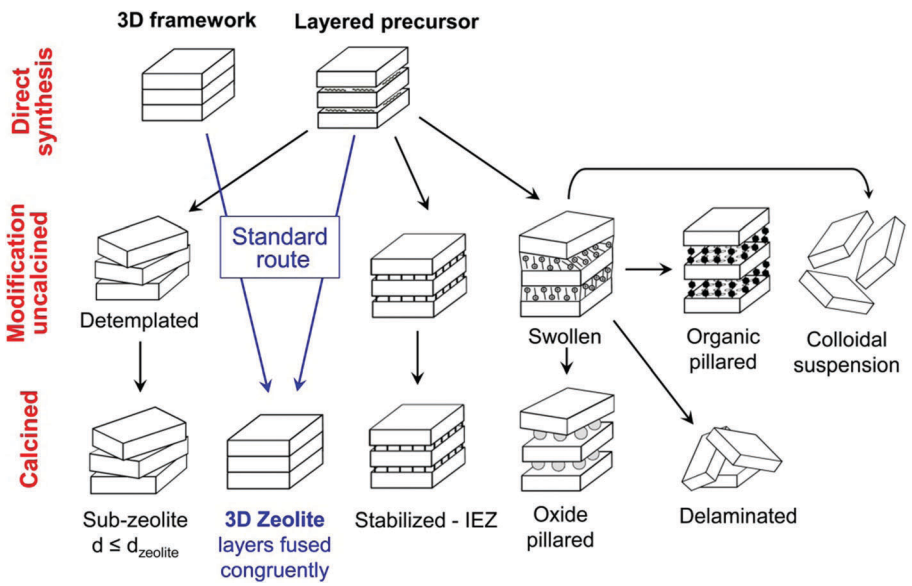

Fig. 9 Post-synthesis modifications of layered zeolites. Reprinted with permission from ref. 182.

the IEZs are not fully connected 3D-frameworks and free silanol groups are present on the bridging atoms.

A critical step in the 2D zeolite modification is breaking of the interlayer hydrogen bonds and expansion of the interlayer space. This process is called swelling (Fig. 9) and it is well described for lamellar materials such as clays, phyllosilicates and layered metal oxides.[242] In the case of 2D zeolites, the swelling was first performed using a concentrated (25 wt%) quaternary ammonium surfactant (*e.g.* cetyltrimethylammonium hydroxide) in a high pH medium.[191] The swollen material exhibits a highly increased interlamellar distance (*e.g.* **MWW**: *d*-spacing 5.2 nm *vs.* 2.6 nm in **MWW**(P)[243]). It should be noted that the materials prepared using a surfactant[203] are swollen intrinsically but in contrast the surfactant tail is not easily removed from interlayer space as it is part of the SDA.

The swelling is not a final step of the post-synthesis modification and once layers are separated, a number of other materials can be prepared. The layers are kept apart from each other by organic surfactants and when these are removed *e.g.* by calcination, the layers collapse. However, if an additional support, which can withstand calcination, is inserted, the interlayer distance can be preserved. It was found that the tetraethyl orthosilicate (TEOS) easily penetrates among the surfactant chains in the interlayer space, where it is converted into mesoporous amorphous silica pillars[242] (Fig. 6 middle). The first pillared zeolite material is **MWW** denoted as MCM-36.[191] Pillaring is nowadays one of the standard modifications of 2D zeolitic materials (as well as of *e.g.* clays[244]); however, the true structure of the pillars remains uncertain because of lack of regularity.[9] Besides pure TEOS, also its mixtures with other metal-alkoxides (*e.g.* titanium(IV) butoxide, tin(IV) iso-propoxide) can be used for pillaring, which results in the formation of additional catalytically active sites.[222,245,246]

Besides amorphous silica-based pillaring, also other groups, such as silsesquioxanes or organic linkers may be inserted.[233,240,247] The latter provide hybrid organic–inorganic materials with interesting adsorption properties. Recently, also covalent insertion of iron, titanium, tin, zinc and europium has been reported into RUB-36 (**CDO** lamellar precursor).[248] Besides that, metallic species, which are turned into metallic nanoparticles upon calcination, can be inserted using the advantage of enlarged space between the zeolite layers.[249,250]

A delaminated material is composed of randomly oriented lamellae (ultimately a house-of-cards morphology). A highly open structure is the main feature of this material and ideally the whole external surface of the lamellae is accessible from the interparticle space or wide mesopores. Corma *et al.* established this group of materials by ultrasonic treatment of swollen **MWW** layers, forming a material denoted as ITQ-2.[251] However, the **MWW** delamination procedure is not generally applicable and examples of other delaminated zeolites are sparse (only **NSI**, **FER**, **RWR** precursors).[9] Several attempts to delaminate nanosheet **MFI** using conditions similar to the ITQ-2 have been made; however, TEM analysis revealed that the product (although having BET area up to 800 $m^2\ g^{-1}$ and total adsorption capacity 1.50 $cm^3\ g^{-1}$) is only a physical mixture of parent nanosheet **MFI** and amorphous silica coming out from partial dissolution of the zeolite in the basic medium.[252]

Last but not least, the swollen material can be dispersed into a single lamellae colloidal solution.[253,254] The so-called exfoliation into single layers has been reported for zeolites **MWW**[255] and **MFI**.[256]

6. Catalytic investigations of 2D *vs.* 3D materials

6.1. Active sites in 2D zeolites

The main advantage of 2D zeolites in comparison with their 3D analogues lies in an improved accessibility of the active sites (resulting from their location on the external surface of the lamellae) while their other characteristics (such as geometry, coordination, strength of acidity *etc.*) are desired to remain the same as for conventional zeolites. Here we review ways of analysis and the literature data confirming or challenging the above statement.

In both 2D and 3D zeolites, active sites in zeolite-based catalysts are usually represented by isomorphously substituted silicon atoms for three- or four-valent elements and/or defects in the crystalline silica structure. To introduce catalytic activity to the structure of zeolites, appropriate heteroatoms (Al, Ti, Sn, Zr, Fe, Ga, Ge, B *etc.*) need to replace silicon atoms in the zeolite frameworks. Exceptionally, various atoms in extra-framework positions or vacancies (defects) as silanol groups (*e.g.* for Beckmann rearrangement) can also be catalytically active. In addition, the concentration of silanol groups defines other important properties such as hydrophilicity.[257]

All mentioned heteroatoms isomorphously incorporated into the framework represent acid sites of Brønsted or Lewis nature. Strong Brønsted acid sites (comparable to mineral acids) are formed by bridging [Si(OH)Al] sites and other trivalent metal ions can also form this type of sites. The other tetravalent (divalent Zn) heteroelements form mostly Lewis acid sites of a different strength. Extra-framework heteroatoms are in a number of cases considered undesirable but there are examples when they significantly contribute to the catalytic activity.[222,245,258]

6.1.1. Aluminum active sites. Aluminum atoms can be directly observed by solid state ^{27}Al-MAS-NMR. Tetrahedrally coordinated framework Al atoms exhibit a signal in the range 51.5–65 ppm (depending on the type of zeolite and Si/Al ratio) while octahedrally coordinated species (which may be extra-framework) exhibit a chemical shift of 0 ppm.[259,260] The shape of spectra and signal position are independent of the crystal size, shape and dimensionality of a particular zeolite.[261,262] In addition, a weak signal around 30 ppm is sometimes reported[218] and ascribed to penta-coordinated species.[263]

Brønsted acid sites can be observed directly using IR spectroscopy as the acidic [Si–(OH)–Al] group exhibits a vibration band clearly distinguishable from other silanol signals. Its precise position alternates with the zeolite structure (*e.g.* **FER**: ν(OH) = 3605 cm^{-1} *vs.* **FAU** ν(OH) = 3645 cm^{-1} (ref. 264)) and

it is also dependent on the zeolite dimensionality (*e.g.* **MWW** 3-dimensional MCM-22: ν(OH) = 3625 cm^{-1} (ref. 264) *vs.* 2-dimensional ITQ-2: ν(OH) = 3620 cm^{-1} (ref. 265)). Molecular modelling showed that the precise position of the band even reflects the crystallographic position of the corresponding aluminium atom;[264] however, distinguishing between several bands corresponding to different positions (which are close to each other) as well as their proper assignment is rarely possible. Laforge *et al.* distinguished acidic OH groups in supercages (ν(OH) = 3621 cm^{-1}) and in the sinusoidal channel (ν(OH) = 3608 cm^{-1}) of the **MWW** zeolite and provided a comparison of its 3-dimensional (MCM-22) and 2-dimensional (MCM-36) forms.[266] The signal belonging to Brønsted sites in supercages was about 7 times weaker for MCM-36 in comparison with MCM-22 reflecting that the supercages are not formed when the zeolite does not condense into a 3D connected structure. In contrast, Lewis sites cannot be observed directly.

To analyze the character (Lewis or Brønsted), location and (relative) strength of the (not only) aluminum acid sites, techniques using basic probe molecules need to be employed. In general there are three approaches for identification and quantification of the adsorbed probe molecules: (i) *in situ* IR analysis,[183,264–268] (ii) ^{31}P-NMR spectroscopy[261,269,270] and (iii) temperature programmed desorption (TPD) experiment.[271,272] The *in situ* IR analysis is a widespread method, used in combination with probe molecules including CO, amines, nitriles, pyridine and its derivatives and others, which exhibit bands characteristic for the corresponding species interacting with Brønsted or Lewis acid sites.[273] ^{31}P-NMR can be used for observation of trialkylphosphine oxides, which adsorb on the acid sites in a one-to-one manner. The TPD experiments give information about the strength of acid sites (the higher the desorption temperature, the stronger the site) but the adsorbed species are not observed directly.[274] The *in situ* IR and TPD techniques can also be combined into so called IRMS-TPD providing a deep understanding of the surface processes as well as quantitative information.[275,276]

The choice of the probe molecule determines the information possible to obtain similarly to Hammett indicators used to estimate acid strength in non-aqueous media (*i.e.* in homogeneous catalysis).[277,278] In fact, it was demonstrated that a carefully chosen set of Hammett indicators can be used to probe even zeolite acidity (namely large-pore zeolite Y); however, steric limitations restrict the application for porous materials.[279] For 2D materials, the enhanced accessibility of the acid sites is the key feature. Therefore, a combination of a small probe molecule, which can access all the acid sites, and a bulky analogue, which cannot enter the system of micropores, provides information about the sites located on the external surface of the crystals or lamellae. For instance, a commonly used pair of such molecules, in connection with IR spectroscopy, is pyridine (kinetic diameter 0.54 nm) together with lutidine (2,6-dimethylpyridine, 0.67), collidine (1,3,5-trimethylpyridine; 0.74 nm)[267] or 2,6-di-*tert*-butylpyridine (DTBpy, 1.05 nm). The pyridine molecule is small enough to enter medium-pore zeolites such as **MFI** or **MWW** while DTBpy in particular is too bulky to enter even the channel systems of extra-large zeolites and its nitrogen atom is strongly hindered so it can interact only with Brønsted acid sites (not Lewis).[265] All the (substituted) pyridines exhibit characteristic vibrations of the aromatic ring attached to different acid sites (and silanol groups) in the region 1400–1800 cm^{-1}, where they do not overlap with *e.g.* framework vibrations of the zeolite.

An accurate quantification of the acid sites requires reliable determination of the extinction coefficients (either for a single wavenumber or integrated molar extinction coefficient for the whole band), which is a complex problem reviewed *e.g.* in ref. 273.

Phosphine oxides are also bases and therefore they can be used similarly to substituted pyridines and other amines. Their size (determining their ability to enter the porous system of the catalyst) can by adjusted by choosing an appropriate length of the alkyl substituents. Trimethylphosphine oxide (TMPO) has a kinetic diameter of 0.55 nm and therefore it can enter even 10-ring pores. On the other hand, *e.g.* tributylphosphine (TBPO, kinetic diameter 0.82 nm) is suitable to assess external surface acidity. The acidic proton interacts with the oxygen atom of the phosphine oxide, resulting in a change in the electron density and thus chemical shift of the phosphorus atom. Hence, the phosphine oxide species can be observed and distinguished using solid state ^{31}P-NMR. Pure solid TMPO exhibits a chemical shift of 30 ppm, TMPO interacting with silanol has a chemical shift of 42 ppm and the signal of TMPO bound to Brønsted acid sites is observed between 66 and 86 ppm depending on the acid site strength.[261] The stronger the acid site, the higher the phosphorus chemical shift. Considerable drawbacks of this method are high demands on experimental equipment (glovebox, MAS-NMR spectrometer) in comparison with FT-IR techniques. In addition, quantification of Lewis sites is complicated and uncertain because the corresponding TMPO signal (37 ppm)[269,270] is very close to the signal of TMPO interacting with silanol (42 ppm), which can be very intensive especially in layered or hierarchical zeolites.

6.1.2. Titanium active sites. Since the disclosure of titanium silicalite 1 (TS-1) by the Eni researchers in 1983,[280] the titanosilicate zeolites have become well established selective oxidation catalysts. They are able to activate hydrogen peroxide in the presence of water. Nature of their active sites has been reviewed in detail in ref. 281.

In titanosilicate zeolites, the titanium atoms can basically adopt 3 different states. Generally, the desired species is an isolated titanium atom (not connected to another titanium atom *via* an oxygen bridge) with tetrahedral coordination, isomorphously incorporated into the framework. Titanium can also be present as isolated 5- or 6-coordinated species in the extra-framework position or it can form clusters of more titanium atoms connected directly with oxygen bridges (referred to as anatase or anatase-like phase). Catalytic activity of isolated extra-framework titanium atoms is a subject of debates. Previously, they were considered inactive; recently multiple pieces of evidence have been found proving their catalytic activity.[222,282–284] On the other hand, the anatase phase is inactive in selective oxidation but it has its irreplaceable role in photocatalysis.

The titanium species can be qualitatively distinguished using UV/Vis spectroscopy in diffuse-reflectance mode (DR-UV/Vis). Tetrahedrally coordinated titanium atoms exhibit absorption centred at about 205–210 nm (corresponding to ligand-to-metal charge transfer from oxygen to titanium atom), 6-coordinated titanium species absorbs in the range 260–290 nm and anatase phase exhibits a band centred at 330 nm. In fact, the position of the absorption band red-shifts with increasing coordination number and a change of the geometry from tetrahedral to octahedral.[281] The isomorphous incorporation of titanium is evidenced by an IR vibration band at 960 cm^{-1}. The true origin of this band was a subject of debates but the most reliable assignment appears to be to antisymmetric stretching mode of a TiO_4 unit.[285]

Isolated titanium atoms act as weak Lewis acids, which are able to coordinate molecules such as H_2O, NH_3, H_2O_2 and organic peroxides. In particular, in the case of peroxides, Ti withdraws electrons from adsorbed species making the O–O bond more susceptible towards a nucleophilic attack *e.g.* of an alkene, which can be then oxidized to the corresponding epoxide.

It is very important to note that the initial step, a titanosilicate catalysed reaction, is the weakening or even hydrolysis of one of the Ti–O–Si bridges, forming a $Ti(OSi)_3(OH)$ defective species (which is then able to extend its coordination).[286] This is proof for the catalytic activity of extra-framework isolated titanium species, which are, most probably, attached to the framework by 2 or 3 oxygen bridges (especially in the case of post-synthesis titanium incorporation).[222,245,258,287] Note however, that leaching of titanium from a titanosilicate zeolite is rarely observed.

6.1.3. Tin active sites. Tin-silicate zeolites are somewhat similar to titanosilicate zeolites but they recieved less attention. The first synthesis of aluminum free Sn-zeolite (Beta) dates back to 1999.[288] Nevertheless, they are interesting solid catalysts showing high activity in Baeyer–Villiger oxidation,[289,290] Meervein–Pondorf–Verley reduction[291] or glucose isomerisation.[292–294] The nature of Sn active sites has been investigated mostly for Sn-beta[289,290] but it apparently fits well also to 2D Sn-silicates.[246,293,295,296]

Just as with titanium, tin can be isomorphously incorporated into the zeolite framework or it can be present in the extra-framework positions or to form the bulk SnO_2 phase. Isomorphously incorporated tin atoms are the desired active sites. The tin species can be observed and to some extent distinguished using DR-UV/Vis spectroscopy. Similarly to titanium, 4-coordinated (framework) tin atoms exhibit an absorption band centred at 205 nm and bulk SnO_2 absorbs at 280 nm.[294,297–299] In contrast to titanium, a Sn active site can be easily hydrated extending its coordination number to 5 or 6 resulting in a red-shift of the absorption band to 220 nm resp. 255 nm. This may cause some confusion, because extra-framework Sn species (or small SnO_2 domains) also absorb in this wavelength range (around 240 nm). The band shifts accompanying dehydration/rehydration can be easily observed and therefere can be used to distinguish qualitatively the framework Sn sites from SnO_2 domains.[294]

The framework Sn site has a Lewis acid character and can be investigated by probes *e.g.* by adsorbed CD_3CN, which exhibits a characteristic vibration band at 2311 cm^{-1}. Physisorbed CD_3CN is observed at 2273 cm^{-1}.[293] Boronat *et al.*[300] and later in more detail Harris *et al.*[294] showed that in fact, two distinct bands of CD_3CN on Sn sites can be observed around 2311 cm^{-1} characterising two different types of sites. One of them (2308 cm^{-1}) characterises adsorption on a closed site (Sn atom is bound by four oxygen bridges) while the other (2316 cm^{-1}) characterises an open site, where two hydroxyl groups (one on Sn, one on neighbour Si) are present instead of one of the oxygen bridges. The latter sites are considered more active in sugar isomerisation.[294] Note the similarity to opening of the titanium site (*vide supra*). However, in most publications these two bands are not distinguised. In some reports, a vibration band at about 970 cm^{-1} (ref. 297 and 301) is reported. A similar band is observed for titanosilicates (being considered as proof of titanium isomorphous incorporation)[285] and vanadium silicates;[302] however, for tin silicates its origin, as well as whether it proves Sn incorporation, is unclear.

An important feature of Sn-silicates, and, in fact, the origin of their unique catalytic activity, is their ability to bind and activate a carbonyl group. This is evidenced *e.g.* by a shift of the cyclohexanone ν(C=O) vibration band (48 cm^{-1} for Sn-Beta) towards lower wavenumbers.[289,290,303]

Sn active sites can also be studied using ^{119}Sn-MAS-NMR spectroscopy. The SnO_2 phase exhibits a sharp signal at −604 ppm.[291,295,298,301] In contrast, 4-coordinated Sn sites are observed at −420 to −450 ppm in dehydrated samples. The signal of 4-coordinated Sn disappears upon hydration and a new signal appears in the range −690 to −740 ppm (characteristic of the hydrated 5- or 6-coordinated Sn).[290,293,295,301] This observation is in accordance with the DR-UV/Vis observations (*vide supra*). It was mentioned above that there exist two types of framework Sn-sites (open and close) and these have been distinguished, besides IR analysis of adsorbed CD_3CN, also in the ^{119}Sn-MAS-NMR spectra: open site −423 ppm; closed site −443 ppm.[304]

6.2. Industrial processes

Zeolites dominate the world catalyst global market due to their enormous use in oil refining and petrochemistry with increasing applications in fine chemical synthesis and environmental catalysis. Fluid catalytic cracking (FCC) and hydrocracking are the most important processes using zeolites, in particular USY (ultra stable zeolite Y, **FAU** topology). FCC catalysts have been developed using hierarchical USY zeolites, stabilized by ion exchange with Rare Earth elements, showing improved hydrothermal stability, increased bottom conversion capacity and better product selectivity in comparison with a conventional commercial USY based catalyst.[305] Additions of **MFI** zeolites are important to increase the ''sharpness'' of the catalyst to produce more propylene. Regardless of the knowledge gained on cracking of oil-based feedstocks, catalytic cracking of other bulky feedstocks remains widely investigated particularly over hierarchical zeolites.[233] Thus, it has been applied to many

diverse raw materials such as vacuum gas–oil,[306] vegetable oils[307] and polyolefins, as main components of plastic wastes.[308]

Zeolites were firstly used in large-scale applications in the 1960s for cracking, which was followed by the breakthrough discovery of high-silica zeolites including the most important ZSM-5 (**MFI** topology). This enabled relating the catalytic behaviour of different structural types of zeolites to different topologies and understanding in detail the structure–activity–selectivity relationship. At present there are about 130 industrial processes using zeolite catalysts from about 850 of total processes.[309] The combination of acid functionalities, uniform micropores providing shape selectivity and easy regeneration allowed zeolites to revolutionise the chemical industry through replacement of hazardous catalysts like H_2SO_4, HF, and $AlCl_3$ in the early 1960s. Table 2 provides a list of the most important processes over zeolites indicating the type of zeolite catalyst employed in each process. An in-depth discussion of industrial applications of zeolites is outside the scope of this review, but for an excellent survey the readers are referred to the chapter by Abdo and Wilson.[310]

It should be noted that further expansion of zeolites as industrial catalysts has been connected with successful isomorphous substitution of Si for Ti by Eni researchers.[280] They succeeded in synthesising a TS-1 zeolite (**MFI** morphology) without the presence of aluminium. The lowest Si/Ti molar ratio is close to 30 and this zeolite is currently used in large scale applications for phenol hydroxylation.[312] In addition to titanium, a Sn-containing zeolite (Sn-Beta, **BEA**) is also currently used for Baeyer–Villiger oxidation of some cyclic ketones to lactones using hydrogen peroxide as the oxidation agent. Last but not least, SAPO-34 (**CHA**) with an 8-ring channel system is used for the methanol-to-olefin (MTO) reaction, providing substantially higher selectivities to ethylene and particularly propylene when compared with **MFI** zeolites.

6.2.1. Hierarchical zeolites in industrially relevant processes. As in the case of cracking (*vide supra*), a remarkable enhancement of the catalytic activity over hierarchical zeolites is observed in most reactions when compared with conventional zeolite samples. This is due to the improvement of the accessibility and mass transport in hierarchical zeolites thanks to their secondary porosity. However, the picture is not so clear in terms of selectivity. In principle, the mesopore surface of hierarchical zeolites lacks the shape selectivity, which is characteristic of the micropores. Accordingly, a decrease in the selectivity towards the target products could be expected for hierarchical zeolites. However, the overall selectivity observed in a specific reaction may depend on other factors. In this way, the changes induced in the acidic features of hierarchical zeolites may also influence the product selectivity and not necessarily in a negative way. Usually, selectivity to primary products can increase over mesoporous zeolites due to a decrease in the contact time.

Hierarchical zeolites have been investigated in the following industrially relevant reactions:

• Aromatization of light alkanes and alcohols to produce aromatic hydrocarbons with applications in the formulation of fuels or as raw chemicals. Aromatization of hexane and propane has been investigated over Pt promoted mesoporous gallium-containing ZSM-11 zeolites, improved conversion and selectivity being obtained owing to the enhanced accessibility to the active extra-framework Ga species due to the presence of mesopores.[313] ZnO-containing ZSM-5 zeolite catalysts with bimodal and trimodal hierarchical pore structures have been studied for the conversion of methanol to aromatics.[173] The authors propose that the presence of highly dispersed ZnO clusters enhances the selectivity towards aromatics by catalysing the dehydrogenation pathway, whereas the hierarchical pore structure facilitates the transfer of reaction intermediates and thus accelerates the formation of aromatics.

• Isomerization and rearrangement reactions of different substrates, such as xylenes, epoxides and oximes.[314–316] Hierarchical Beta zeolites have been investigated as catalysts for epoxide rearrangement reactions, being compared with hybrid zeolitic-mesoporous materials. When tested in the liquid phase rearrangement of cyclic, branched, and linear epoxides, hierarchical Beta zeolites exhibited the best combination of catalytic activity and selectivity due to enhanced accessibility and appropriate balance of Brønsted and Lewis acid sites.[315] Likewise, hierarchical Beta zeolites with different Si/Al molar ratios showed significant improvements in the catalytic behaviour in liquid-phase Beckmann rearrangement of cyclohexanone and cyclododecanone oximes compared to conventional Beta

Table 2 Commercial zeolite catalytic processes and types of catalysts; based on ref. 311

Structural type	Catalytic process
FAU (zeolite Y)	Catalytic cracking, hydrocracking, NO_x reduction, acylations
MOR (mordenite)	Alkane hydroisomerisations, hydrocracking, dewaxing, aromatic alkylations, olefin oligomerisation
MFI (ZSM-5, TS-1)	MTO, MTG, olefin cracking, olefin oligomerisation, aromatic alkylations, isomerisations, disproportionations, aromatisation, NO_x reduction, selective oxidations, hydration, amination, Beckmann rearrangement, cyclodimerisation
***BEA** (Beta)	Benzene alkylations, aliphatic alkylations, acetylation, Baeyer–Villiger reaction, etherification
LTL (zeolite L)	Alkane aromatisation
MWW (MCM-22)	Benzene alkylations
CHA (SAPO-34[a])	MTO
AEL (SAPO-11)	Long-chain alkane hydroisomerisation, Beckmann rearrangement
ERI (Erionite)	Selectoforming
RHO (Rho)	Amination
TON (Theta-1)	Long-chain alkane hydroisomerisation

[a] Zeotype – silicoaluminophosphate.

samples due to a number of factors: faster intracrystalline diffusion, availability of non-sterically hindered mesopore/surface area and lower deactivation through product inhibition.[316]

• Incorporation of noble metals into hierarchical zeolites has allowed preparing catalysts for hydrotreating processes, such as alkane hydroisomerization and hydrogenation of aromatic compounds. Hydroisomerization and hydrocracking of *n*-decane, *n*-nonadecane and pristane (2,6,10,14-tetramethylpentadecane) over a hierarchical Pt/ZSM-22 zeolite noted the contributions of both the acid sites located in the pore mouths and within the micropores to the skeletal rearrangement and cracking reactions.[317] Pd supported on a hierarchical Beta zeolite evaluated in both absence and presence of 4,6-dimethyldibenzothiophene showed a better sulphur tolerance than a Pd/Al-MCM-41 catalyst in hydrogenation of naphthalene and pyrene.[318] Likewise, hierarchical Ni/Beta zeolites have been studied in the hydroreforming of the oil obtained from the thermal cracking of low-density polyethylene, showing to be an adequate catalyst for obtaining gasoline and diesel fractions that could be employed in the formulation of transportation fuels.[169]

• Transesterification reactions of fatty feedstock. Transesterification of fatty acids to produce bio-diesel is traditionally a domain of homogeneous base or acid catalysts (KOH, NaOH, H_2SO_4);[319] however, heterogeneous catalysts are also a subject of investigation due to their obvious advantages. Among these, hierarchical Beta zeolites exhibited a remarkable activity in biodiesel production using microalgae lipids as feedstock. Hierarchical character of the catalyst is essential in this case.[320] Likewise, hierarchical zeolite Beta has exhibited significant activity in the transesterification of triolein to afford methyl oleate.[321]

• Hydrodesulfurization of oil fractions has also been studied over hierarchical zeolites. Thus, zeolite L containing mesopores[322] has been incorporated as a component of a catalyst for gasoline hydrodesulfurization, showing excellent performances in terms of desulfurization, aromatization, isomerization and preservation of the RON value compared with the catalyst into which ordinary microporous zeolite L was introduced.[323] CoMo catalysts supported on ZSM-5 zeolite–alumina composites have been tested in the hydrodesulfurization of 4,6-dimethyldibenzothiophene.[324]

• Finally, an emerging and relevant field of application of hierarchical zeolites is their use in catalytic treatments for the removal of pollutants in gaseous and liquid streams. Hierarchical Cu/H-ZSM-5 zeolite-based systems, with improved Cu dispersion, have been employed with remarkable performance as a catalytic trap for the retention of propene and toluene, enabling their further conversion to carbon dioxide and water instead of being emitted in the exhaust.[171] Cu-Modified ZSM-5 and ZSM-11 type zeolite catalysts, both containing mesopores, have been used as catalysts for direct NO decomposition, concluding that the presence of mesoporosity leads to a significant improvement of the catalytic activity regarding conventional zeolites.[325] Fe-Containing ZSM-5 and ZSM-12 catalysts, possessing mesoporosity, have been tested in the selective catalytic reduction (SCR) of NO_x with NH_3, exhibiting a significantly higher activity than conventional samples.[326] This difference has been assigned to both faster diffusion of reactants and products in the mesopores and better dispersion of the iron particles. Pd-Containing hierarchical ZSM-5 zeolites have been explored in hydrodechlorination of trichloroethylene in the aqueous phase, showing enhanced catalytic performance compared to the use of a pure microporous zeolite sample.[327] Hierarchical ZSM-5 zeolites, containing iron, have been tested in H_2O_2 decomposition reactions in the absence and presence of an iron-complexing agent, as well as in oxidation of low and high molecular weight organic compounds by H_2O_2, noting that the presence of secondary porosity in the zeolite resulted in a significant improvement of the catalyst properties.[328]

6.3. Biomass transformations

The versatility of the catalytic properties of zeolites has allowed their expansion to new applications demanded by worldwide socioeconomic progress. This is the case of the search for new and sustainable routes to deliver for the needs of humanity driven by the climate change. Among these routes, there are all those processes based on the use of biomass as a raw material, such as the production of bio-based chemicals and biofuels within the ''biorefinery'' concept.[329]

Biomass is defined as any kind of organic material of either animal or plant origin.[330] Its renewable character, abundance and worldwide distribution have prompted its use as an energy source. This encouraging scenario is even more attractive when the biomass feedstocks comprise any material not competing with the food sector, such as forestry and agricultural residues.

The routes to convert biomass into both bio-based chemicals and biofuels can be grouped in terms of the chemical nature of the biomass feedstock (sugars, lipids or lignocelluloses). Some general aspects regarding the most relevant conversion routes are outlined here:

Sugars or starch as feedstocks are used to produce biofuels, in particular bio-ethanol. The process comprises saccharification or hydrolysis into simple sugars and fermentation. Recently, the use of sugars has been expanded to produce platform molecules by catalytic routes, such as isomerization (*e.g.* from glucose to fructose), dehydration (*e.g.* production of 5-(hydroxymethyl)furfural (5-HMF), furfural and levulinic acid) and hydrogenation (*e.g.* conversion of glucose and xylose into sorbitol and xylitol, respectively).

Lipids or oleaginous materials can be transformed into biodiesel by the transesterification reaction with alcohols. Together with bioethanol they are currently commercially available as biofuels and blended with conventional fossil-derived fuels in the transportation sector. Both of them represent the so-called ''first generation biofuels'' as they are produced from raw materials competing with the food industry. However, lipidic feedstocks may be achieved from non-edible plants, called energy crops, solving the sustainability concerns associated with the first generation biofuels. In addition, alternative technologies have been proposed, such as hydroprocessing and catalytic cracking, to yield hydrocarbons with similar properties to those of conventional fossil-fuels.

Lignocellulose, according to its more complex composition, has been evaluated as feedstock for different thermochemical and biochemical routes to obtain biofuels or bio-based chemicals. Syngas is the main product of gasification for Fischer–Tropsch synthesis. Sugars can be extracted from lignocellulose by means of hydrolysis. Such sugars are further processed into bioethanol (*via* fermentation) or into chemicals and/or biofuels by other catalytic processes. Residual lignin from the hydrolysis treatment can be pyrolyzed or gasified. Finally, pyrolysis of lignocellulose yields bio-oils which, after catalytic upgrading, may produce valuable chemicals and biofuels. This catalytic upgrading can be classified into two main groups: (a) hydroprocessing of the liquid bio-oil (hydrodeoxygenation; HDO) and (b) bringing the pyrolysis vapours into contact with a catalyst (catalytic pyrolysis) promoting dehydration and decarboxylation as preferred deoxygenation routes.

A detailed discussion of each technology is outside the scope of this review and it can be found in the literature.[331–334] All these processes incorporate one or several catalytic steps. Zeolites may be especially relevant catalysts because of their acidic and porous properties.[335–337] The main reactions over zeolites are summarized in Fig. 10. However, their application in the field of biomass transformation is quite challenging as they face several difficulties intrinsic to the features of the raw material: (a) complex composition, with bulky compounds and multiple functionalities; (b) presence of heteroatoms affecting the quality of the final product (*e.g.* oxygen in biofuels), interfering the catalytic processes (*e.g.* Na^+, K^+) or poisoning the catalyst (*e.g.* sulphur); (c) high water content, which may deteriorate the catalyst structure and activity, and (d) strong trend to form carbon deposits (coke) over the catalysts, causing their deactivation.

This section focuses on the role of zeolite properties in the performance of the most relevant biomass transformation processes and, in particular, on the impact of moving from 3D to 2D topologies in terms of their activity, selectivity and stability to deactivation.

6.3.1. Selected biomass conversion reactions. Many biomass transformations shown in Fig. 10 are promoted by acid catalysts. Nevertheless, some undesirable reactions, such as excessive cracking and coke formation, are also acid-catalysed and may dramatically affect the reaction viability. Both density and strength of catalyst acid sites must be controlled carefully, depending on the feedstock and reaction conditions. Porous properties, as they determine the accessibility of acid sites and the existence of shape selectivity effects, are also key properties.[338]

6.3.1.1. Catalytic pyrolysis of solid biomass. Zeolites exhibited excellent performance in catalytic pyrolysis of solid biomass, demonstrating their ability to increase the production of aromatics and, therefore, yielding final oils with lower oxygen content and higher quality as biofuels.[332,333,338–343] Acid sites promote the dehydration of levoglucosan into furans, and their further conversion into aromatics by Diels–Alder reactions with light olefins. Brønsted acid sites are particularly active because of their higher acid strength. Li *et al.*[344] tested zeolites with different acidity in the pyrolysis (500 °C) and subsequent catalytic upgrading (550 °C) of corncob hydrolysis residue using an Auger-type reactor coupled to a downstream fixed-bed reactor. Specifically, **FAU** and **MFI** zeolites were used as catalysts. In the case of the **FAU** zeolite, the strength of acid sites is rather low, whereas **MFI** presents both mild and strong acid sites. Accordingly, **USY** zeolites exhibited very low activity yielding oxygenate amounts (50%) very close to the non-catalytic bio-oil (51.3 area%). In contrast, ZSM-5 was able to catalyse the bio-oil transformation reducing the amount of oxygenated compounds below 10 area% and increasing the content of phenols and aromatics (above 80%).

Increasing the density of zeolite Brønsted sites is an effective route to upgrade pyrolysis-oils *via* deoxygenation and aromatization.[333] The concentration of Brønsted acid sites in **MFI** zeolites from 17 to 212 has been explored.[345–347] However, together with a higher yield of aromatics, the acidity of **MFI**

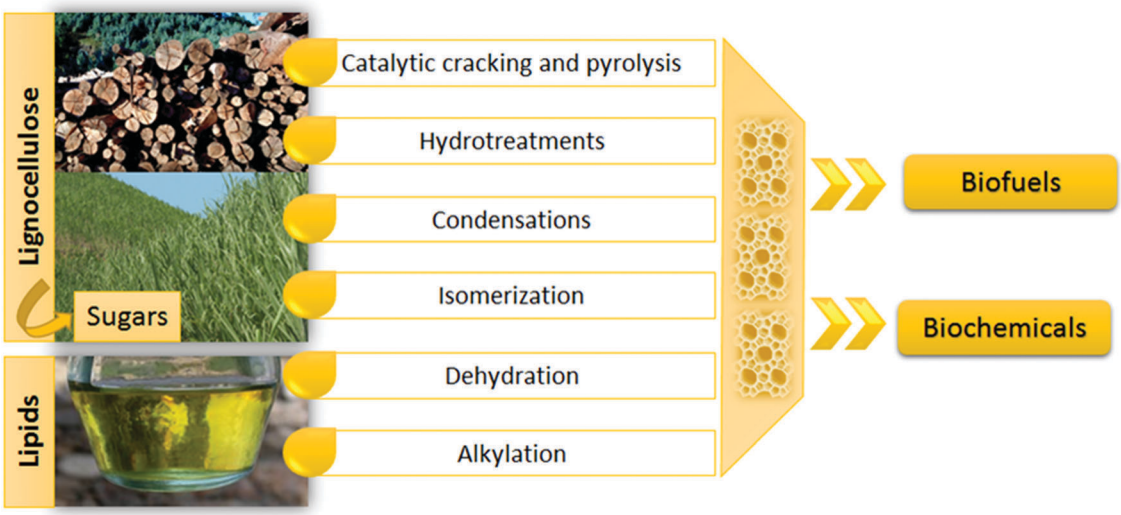

Fig. 10 Main catalytic routes of biomass conversion involving zeolites.

at low Si/Al ratios has been found to be detrimental leading to the formation of gases and coke.

Alternatively, cation-exchange and impregnation with metals or metal oxides have been explored to modulate the acidity of zeolites to slow down the coke formation while keeping or even maximizing the deoxygenation and aromatization activity.[329] The most successful results have been attained when metallic species, exchanged or impregnated on the zeolite, possess some intrinsic catalytic activity for any deoxygenating reactions. For instance, when Ga, Ni or Zn are either cation exchanged[348] or impregnated[338,349] in **MFI**, the selectivity to aromatics in the upgraded bio-oil is increased. Similar effects have been found with Pt dispersed on **MFI** in the catalytic pyrolysis of Miscanthus to promote cracking, hydrogenolysis, hydrocracking, and dehydrogenation reactions.[350] It has been reported that impregnation of **MFI** with NiO–MgO also leads to a higher selectivity to alkylbenzenes and less coke formation.[351] In particular, the authors found that using **MFI** (Si/Al ratio = 50) having 6% Ni + 2% Mg, the upgraded bio-oil contained the highest amount of hydrocarbon compounds, with a yield of 35.52 chromatogram area% (12.94% for aliphatic hydrocarbons and 22.58% aromatic hydrocarbons), *versus* 10.22% in the case of the non-catalytic run. Moreover, coke formation was half (1.65 wt%) of the value attained with the parent zeolite (3.75 wt%). Nevertheless, there is an optimum amount of metallic or metal oxide species to be incorporated into zeolites as excessive loadings may lead to a dramatic loss of acidity, especially Brønsted acid sites, also necessary to drive the formation of aromatics *via* cyclization and oligomerization of light components.[352,353]

In addition to acidity, porosity is also a key feature of zeolites in terms of activity, selectivity and deactivation resistance by coke deposition in catalytic pyrolysis.[332,333,338] It is quite difficult to correlate its direct impact on the product yield and distribution as changes in porosity are usually accompanied by variations in acidity (strength and accessibility). However, there is consistent evidence that zeolites with too small micropores (*e.g.* SAPO-34, with 6 and 8-rings) are hardly active in upgrading pyrolysis vapours, which are mostly composed of bulky molecules that cannot access the internal zeolite space.[354] On the other hand, zeolites with large mesopore volumes[39] or relatively large micropores (*e.g.* ***BEA** and **FAU**, having 12-membered rings)[355,356] are prone to generate more coke as polymerization of large molecules is less restricted. The combination of acidic properties and a micropore size of 10-rings makes ZSM-5 one of the most promising zeolites for catalytic pyrolysis.

6.3.1.2. Hierarchical zeolites in catalytic pyrolysis. Pyrolysis vapours contain many large molecules, including phenolic oligomers coming from lignin decomposition, whose dimensions are too large to enter into any zeolite micropores. For that reason, zeolites with larger external surface areas and hierarchical structures have also been recently explored. Typically, good results have been obtained over hierarchical ZSM-5 due to a strong aromatization activity of this zeolite, which leads to the production of a highly deoxygenated bio-oil.[357–359] In the case of hierarchical ZSM-5 prepared by desilication,[359] it has been proposed that the mesopores can be seen as "highways" where big molecules (such as levoglucosan) can diffuse to the micropore mouths, where the Brønsted acid sites present are active for their conversion into small fragments. Moreover, mesopores also promote the transport of reaction products, thus enhancing the selectivity of mono-aromatic hydrocarbons.

It seems that the key is a right balance between high mesopore accessibility and external acid density. By this way, conversion of bulky char precursors and oxygenates could be promoted on the external surface, hindering their polymerization to coke within the micropores, and increasing the aromatic yields. This was evidenced by Gamliel *et al.*,[358] when comparing different synthetic routes to introduce mesoporosity in **MFI** zeolites: (a) desilication with organic hydroxides; (b) desilication with NaOH at different concentrations (mild and strong desilication) and (c) surfactant-assisted desilication. The best performance was achieved with mildly-desilicated zeolite as it was able to increase the production of monoaromatics from 11.3% (measured as carbon yield) for the parent zeolite to 19%. However, a harsher desilication, despite generating a larger mesopore volume, reduced the monoaromatics to 15.9% and increased the coke yield (from 43.4 to 46.5%, measured as coke + char).

Hydrodeoxygenation of bio-oils (from biomass pyrolysis) and fatty compounds has also been investigated using hierarchical zeolites as supports of different active phases. Thus, hydrodeoxygenation of bio-oil model compounds has been probed using catalysts based on Pt and Ni_2P, respectively, supported on hierarchical ZSM-5 zeolites.[176,360] Likewise, Ni supported on hierarchical USY zeolites has exhibited a high efficiency in the hydrodeoxygenation of fatty acids, esters, and palm oil.[361]

6.3.1.3. 2D vs. 3D zeolites in catalytic pyrolysis. Very recently, MCM-22 zeolite samples (**MWW** framework) with different Si/Al ratios have been studied in the catalytic pyrolysis of acid-washed wheat straw at 400–450 °C.[362] The materials were characterized by a significant contribution of external surface area (160–190 $m^2\ g^{-1}$) and a higher concentration of Brønsted acid sites than Lewis ones. In terms of overall deoxygenation degree and aromatics production, both zeolites exhibited similar behaviour being worse than the **MFI** reference catalyst. In addition, a higher amount of coke was deposited over the **MWW** zeolites. This coke was lighter and presented significant oxygen content, denoting that its formation was mostly mediated by oxygenated compounds.

2D zeolites have been applied in catalytic pyrolysis of solid biomass to take advantage of their higher external surface areas and pore dimensions, diminishing the effect of diffusion, for converting bulky compounds in primary pyrolysis vapours. Lee *et al.*[363] employed unilamellar mesoporous **MFI** nanosheets (UMNs) to upgrade the pyrolysis vapours generated from the individual fractions of lignocellulose: cellulose, hemicellulose and lignin. For comparison purposes, the same reactions were carried out without a catalyst (thermal pyrolysis) using Al-SBA-15 as the representative of an acid mesoporous catalyst. The UMN catalyst

was composed of randomly assembled zeolite nanosheets with a thickness of 2.5 nm (see Section 5.2), BET area of 600 m^2 g^{-1} and a mean mesopore size of 6.3 nm. BET area and mean pore size of the Al-SBA-15 sample was 500 m^2 g^{-1} and 7.8 nm, respectively. Regarding acidity, unilamellar **MFI** exhibited both weak and strong acid sites whereas the ordered mesoporous Al-SBA-15 contained only weak acid sites. Due to the superior acidity, the UMN catalyst exhibited higher activity for cracking and deoxygenation and it produced a bio-oil with lower oxygen content and with a better overall quality. While monoaromatics were hardly detected in bio-oils from thermal pyrolysis of each lignocellulose fraction, their production was promoted using the catalysts. This effect was especially important over the zeolite which almost tripled the monoaromatics selectivity compared to the Al-SBA-15 catalyst (*e.g.* 16% of total distribution of compounds *vs.* around 5%, respectively, in catalytic pyrolysis of lignin).

MCM-22 and its delaminated derivative, ITQ-2, have been tested in the catalytic pyrolysis of rice husk by Naqvi *et al.*[364–367] at 450 °C in a lab scale fixed-bed pyrolyzer and compared to conventional zeolites with different micropore sizes (8, 10 and 12-rings). Despite scarce information that is given regarding the formation of coke, some conclusions were provided. As expected, small pore zeolites (8-rings: SAPO-34) did not produce aromatics and exhibited the lowest deoxygenation capacity. Large pore size zeolites (12-rings: **MOR**) exhibited high solid yields (char + coke) and low aromatics production. Medium pore sizes with 10 membered rings, and specially ZSM-5 and ITQ-2, resulted in the best performance with similar results. The combination of medium pore size and high acid strength of ZSM-5 was considered to be mainly responsible for achieving the highest deoxygenation degree and increased aromatics production when compared with thermal pyrolysis. In the case of ITQ-2, its higher external surface area than the parent MCM-22 (442 m^2 g^{-1} *vs.* 100 m^2 g^{-1} of MCM-22) effectively reduced the steric hindrance allowing a higher conversion of sugar compounds, which resulted in higher aromatics production and the second position in the deoxygenation capacity.

Lamellar and pillared **MFI** zeolites, and their modifications by MgO or ZnO impregnation, have also been studied for the catalytic pyrolysis of eucalyptus woodchips in a lab-scale fixed-bed reactor operating at 500 °C.[368] The use of zeolites promoted decarboxylation and decarbonylation as deoxygenation routes for pyrolysis vapours. The parent layered ZSM-5 and pillared ZSM-5 produced the monocyclic aromatic hydrocarbons most effectively. Their share in the total bio-oil increased from 1.4 (thermal pyrolysis) to 11.9 and 7.5%, respectively. The modification with both metal oxides remarkably reduced the porosity and acidity of the zeolitic supports. As a result, the formation of aromatic hydrocarbons was reduced in favour of oxygenated aromatics (3,4,5-trimethoxytoluene, 1,2,4-trimethoxybenzene and 2,6-dimethoxyphenol being the most abundant, Fig. 11). On the other hand, formation of coke and undesired polyaromatic hydrocarbons was also reduced.

6.3.2. Condensation reactions. Condensation reactions have gained special interest in biomass transformation for both biofuels and production of valuable chemicals. These reactions involve the formation of C–C bonds and the release of oxygen in the form of water. Therefore, these reactions allow small, oxygenated and reactive compounds, typically present in pyrolysis bio-oils (*e.g.* acids, aldehydes, esters, phenolics, furanics, *etc.*),[369] to be transformed into larger, deoxygenated, and more stable molecules.[370,371]

Numerous condensation reactions have been traditionally applied in organic chemistry where homogeneous acid or base catalysts are mostly used. Homogeneous catalysts cannot be recovered, and there are economic and environmental concerns to initiate searching for solid catalysts as substitutes. One example is aldol condensation of aldehydes or ketones in the presence of homogeneous base catalysts, such as sodium hydroxide.[372–374] As aldehydes and ketones are present in pyrolysis bio-oils in significant amounts, this reaction has been considered as a very reasonable way to upgrade them. Aldol condensation can be performed in both liquid and vapour phase. Particularly the vapour phase option allows its direct coupling to the exhaust of the pyrolysis reactor without necessity to condensate the primary vapours. Although most of the solid catalysts under investigation possess basic properties, some acidic materials (in particular zeolites) have also been tested showing promising results.[375–378] Large pore zeolites, especially ***BEA** zeolites, were found to be good catalysts of aldol condensation. However, the existence of Brønsted acid sites in this kind of zeolite promotes the catalyst deactivation by coke formation. Therefore, efforts in the development of catalysts with enhanced resistance to deactivation have been made. Puértolas *et al.*[379] attempted to modulate the USY zeolite acidity by impregnation with a second active phase and used the resulting catalysts in aldol condensation of oak wood pyrolysis vapours at 400 °C. The authors modified the zeolite by K-exchange or supporting MgO. The exchanged catalyst exhibited better performance than MgO/USY (24.7% oxygen reduction *vs.* 15.2%, respectively), but at the expense of producing more coke (26.1 *vs.* 16. 5 wt%, respectively).

Similarly, hierarchical ZSM-5 zeolites have shown much higher catalytic activity than their conventional counterparts for aldol condensations involving large molecules, especially in the synthesis of vesidryl.[370] Impregnation of hierarchically structured ZSM-5 zeolites with metal cations (Sn, Cu, Ni, or Mg) has led to catalysts that promote selectively bio-oil oxygen removal reactions. Ketonization reactions of acids with aldehydes to produce ketones seem to be favoured over the Lewis acid sites created after incorporation of Mg cations by ion exchange.[371]

6.3.2.1. 2D vs. 3D zeolites in aldol condensation. Owing to their enhanced external surface areas compared to conventional zeolites, two-dimensional zeolites are considered more appropriate catalysts for aldol condensation reactions involving bulky compounds, as they occur in primary pyrolysis vapours from biomass. Kikhtyanin *et al.*[380] explored a variety of layered zeolites belonging to the **MWW** family in aldol condensation of furfural and acetone. A batch reactor operating at 100 °C under

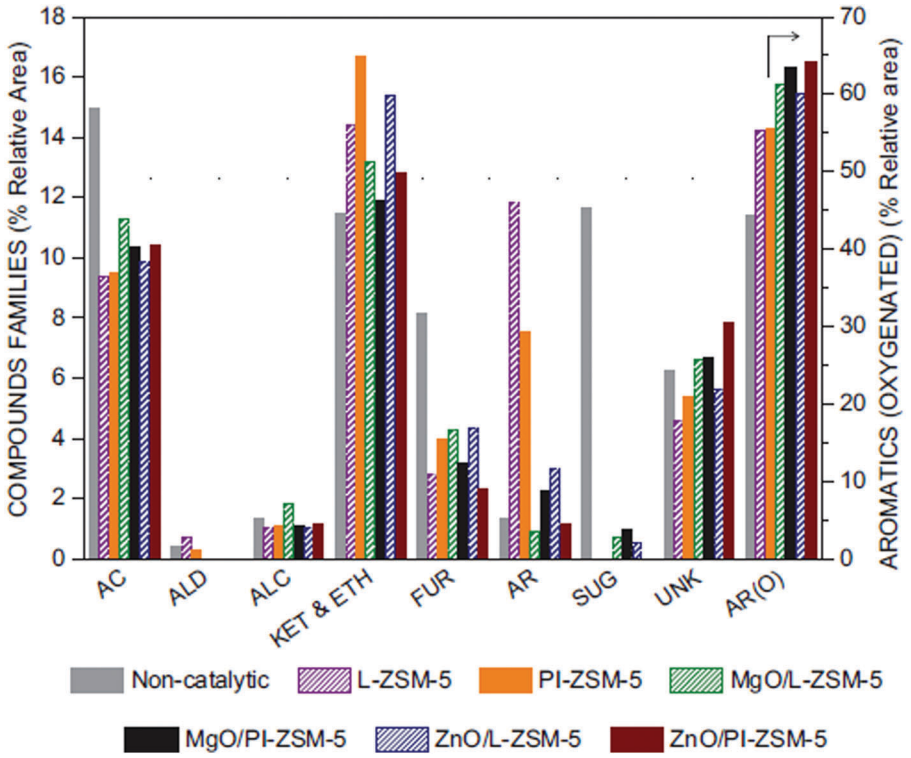

Fig. 11 Impact of catalyst type on the deoxygenation degree of the bio-oil obtained by catalytic pyrolysis of rice husk. Reprinted with permission from ref. 368.

autogenous pressure was employed and their activity was compared with that of Beta zeolites. All the **MWW**-type catalysts (MCM-22 and MCM-49, characterized by a 3D layered structure, as well as their delaminated and pillared derivatives, MCM-56 and MCM-36) were more active than the ***BEA** zeolite and other conventional zeolites previously tested by the same authors.[378] Moreover, selectivity to FAc (4-(2-furyl)-3-buten-on) was always above 80%. Among the four **MWW**-type zeolites, MCM-22 gave the best performance, which was attributed to the participation of the active sites located within the supercages, in addition to those located on the external surface. On the other hand, the pillared MCM-36 showed the lowest conversion of its family, denoting that introducing the silicate pillars deteriorated its activity. Moreover, MCM-36 was deactivated much faster by coke due to polymerization reactions on the easily accessible external active sites created by delamination and pillaring.

6.3.3. Isomerization. Valorisation of some molecules present in biomass, such as sugars and terpenes, into fine chemicals or higher quality biofuels can be accomplished by isomerization reactions. In the particular case of sugars, there are already commercial bio-catalytic isomerisation processes for glucose into fructose.[381] Nevertheless, the use of immobilized enzymes brings important operational limitations including fast activity decay, rigid operation conditions and also the necessity to apply purification treatments to the feed. In this context, heterogeneous inorganic catalysts are being investigated with the aim to replace enzymes as isomerization catalysts of glucose. Zeolites, due to their high versatility, have also been explored in this type of reaction. Results employing both basic (NaX and KX)[382] and acidic zeolites (Sn-**BEA**, Sn-**MFI**, Ti-**BEA**, Y zeolite)[381,383–387] are available. Basic NaX and KX zeolites achieved high selectivity to fructose (about 90%) but rather low conversions of glucose (10–20%).[382] Acidic zeolites have shown better performance, and particularly, Sn-Beta, thanks to its ability to activate the carbonyl group, exhibited activities very close to the enzymatic route.[381,384] Moreover, the zeolite catalysts have the advantage of allowing the use of broader ranges of both temperature and pH conditions. Moliner *et al.*[381] reported a product distribution of 46 wt% glucose, 29 wt% fructose and 8 wt% mannose after reacting a 45 wt% glucose solution using Sn-Beta (1 : 225 Sn : glucose molar ratio) as the catalyst for 60 min at 110 °C. The reaction occurred without any decrease in catalyst activity even at pH = 2. This is beneficial either for combination of the isomerisation with acid hydrolysis of starch to produce glucose for isomerisation, or to combine the isomerisation with further acid catalysed dehydration leading *e.g.* to 5-HMF.

Another interesting isomerization reaction using acidic zeolites is the conversion of xylose into xylulose.[385,388–390] M. Paniagua *et al.*[389] compared zeolites **FAU** (Y), ***BEA** (Beta) and **MFI** (ZSM-5), observing the first one as the most active leading to xylulose yields up to 47%. Li *et al.*,[391] used periodic DFT calculations to determine the mechanism of glucose isomerization to fructose over a variety of Sn-zeolites (**MOR**, ***BEA**, **MFI** and **MWW**). Despite a higher glucose adsorption energy

caused by the narrower 10-ring micropores of **MWW**, it was predicted that Sn-**MWW** could provide high conversions due to the presence of a small fraction, but highly reactive, of accessible sites.

The presence of mesopores to overcome limited accessibility of the active sites was also found to be beneficial in isomerisation reactions. Hierarchical Sn-ZSM-5 materials have been able to isomerize selectively glucose, xylose, and lactose, which suffer from access or diffusion limitations in purely microporous Sn-ZSM-5.[392] Likewise, Sn-Beta facilitated a selective conversion of sugars into important intermediates for producing alkyl lactate.[393] Ethanolysis of renewable furfuryl alcohol has been performed over hierarchical ZSM-5 with high yield into ethyl levulinate.[394] In the same way, hierarchical niobium-containing zeolites have been applied for isomerization of dihydroxyacetone to alkyl lactate and lactic acid with a yield over 95%.[395]

6.3.3.1. 2D vs. 3D zeolites in isomerization reactions. The application of layered zeolites in the isomerization reaction of biomass-derived compounds has been scarcely explored so far. Sn-self-pillared-pentasil (Sn-SPP)[293] and pillared Sn-**MWW**(SP)-SSE[396] (analogue of aluminosilicate MCM-36) were demonstrated to be very effective catalysts in glucose to fructose isomerisation using an alternative approach, when glucose is turned into ethylfructoside (which helps in shifting the isomerisation equilibrium) and fructose is obtained after hydrolysis of the fructoside with water at the end of the reaction. Fructose yield up to 60% has been reported. These self-pillared resp. pillared catalysts isomerize even disaccharides (lactose to lactulose resp. maltose to maltulose), where catalysts such as Sn-**BEA** fail because the substrates are too sterically demanding.[293,396]

Isomerization of β-pinene, as a representative of terpenes present in the essential oil of pine trees, has been attempted over MCM-22 and its hierarchical microporous-mesoporous derivatives obtained by acid post-treatment.[397] The purpose of such a reaction is to produce a mixture of limonene and camphene, compounds of particular interest in the field of cosmetics and medicine. An excellent performance was obtained over the hierarchical MCM-22, with full conversion and 93.7% selectivity to the mixture of limonene and camphene (76.2% limonene and 17.5% camphene) under the reaction conditions employed. Such good catalytic behaviour was attributed to the right balance between acidic and textural properties. Moreover, the catalyst could be efficiently recycled by mild washing treatments, denoting good structural stability and removal of organic compounds facilitated by the existence of mesopores.

6.3.4. Dehydration reactions. Important platform molecules can be produced by inducing dehydration reactions on organic compounds derived from biomass. For instance, sugars can be converted into 5-HMF (5-(hydroxymethyl)furfural) and furfural by dehydration reactions catalysed by zeolites.[332,333]

The dehydration of hexoses (glucose and fructose) to 5-HMF revealed that the yield of 5-HMF is highly dependent on the reaction conditions, type of sugar used and zeolite properties. For instance, fructose leads to higher 5-HMF yields than glucose. On the other hand, Brønsted acid sites are poorly active in the conversion of glucose; thus most efforts are made in the development of zeolitic catalysts with well-balanced Lewis and Brönsted acidity. This can be addressed by preparing mixtures of catalysts, such as Ti-Beta + Sn-Beta, as Lewis center carriers, and HCl as Brönsted acid,[398] or Sn-Beta (as Lewis center carrier) + Amberlyst (as Brønsted center carrier).[399] However, it would be more practical to apply bifunctional zeolite catalysts containing both types of acidity.

The use of zeolites to produce furfural by dehydration of biomass derived xylose is also a field of interest as it would allow replacing the hazardous and non-recoverable sulphuric acid used industrially as a catalyst. However, it is a tricky issue because dehydration of C_5 sugars to furfural, which is promoted by Brønsted acid sites, can interfere with isomerization reactions to -xylulose, which are catalysed by Lewis acidity.[332] A variety of 3D zeolites have been used for xylose dehydration, including **MFI** (ZSM-5), **MOR** (Mordenite), **FAU** (Y), ***BEA** (Beta) and silicoaluminophosphates (SAPO-5, SAPO-11, SAPO-40).[400–404] Excellent results have been reported while combining the use of Mordenite with a solvent composed of γ-valerolactone (GVL) and 10 wt% of water.[403] Under these conditions 80% yield of furfural was achieved, which was attributed to hindering of side condensation reactions between furfural and pentose intermediates. More recently, Iglesias *et al.*[404] reported that zeolites with smaller pores (ZSM-5) are poorly active in xylose dehydration. They also found that the nature of the acid sites was the key parameter driving the main reaction pathways for transforming xylose into furfural. Thus, Lewis acid sites promoted the direct dehydration of xylose, whereas Brønsted-type catalysts produce alkyl xylosides as intermediates. In addition, Beta-zeolite with a proper balance between Brønsted and Lewis acidity was postulated as the most promising catalyst to maximize furfural production.

6.3.4.1. 2D vs. 3D zeolites in dehydration reactions. Lima *et al.*[400] applied a delaminated zeolite (Si/Al = 29) as a catalyst for the liquid phase dehydration of xylose to furfural at 170 °C, using a water–toluene biphasic reactor system. The delaminated zeolite was prepared by swelling and ultrasonication of a laminar precursor of Nu-6(2), resulting in a BET surface area close to seven times higher (151 $m^2 g^{-1}$) than that of the parent material (25 $m^2 g^{-1}$). Such an increase in the textural properties and its consequent accessibility enhancement, led to a significant improvement with a furfural yield of 47%, higher than that (34%) obtained over H-Mordenite used as a reference catalyst. Moreover, the authors evidenced no Al-leaching and quite stable activity in recycling.

Very recently, Abdelrahman *et al.*[405] proposed an alternative thermochemical pathway to produce butadiene from biomass based on the dehydration of sugars to furfural, followed by decarbonylation and hydrogenation to THF and a final dehydration and decyclization step. Regarding the last catalytic step, dehydration and ring opening of THF, they compared a phosphorous-containing siliceous self-pillared pentasil sample

(P-SPP) with a wide variety of catalysts, including ZSM-5, HY, Sn-Beta, ZrO_2 and silica–alumina. Among them, P-SPP demonstrated very promising performance with very high selectivity to butadiene (87–92%) and conversions up to 83%.

Another interesting application of zeolites based on dehydration reactions of biomass-derived molecules is the conversion of glycerol to acrolein. Acrolein is an intermediate for the production of acrylic acid, the platform molecule used in the manufacture of paints, plastics, adhesives and super-adsorbents. Recently, two similar studies employing **MWW**-type catalysts in this reaction have been reported.[406,407] In both cases, MCM-22, pillared MCM-36 and delaminated ITQ-2 zeolites were compared under gas phase conditions. ITQ-2 stood out as the best catalyst in terms of conversion, selectivity (Fig. 12) and regeneration capability. The observed features were explained by the higher accessibility of their active sites (ITQ-2 possesses a house-of-cards morphology) together with an easier removal of coke from mesopores.

6.3.5. Other biomass conversion reactions. As was mentioned at the beginning of this section, the exploration of zeolites in the field of biomass transformation covers numerous pathways due to the large variety of molecules derived from that feedstock and consequently, the wide range of products to be obtained from them. In particular, it has already been evidenced that layered 2D and 3D zeolites have high potential in the reactions involving bulky compounds (catalytic pyrolysis, aldol condensation, isomerization and dehydration) due to the enhanced accessibility of their active sites. But these high capabilities have also been revealed in other catalytic reactions related to the biomass-derived compound conversion.

One example is the study reported by Yoon *et al.*,[408] in which they demonstrated an improved activity of Rh supported on swollen MCM-22 and its pillared derivative MCM-36 compared with other acidic supports (MCM-41 and silica–alumina aerogel), when they were applied in the hydrodeoxygenation (HDO) of guaiacol and 1,3,5-trimethoxybenzeze (1,3,5-TMB). Among the zeolites tested, MCM-36 was particularly the most efficient catalyst, due to a higher dispersion of Rh particles. Despite Rh dispersion onto MCM-41 and silica–alumina aerogel being even higher, the activity over Rh/MCM-36 was the largest due to the higher accessibility of the acid sites located on the external surface, thus, minimizing mass transfer limitations.

Alkylation using conventional zeolites, layered 2D and 3D acidic zeolites has been explored as a useful reaction for either improving the H/C ratio in bio-oils,[409] producing biofuels[410] or for the production of high value chemicals, such as xylenes, ethylbenzene and ethyltoluene.[411] Large pore zeolites are more convenient than small and medium pore size ones due to lower mass transfer restrictions. Among 2D zeolites, delaminated ITQ-2 is specially active and selective to alkylation products thanks to the enhancement of accessible surface and to the shorter diffusion path lengths.

Encapsulation of cobalt clusters in a hierarchical ZSM-5 zeolite has afforded a catalyst for the direct production of middle isoparaffins[412] by means of the hydrogenation of carbon monoxide into hydrocarbons (the Fischer–Tropsch (FT) synthesis). In the same way, hierarchical zeolite Y supported Co catalysts has been tested in FT synthesis.[413] Middle hydrocarbons, with a remarkable selectivity to isoparaffins, were the main products due to the optimized hydrocracking and isomerization function brought by the hierarchical zeolite. Also for this reaction, addition of Mn to Co/Na-hierarchical zeolite Y caused a significant improvement in the diesel fuel selectivity by suppressing the formation of CH_4 and lighter hydrocarbons.[414]

Delaminated and pillared MCM-22 zeolites have also been applied as a support of cobalt for the FT reaction.[415] It has been found that using either delaminated or pillared derivatives allows narrowing the product distribution of the FT reaction as the selectivity to C_4–C_{12} molecules is increased. Nevertheless, compared to the parent MCM-22, the delaminated support leads to a higher proportion of C_{21+} hydrocarbons, which was attributed to the loss of acidity caused during the swelling and delaminating process. Last but not least, a Co impregnated nanosponge ZSM-5 catalyst exhibited high selectivity for branched hydrocarbons and olefins in the gasoline range (C_5–C_{11}).[416]

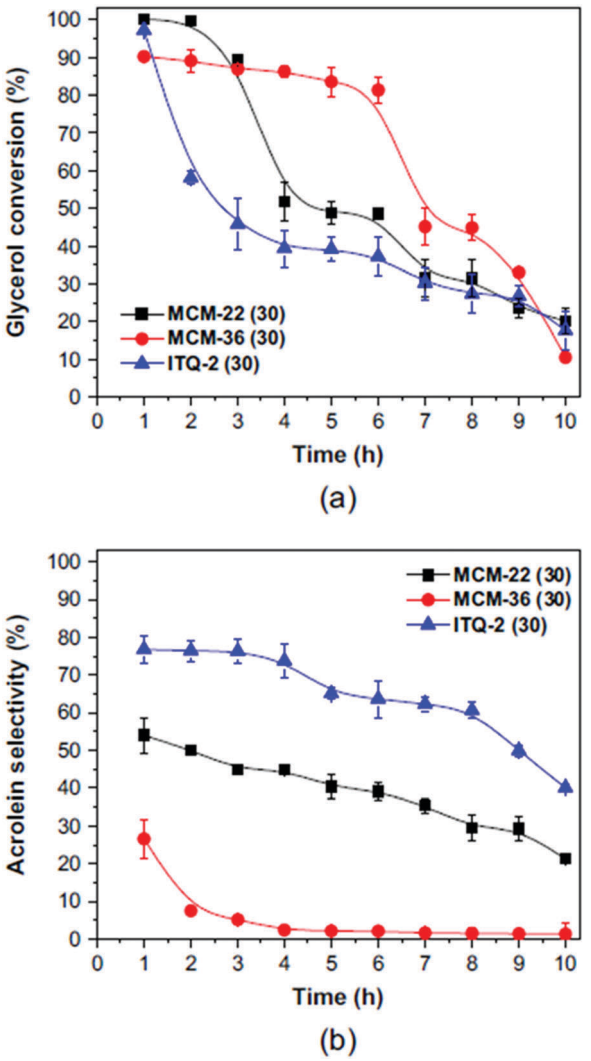

Fig. 12 Glycerol conversion and acrolein selectivity over MWW catalysts. Reprinted with permission from ref. 407.

The above observed selectivity towards lighter and branched hydrocarbons results from close intimacy between the metal and zeolite active phase resulting in an *in situ* processing of the primary (linear) FT hydrocarbons.

6.4. Selective oxidation/reduction reactions

Selective oxidation is an important part of heterogeneous catalysis. For instance the world ethylene oxide production capacity was 34.5 million tons per year in 2016[417] and all the production was perfomed by direct oxygen or air oxidation of ethylene over a silver oxide-based catalyst. Here we discuss 3D and 2D zeolite based oxidation catalysts including epoxidation as one of the important reactions.

Zeolites with Lewis acid sites (namely titanosilicates, tinsilicates, and zirconium silicates) catalyse a number of selective oxidation/reduction reactions, of which the epoxidation, hydroxylation of aromatics, ammoxidation, Baeyer–Villiger oxidation and Meervein–Ponndorf–Verley reduction/Oppenauer oxidation are the most important; the titanosilicate catalysed propylene epoxidation, cyclohexanone ammoxidation and phenol hydroxylation are carried out even at the industrial scale.[312,418,419] One of the strong points of oxidation reactions catalysed by zeolites is the use of a ''green'' and simple oxidant: hydrogen peroxide. Unfortunatelly, to our best knowledge, there are no data (except for phenol hydroxylation over IEZ-Ti-**CDO** (denoted as Ti-COE-3, Ti-COE-4[420])) on phenol hydroxylation and ammoxidation using 2D titanosilicates.

6.4.1. Epoxidation. The epoxidation of the C=C double bond is an important selective oxidation reaction and epoxides are important reactive intermediates. Except for ethylene oxide and propylene oxide, it is traditionally performed by the so-called chlorhydrine route in which a hypochloric acid is added to the C=C bond and the epoxide is obtained by subsequent dehydrochloration with a strong base. Alternatively, it can be performed directly using hydrogen peroxide or organic hydroperoxides (*e.g. tert*-butyl hydroperoxide (TBHP) or cumeme hydroperoxide). However, peroxides require activation, which can be performed effectively with titanosilicate zeolites. Titanium-zeolite catalysed epoxidation occurs under mild conditions in a liquid phase and is advantageous for suppression of consecutive reactions, safety, and particularly for a considerable side product/waste reduction when hydrogen peroxide is used. Data from a continuous setup experiments are rare (Deng *et al.*[421] is one of the few examples); typically the epoxidations are carried out batchwise using acetonitrile or methanol as solvent at temperatures between 30 and 60 °C (depending on substrate).

Titanium silicalite-1 (TS-1)[280] and Ti-**MWW**[422,423] based materials are the most studied. Both of them exist in 3D and 2D forms; see recent review.[424]

The substrates subjected to the epoxidation can be divided into two groups. Small substrates (linear alkenes up to about C_8, allylchloride, allylalcohol, *etc.*) and bulky substrates (cyclic alkenes, terpenes, branched alkenes *etc.*). For the first group, the highest yields and selectivity (when using H_2O_2 as oxidant) are obtained using conventional 3D catalysts while their two dimensional analogues provide significantly lower conversions and yields, although *e.g.* the titanium content and characteristics of the titanim species are the same. Such behaviour is nicely documented in epoxidation of 1-hexene *e.g.* in the case of conventional TS-1 (conversion 5.5% after 2 h) *vs.* nanosheet TS-1 (conversion 3.8 resp. 3.8% after 2 h under the same conditions).[257,258] Similarly, IEZ-Ti-**MWW** (Si/Ti = 94)[425] fails in comparison with Ti-**MWW** (Si/Ti = 44)[426] (conversion 12.1% *vs.* 54.2% after 2 h, under the same conditions, exhibiting similar selectivity (95%)). Note that the difference in titanium content is about 2 times while the difference in conversion is almost 5 times. Qualitatively the same results were also observed when comparing data for 1-octene.[424,427,428] Reasons for such behaviour are not fully clear, but different hydrophobicity of the 3D frameworks, confinement effects or slight differences in Ti sites geometry are assumed to be responsible.

A direct relationship has been identified also between the catalytic activity and the mesopore surface area of hierarchical TS-1 in 1-hexene and cyclohexene epoxidation (Fig. 13).[429,430] In addition, the connectivity between micro- and mesopores may have also a relevant effect on the catalytic properties.

For bulky substrates, the data show the expected advantages of the open structures of hierarchical and 2D catalysts. Cyclohexene is the most frequently reported bulky substrate, although it is the smallest, and it is strongly prone to side reactions such as allylic oxidation (using the H_2O_2). Nevertheless, it is epoxidised with higher yield and selectivity over IEZ-Ti-**MWW** catalysts[426,431,432] (*e.g.* yield 33.3% after 5 h) in comparison with Ti-**MWW** (yield 4.7% after 5 h) and TS-1.

Cyclooctene and cyclodecene oxides are more stable than cyclohexene oxide under the reaction conditions and less prone to oxidation of allylic carbon and in contrast their diffusion even in large pore titanosilicates such as Ti-Beta is more limited. The difference between cyclooctene conversion over TS-1 (0.2% after 2 h) and layered TS-1 (2.8% after 2 h) reaches an order of magnitude.[258] In different experimental setups, silica–titania pillared TS-1 (Si/Ti = 20) provided 21% conversion[222] and silica–titania

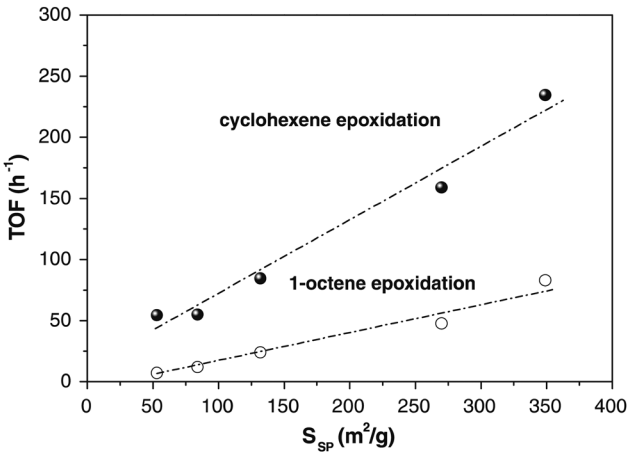

Fig. 13 Variation of the catalytic activity (TOF) in olefin epoxidation with the surface area related to the secondary porosity of TS-1 samples. Reprinted with permission from ref. 430.

pillared Ti-IPC-1-PITi (Si/Ti = 69) provided even 35% conversion[245] of cyclooctene both exhibiting 80% selectivity while Ti-Beta (Si/Ti = 119) provided only 14% conversion with 32% selectivity and TS-1 8% conversion with 42% selectivity. Note that the silica–titania pillared catalysts bear additional titanium sites on their external surface. In the case of cyclodecene the difference between conventional and layered TS-1 is expectably higher (TS-1: 0.2% conversion *vs.* layered TS-1 5.1% conversion[258]).

Epoxidation over 3D medium pore titanosilicates (TS-1, Ti-**MWW**) using TBHP as an oxidant is not possible (or at least not convenient) because the TBHP is too bulky to penetrate the microporous system and therefore only the active sites on the external surface participate in the reaction (*e.g.* TS-1: conversion 1.2% after 2 h,[221] Ti-**MWW**: 4.2% after 2 h[210] in epoxidation of cyclohexene). In contrast, hierarchical catalysts (*e.g.* TS-1 prepared using silanized zeolite seeds[433]), the 2D catalysts, have well accessible external surface of the layers with titanium sites[434] and therefore, they are much more effective (layered TS-1: conversion 17% after 2 h under the same coditions[210]). Note, that in contrast to the epoxidation with hydrogen peroxide, epoxide selectivity of 90–100% is observed even at cyclohexene conversion above 40%.[424] In addition to 2D zeolites, also mesoporous molecular sieves (*e.g.* Ti-MCM-41) are effective catalysts, when TBHP is used instead of H_2O_2.[210,435] Recently, a layered silicate (not a zeolite) HUS-7 intercalated with Ti(IV) acetylacetonate was reported to be very active in epoxidation of cyclohexene with TBHP (TOF up to 266 h^{-1}). In this case, the catalyst is not calcined and the mentioned TOF is achieved in the 3rd recycling of the catalyst. Changes in the catalyst structure during the reaction were observed (changing of the interlamellar spacing) but titanium species leaching was not observed. Thus the results can be interpreted as successful immobilization/stabilization of a titanium organometallic complex, which provides the catalytic activity.[436]

The results observed for the cyclic alkenes are illustrative also for substrates like norbonene. The readers are invited to check the review[424] for a detailed comparison.

6.4.2. Baeyer–Villiger oxidation. Baeyer–Villiger (BV) oxidation is a direct conversion of ketones to esters and cyclic ketones to lactones.[437] In organic synthesis, the reaction is performed using peracids or persulfate salts; however, use of a suitable heterogeneous catalyst together with hydrogen peroxide has obvious advantages. A number of heterogeneous catalysts have been used including acidic anionic resins,[438] hydrotalcites,[439] titanosilicates,[440] aluminosilicates[438] and germanosilicate[441] zeolites, all of them activating the hydrogen peroxide. In contrast, tin(IV) containing catalysts (Sn-Beta being the first Sn-silicate zeolite[289]) activate the carbonyl group, thus strongly increasing the selectivity of the reaction. Sn-Beta is a large pore tin-silicate zeolite and thus its activity does not suffer too much from diffusion restriction even when oxidising substrates such as 2-adamantanone. As a result, Sn-Beta is so far the most studied tin-silicate catalyst[442,443] in BV oxidation but other – in particular 2D dimensional – catalysts have been reported recently; namely: (I) the Sn-**MFI** familly including conventional 3D Sn-**MFI**, 2D Sn-**MFI** nanosheets,[296] Sn-selfpillared pentasil catalyst[293] and tin-silica pillared **MFI**;[246] (II) the **MWW** family including 3D Sn-**MWW**, partially delaminated Sn-MCM-56[295] and Sn-DZ-1[444] and pillared Sn-**MWW**(SP)-SSE[396] (MCM-36 analogue); (III) tin-silica pillared ICP-1[246] (a **UTL**-based material) and (IV) IEZ-Sn-PLS-3 which is an interlayer expanded zeolite with **FER** layers.[445] For complete image we should mention that also several Sn mesoporous molecular sieves (*e.g.* Sn-MCM-41) were reported.[303]

BV oxidation of 2-adamantanone is the most used model reaction when investigating novel BV catalysts. The kinetic diameter of 2-adamantanone is about 7 Å which makes it too bulky not to enter the 10-ring pores but small enough to enter large pores of Sn-Beta. Its polycyclic structure also brings high stability and rigidity to the molecule and therefore high selectivity of the BV oxidation is usually observed (typically >98%).[301] Similar behaviour can be observed *e.g.* in BV oxidation of norcamphor.[303] On the other hand cyclopentanone and cyclohexanone are not so easy to oxidise and observed selectivities are usually lower (<80%).[246,442] In most cases the above 2D catalysts (particularly the **MFI** and **MWW** families) provide only similar or lower conversions and lactone yields in BV oxidation of 2-adamantanone with hydrogen peroxide (*vide infra*). In this sense, a strong difference in comparison with titanosilicate catalysed epoxidation with hydrogen peroxide was observed, where the 2D catalysts brought strong enhancement of the catalytic performance. Also within a group of germanosilicate zeolites tested in BV oxidation of 2-adamantanone, ITQ-17 (**BEC**, Beta polymorph C) was also the most active catalyst, followed by extra-large pore zeolite IM-12 (**UTL**)[441] but in comparison with Sn-**UTL** and Sn-Beta, germanosilicate **UTL** provided significantly lower conversion in BV oxidation of 2-adamantanone and cyclohexanone.[446]

Luo *et al.*[296] tested Sn containing **MFI** nanosheets, which were considerably more active than 3D Sn-**MFI** (initial turnover-frequency TOF = 38 h^{-1} resp. 5 h^{-1}) but Sn-Beta provided initial TOF = 210 h^{-1}. The authors suggest that lower TOF of Sn-**MFI** nanosheets (and Sn-MCM-41) in comparison with Sn-Beta can be caused by the more hydrophilic character of the 2D (resp. amorphous silica) catalyst which results in stronger concurrent adsorption of water (introduced with the H_2O_2). Decreasing of the H_2O_2 dose (and therefore also water concentration in the reaction mixture) resulted in an increase of TOF (Sn-**MFI** nanosheets 86 h^{-1}). On the other hand, silylation (hydrophobisation) of the surface resulted in blocking of the access to the Sn sites rather than improvement of the catalytic activity. Liu *et al.*[295] investigated BV oxidation of 2-adamantanone with Sn-**MWW** based catalysts in comparison with Sn-**MFI** and Sn-Beta. An advantage of the partially delaminated structure of Sn-MCM-56 over 3D Sn-**MWW** was observed, but still Sn-Beta provided higher conversion (Sn-Beta 57% > Sn-MCM-56 42.3% > Sn-**MWW** 29.5% > blank 3.5% after 2 h at 90 °C). Recently Ren *et al.*[396] reported pillared Sn-**MWW**(SP)-SSE (MCM-36 analogue) to provide 90.5% conversion of 2-adamantanone while Sn-Beta with the same Sn content gave 82.3%.[396] In addition, much stronger difference was observed when the catalysts were tested

in sugar isomerisation (see Section 6.5). The observation evidences that 2-adamantanone is still too small to assess the advantages of 2D stannosilicates in BV oxidation.

Regarding the pillared catalysts, Přech *et al.*[246] recently extended his silica–titania pillaring concept,[222,245] which was successfully used to prepare highly active epoxidation catalysts, also to tin-silica pillaring. The layered **MFI** based and (**UTL** based) ICP-1-SnPI catalysts showed remarkable activity in BV oxidation of 2-adamantanone, norcamphor and cyclopentanone. Although reference Sn-Beta exhibited higher turn-over-numbers (Sn-Beta **TON** = 69 *vs. e.g.* IPC-1-SnPI **TON** = 28 in BV oxidation of norcamphor) than the tin-silica pillared catalysts, the overall conversions (*e.g.* norcamphor conversion: Sn-Beta: 13% *vs.* IPC-1-SnPI: 36% after 8 h) and yields were higher for the pillared catalysts because the tin-silica pillaring creates a large amount of well accessible Sn sites located preferentially on the external surface of the crystalline layers. A similar feature (Sn sites close to the external surface of crystals) is probably responsible also for the high performance of the Sn-Y (Sn-**FAU**) catalyst prepared by dealumination of zeolite Y and subsequent tin incorporation by $SnCl_4$ vapour.[301]

6.4.3. Meervein–Ponndorf–Verley reduction/Oppenauer oxidation. Meervein–Ponndorf–Verley reduction (hereafter MPV)[447–449] and Oppenauer oxidation[450] are two complementary hydrogen transfer reactions catalysed by Lewis acid catalysts such as Ti-, Sn-, Zr- and Hf- but also Al-zeolites. In the MPV reaction, a ketone (or aldehyde) is reduced by an excess of secondary alcohol (typically 2-propanol) to the corresponding secondary (primary) alcohol while acetone is the side product; *vice versa* in the case of Oppenauer oxidation. Al-Beta, modified by mild steaming or activated at high temperature (700 °C) to increase it Lewis acidity, is known to catalyse MPV reduction of 4-*tert*-butylcyclohexanone for quite long time.[451,452] Note that due to the shape selectivity effect a *cis*-4-*tert*-butylcyclohexanol is formed although it is thermodynamically the less favored product. Shortly after that, the same ability for Ti-Beta was reported[453] and later, Sn-Beta was found to be even more active than Ti- and Al-Beta.[454] While 4-*tert*-butylcyclohexanone and 4-methylcyclohexanone were converted easily over Sn-Beta, MPV reduction of 2-methylcyclohexanone was slower and 2-*tert*-butylcyclohexanone was not converted at all; most propably as a result of the steric hinderance of the carbonyl group by the *tert*-butyl substituent rather than because of the shape selectivity effect because in such a case, at least the external surface acid sites should contribute to the catalytic activity and conversion would be low but not zero.[454] Until now, a number of studies on MPV reduction of many carbonyl compounds including cyclohexanone,[446] 4-methoxybenzaldehyde,[455] nopinone, norcamphor, acetophenone, benzylacetone, cinnamaldehyde or citral[456,457] have been reported using Sn- and Zr-Beta; however, the potential of 2-dimensional catalysts, particularly 2D Lewis acid zeolites, remains undisclosed. Al-Naiyli *et al.* reported MPV reduction of cyclohexanone, cyclooctanone and cyclododecanone over Sn-Beta and hierarchical Sn-Beta. The reaction rate of cyclohexanone reduction was almost the same over both conventional and hierarchical Sn-Beta, while reduction of the two latter substrates was considerably faster over the hierarchical catalyst (*e.g.* reaction rate of cyclooctanone reduction was 1.4×10^{-4} s^{-1} over hierarchical Sn-Beta *vs.* 1.6×10^{-5} s^{-1} over conventional Sn-Beta).[291] Recently, catalytic activity of (aluminosilicate) IEZ-**MWW** containing Lewis acid sites was demonstrated in MPV reduction of 4-methylcyclohexanone and butanone.[458] Therefore, benefits from 2D catalysts are highly expectable, particularly because the MPV reaction has a sterically demanding transition state where both alcohol and ketone are co-adsorbed.[457]

6.4.4. Oxidative desulphurization and sulphide oxidation. In addition to hydrodesulphurization (HDS) processes, a completely different approach for the removal of sulphur in oil fractions is by catalytic oxidative desulphurization, which presents the advantage of not requiring hydrogen or a high pressure. A TS-1 zeolite possessing mesopores has demonstrated a high catalytic activity and a convenient recyclability in thiophene oxidation, due to the decreased hydrophobicity and mesoporous structure of this material.[459] Likewise, catalytic oxidative desulphurization (ODS) of S-containing aromatic compounds has been investigated over both hierarchical and conventional TS-1 zeolites.[460] The influence of both the solvent (*n*-heptane and acetonitrile) and the oxidizing agent (hydrogen peroxide and *tert*-butylhydroperoxide, TBHP) was studied using dibenzothiophene (DBT) as a model substrate. The catalytic activity exhibited by the hierarchical TS-1 was much higher than that obtained with the conventional TS-1; a very high desulphurization activity was obtained with the combination of heptane and TBHP, leading to almost total DBT conversion.

In the same way, organic sulphones and particularly sulphoxides (intermediate products in the S-oxidation) can be prepared by oxidation of corresponding sulphides with hydrogen peroxide over titanosilicate catalysts. When 2D TS-1 and Ti-IPC-1-PI catalysts were tested in this reaction, it was found that the use of these 2D catalysts with a highly open structure is beneficial for both small and bulky substrates.[461] In the case of small substrates (represented by methylphenyl sulphide), selectivity of the reaction is diffusion driven enabling the attainment of a sulphoxide:sulphone ratio of 94 : 6 at 40% conversion (3D TS-1 exhibited only 60–74% sulphoxide selectivity depending on crystal size under the same conditions). In the case of bulky substrates (represented by diphenyl sulphide, dibenzothiophene and dioctyl sulphide) the enhanced accessibility of the active sites resulted in a significantly increased conversion in comparison with 3D counterparts.

6.5. Chemical specialities

Zeolites are traditionally considered as catalysts for large-scale industrial processes and much less they represent a toolkit for synthetic organic chemists. However, researchers and manufacturers, dealing with pharmaceuticals, fragrances or food additives, can benefit from the same advantages known from large-scale processes. In most research papers from the area of molecular sieves, thorough characterisations of novel catalysts are reported and catalytic testing serves in the first instance as a characterisation tool. Properly chosen standard catalytic tests may provide ultimate information on the abilities of the catalyst

under investigation. However, beyond standard reactions such as toluene alkylation and disproportionation,[1] methanol-to-olefins breakthrough curves,[203,206] cyclohexene epoxidation and Baeyer–Villiger oxidation of adamantanone (*vide supra*), there exist many other interesting and useful transformations (*e.g.* acylation of methoxynaphthalene, vitamin E synthesis), which can be performed over zeolites[383,462] (the referenced book[462] contributes to bridging the gap between materials science and organic chemistry) and many of them are still waiting for disclosure or more detailed investigation.[463] In this section, there are highlighted examples of transformations, that are performed over 2D catalysts and which either represent non-classical zeolite-catalysed reactions or extend a classical approach to unusual substrates. Note also the overlap of fine chemical area with biomass processing (Section 6.3).

6.5.1. Friedel–Crafts reactions. Friedel–Crafts alkylation reactions are probably the most classical transformations in petrochemistry over zeolite based catalysts. Alkylation and acylation of *e.g.* benzene, toluene, and phenol yield also products with interest in Fine Chemistry.[464–468] Benzylation of benzene with benzyl alcohol has been used to evaluate the catalytic activity of the hierarchical zeolite catalysts in Friedel–Craft alkylations, showing that the ZSM-5 zeolite containing mesopores exhibits a much higher catalytic activity than conventional ZSM-5.[464] Likewise, the hierarchically structured ZSM-5 zeolite has shown high catalytic activity and stability for the alkylation of phenol with isopropanol due to its shortened microporous channel and presence of mesopores.[466]

The use of 2D catalysts opens possibilities to effectively couple two relatively bulky molecules. In this sense, alkylation of benzene or more bulky mesitylene with benzyl alcohol was demonstrated in the liquid phase. Kim *et al.*[469] performed the benzylation of benzene over nanosponge and conventional zeolites (***BEA**, **MTW**, **MRE**, **MFI**). Both reactants can enter the zeolite micropores but the bulky product diphenylmethane is, most probably, unable to leave the micropores, particularly of **MTW**, **MRE** and **MFI** resulting in almost zero conversion per Al site (a turn-over-number, **TON**). The active sites on the external surface, strongly augmented in the nanosponge form, catalyse the reaction effectively. Selective poisoning of the external acid sites then switches the catalytic behaviour of nanosponge Beta into commercial Beta. The nanosponge Beta provided 15% conversion after 1 h and the conversion increased steadily up to about 80% conversion (after 50 h) while reference commercial Beta and poisoned nanosponge Beta provided 10% resp. 7% conversion after 1 h and the reaction died out after about 10 h, reaching conversion below 20%. High conversion (93% *vs.* 30% over 3D **MFI**) and diphenyl methane selectivity (94%) have also been reported using single-pore nanosheet **MFI.**[212]

Mesitylene has a kinetic diameter of 0.87 nm not entering the micropores even of large-pore zeolites. Therefore, its alkylation is restricted to the external surface of the catalyst. Selective poisoning of external acid sites switches the selectivity from 1-benzyl-2,4,6-trimethylbenzene to dibenzylether because the concurrent etherification of benzyl alcohol can occur in the micropore system of catalysts,[470] but the main reaction cannot (Scheme 1). Almost complete suppression of the diffusion limitations is observed for pillared **MFI** and self-pillared-pentasil as their observed effectiveness factors are close to 1 (Fig. 7) in the etherification of benzylalcohol while external acid sites are switched-off (poisoned) with di-*tert*-butylpyridine[208] not to influence the observation of transport phenomena.

Mesostructured molecular sieves with zeolite-like walls (materials combining features of nanocrystalline and nanosheet **MFI** and ***BEA**, prepared by surfactant templating) were demonstrated to catalyse even alkylation of pyrene with 9-phenyl-9-fluorenol (Scheme 2).[213] The reaction was performed in an autoclave at 130 °C and the substrate/catalyst mass ratio was 2; however, in 2 h, the hexagonally mesostructured sieve with **MFI** walls provided 82% conversion, while the conventional Beta zeolite and mesoporous MCM-41 were almost inactive (conversion <5%). The mesostructured catalysts were composed of crystalline **MFI** phase with a similar Si/Al ratio to reference catalysts. Thus the observed catalytic activity can be ascribed to the improvement of the active site accessibility even for very bulky molecules such as the mentioned polyaromatic hydrocarbons. Similarly, these catalysts were active in Friedel–Crafts acylation of 1-methoxynaphthalene with benzoic anhydride to form 4-benzoyl-1-methoxynaphthalene (with more than 95% selectivity),

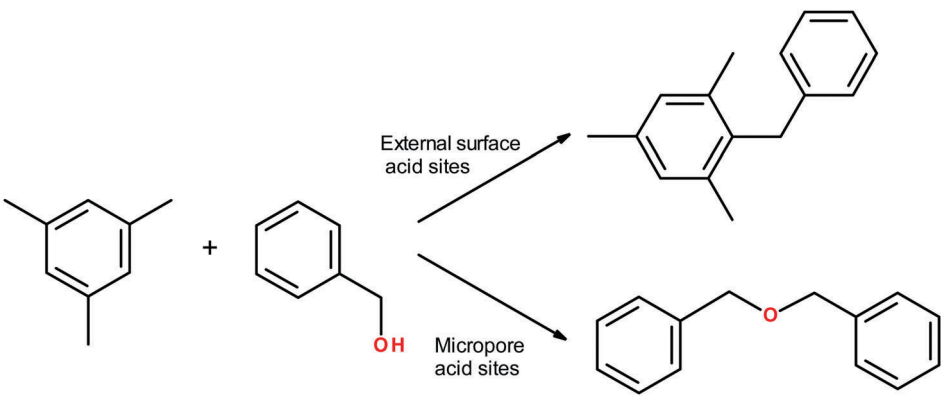

Scheme 1 Mesitylene alkylation with benzylalcohol and parallel self-etherification of benzyl alcohol.

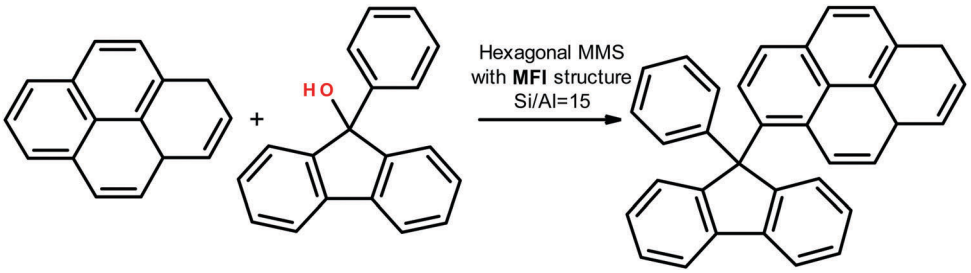

Scheme 2 Alkylation of pyrene with 9-phenyl-9-fluorenol.

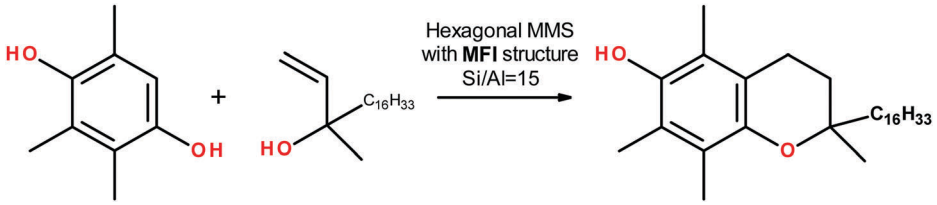

Scheme 3 Annulation of trimethylhydroquinone with isophitol yielding vitamin E.

and annulation of trimethylhydroquinone with isophytol (1-ethylen-1-methylheptadekan-1-ol) to form α-tocopherol (vitamin E, Scheme 3). Opanasenko *et al.*[471] reported annulation of phenol, 1- and 2-naphthol with 2-methyl-3-buten-2-ol. This reaction combines alkylation of the corresponding phenol in the first step with a subsequent intramolecular ring closing reaction of isoprenylphenol to form 3,4-dihydro-2*H*-1-benzopyran (chromane). The reaction was performed over unilamellar **MFI** and several mesostructured **MFI** zeolites prepared by surfactant templating. These catalysts provided the highest conversion while the selectivity of the reaction was, particularly for 1-naphthol and 2-naphthol, independent of the used catalyst.

Similarly, acylation of anisole with acetanhydride to *p*-acetophenone occurs considerably faster over lamellar and pillared ECNU-7 (**MWW** layers), and delaminated MCM-56[194] in comparison with 3D **MFI** and ***BEA**. Interlamellar expanded IEZ-PLS-3 (**FER** layers) having 12 × 10 ring channels instead of a 10 × 8 ring, characteristic of **FER**, provided conversion comparable with ***BEA**.[472] Partially delaminated ERB-1-del-135 (**MWW** layers) catalysed acylation of 2-methoxynaphthalene with acetic anhydride giving 1-acetyl-2-methoxynaphthalene,[473] which is kinetically favoured but more sterically demanding than 2-acetyl-6-methoxynaphthalene. Position 2 was favoured when large-pore zeolites (**FAU**, **MOR**, ***BEA**) were used to catalyse naphthalene acylation.[474] However, in the above case, the partial delamination brought no significant improvement in comparison with 3D **MWW**. Note that the 2-methoxynaphthalene acylation is a key reaction in one of the syntheses of a pain-reliever drug naproxen (Scheme 4).[475]

6.5.2. Aldolization and acetalization. Aldolization and acetalization are acid catalysed (aldolization also base catalysed) addition reactions on a carbonyl group with a wide use in organic chemistry; the former being able to form a C–C bond releasing water and thus decreasing the oxygen content in the product, while the latter being used to protect the carbonyl group. Besides biomass valorisation (see Section 6.3.2), nanosheet **MFI** was demonstrated to catalyse condensation of benzaldehyde with heptanal to jasminaldehyde[212] (85% conversion with 70% selectivity

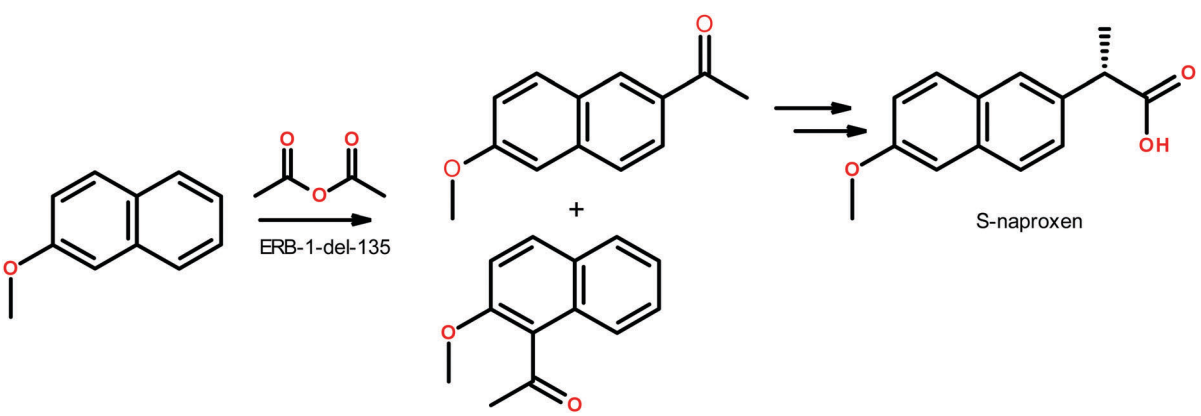

Scheme 4 Acylation of 2-methoxynaphthalene with acetanhydride and illustration of the route to S-naproxen.

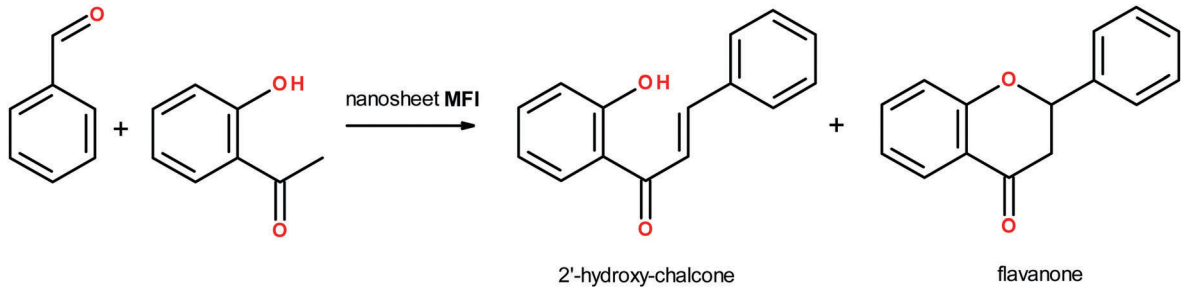

Scheme 5 Claisen–Schmidt condensation of 2-hydroxyacetophenone with benzaldehyde.

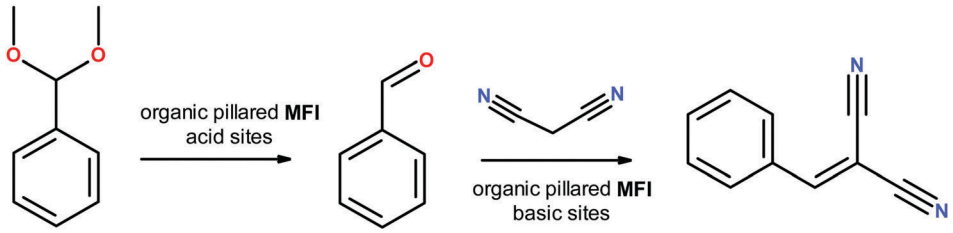

Scheme 6 Cascade deprotection of benzaldehyde dimethylacetal and subsequent Pechmann condensation with malononitrile yielding benzilidene malononitrile.

against 9% conversion over 3D **MFI**) and Claisen–Schmidt condensation of benzaldehyde with 2-hydroxyacetophenone to form flavanone and 2′-hydroxychalcone (Scheme 5).[203] In contrast to 3D **MFI**, the nanosheet **MFI** exhibited increased flavanone selectivity (62% *vs.* 50%) because the formation of flavanone is a reaction consecutive to 2′-hydroxychalcone formation and 2′-hydroxychalcone is sterically more demanding than the initial reactants.

Abilities of 2D catalysts can be demonstrated by protection of aldehydes (*e.g.* benzaldehyde) with pentaerythritol forming bulky spiro-diacetal.[203] In contrast, an opposite reaction (deprotection of carbonyl group) is used, when it is desired to perform a cascade reaction involving several types of active sites. In this way, for instance, organic pillared **MFI** was used for one-pot hydrolysis of benzaldehyde dimethylacetal to benzaldehyde and subsequent Knoevenagel condensation of benzaldehyde with malononitrile yielding benzylidene malononitrile (Scheme 6).[247] In this case, acid sites of the zeolite were responsible for the deprotection, while basic sites located on the organic pillars catalysed the condensation.

6.5.3. Miscellaneous. Structure-directing agents are usually removed from the zeolite structure before catalysis. However, Li *et al.*[476] demonstrated that in reactions, where namely the quaternary ammonium salts serve as catalysts, the zeolite can be used as a support for them. In this way, as-synthesised layered **MFI** was used as the catalyst of cycloaddition of CO_2 on epoxides, yielding cyclic carbonates (Scheme 7). The surfactant template, used for the synthesis, contains two quaternary ammonium groups. One of them is hidden in the channel system (acting as an anchor), while the other one is located at the pore mouth and thus accessible (acting as an active site).

The nanosponge **MFI** (and also self-pillared-pentasil catalyst) exhibited remarkable activity (in comparison with 3D zeolites **MFI**, ***BEA** and **FAU**) also in Pechmann condensation of pyrogallol and resorcinol with ethylacetoacetate in the liquid phase yielding corresponding dihydroxy-4-methylcoumarins.[207]

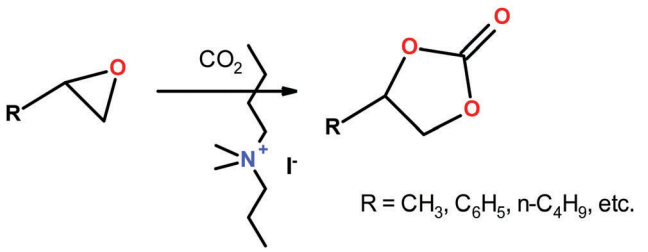

Scheme 7 Quaternary ammonium salt catalysed cycloaddition of CO_2 on epoxides.

Taking into account the number of various transformations that can be catalysed by 2D zeolite-based catalysts, we believe that appropriately shaped 2D zeolite catalysts might become, for organic chemists, a common tool for acid catalysed reactions as, for instance, 4A molecular sieve (**LTA** zeolite) for solvent drying.

7. Conclusions and perspectives

This review covers the current state-of-the-art of synthesis and catalytic properties of zeolites highlighting the most important achievements in recent years and discussing the progress in the research on conventional zeolites, nanozeolites, hierarchical zeolites up to two-dimensional ones.

Synthetic zeolites are typically prepared by crystallization of gels containing water, alkali cations, silica and alumina sources under hydrothermal conditions, basic pH, temperatures in the range 60–200 °C and autogenous pressure. Incorporation of

organic compounds into the synthesis gel enabled discoveries of new zeolite structures, mainly with high silica compositions, since the organics act as structure-directing agents.

Seeding has been widely applied in zeolite synthesis, not just to accelerate the crystallization process, but also as a green route for the organotemplate-free synthesis of zeolites, to decrease reagent cost and environmental impact. Synthetic protocols to minimize the water content during the zeolite crystallization, such as dry-gel conversion, vapour-phase transport, steam-assisted conversion and hydrothermal treatment of wetness-impregnated xerogels have been described recently.

Fluoride-containing media have been employed for the crystallization of zeolites at neutral or even slightly acidic pH to provide large crystals with a low concentration of defects and highly hydrophobic properties. Similarly, microwave heating and ultrasound have been used in zeolite synthesis to reduce the synthesis times allowing a better control of the size and morphology of the crystals.

Although a great number of zeolitic structures have been theoretically predicted, in practice, just a relatively small number has been identified due to the limitations existing for their real synthesis. Thus, by April 2018 the International Zeolite Association recognized 235 different zeolite structures (represented by three-letter framework codes). Recently, the ADOR (assembly–disassembly–organisation–reassembly) methodology has been developed for the preparation of novel zeolite structures that could not be obtained by conventional hydrothermal synthesis. This approach started from zeolite **UTL**, which has been subjected to a number of post-synthesis transformations (hydrolysis, organisation and condensation) in order to generate different zeolite structures. This strategy has been very effective for the development of new zeolite structures, affording in many cases topologies, which are not feasible by direct hydrothermal synthesis.

Classical zeolites are very well known for their acidic and cation-exchange properties, which derives from the extra negative charge associated with the Al tetrahedral sites. Acidity in zeolites arises from Brønsted acid sites associated with framework Al atoms, although they may also contain significant amounts of Lewis acids sites, formed by dehydroxylation of the former or linked to extra-framework Al species. Zeolites may also present basic properties, which are generated by ion-exchange with alkali cations or by incorporation of basic metals and metal oxides.

Increasing the Si/Al ratio has been commonly employed as a method for enhancing the zeolite stability. While this can be achieved in high silica zeolites just by varying the gel composition, for low silica zeolites it is usually accomplished by post-synthesis treatments *via* extraction and removal of Al species. Isomorphous substitution of the Al^{3+} or Si species by other cations leads to different families of zeolitic materials, such as metallosilicates, aluminophosphates and silicoaluminophosphates. These modifications have a strong effect on the zeolite properties, making possible the synthesis of materials with controllable acidity in terms of both strength and type. In this way, replacement of Al by tetravalent cations has yielded materials showing very specific Lewis acidity and redox properties.

Other fundamental features of zeolites are shape selectivity and molecular sieving properties. Since zeolite micropores present diameters very close to the size of many molecules, they are able to discriminate between compounds having just a small variation in their size, so the largest ones cannot penetrate the zeolite structure or diffuse very slowly through the zeolite channels. This fact has a strong effect on the product distribution and, therefore, on the outstanding selectivity exhibited by zeolites in many reactions.

However, at the same time, the small pore size of zeolites strongly limits the application of these materials in processes involving large substrates, which is the case of many transformations within the biomass conversion and fine chemical synthesis. Accordingly, in recent years, an enormous research effort has been devoted to tailoring zeolite properties directly related to their porosity and active site accessibility. New zeolitic materials showing enhanced accessibility and external/mesopore surface area have been developed, which include nano-sized, hierarchical and two-dimensional zeolites. A sequential process can be envisaged in the evolution of conventional 3D zeolites, passing by the reduction of their crystal size below 100 nm (nanozeolites), *i.e.* introduction of a secondary porosity in the mesopore range (hierarchical zeolites) to finally reach lamellar particles (2D zeolites).

A number of relevant advantages have been widely reported when using zeolitic materials with enhanced accessibility as catalysts: possibility of converting bulky compounds that could not enter the micropores, enhanced transport of reactants, intermediates and products, and less pronounced deactivation effects by formation of coke deposits. The overall result coming out is that in many cases these new classes of zeolitic materials show quite better catalytic properties than the conventional zeolites. Moreover, the presence of a high proportion of external/mesopore surface is a very positive aspect when the zeolite is used as a support for other catalysis phases, as it leads to an improved dispersion of the latter with a stronger interaction with the zeolite. The resulting materials present bifunctional or even multifunctional properties, which opens the way for their use in many sectors, beyond the typical fields of zeolite applications.

One example of new catalytic applications of zeolites is the search for sustainable routes to use biomass as a raw material, according to the ''biorefinery'' concept. Catalytic pyrolysis, hydrotreatment, isomerizations, dehydrations, *etc.*, to produce either biofuels or bio-based chemicals, are promoted by acid zeolite catalysts. However, biomass transformation is a complex issue as there are difficulties intrinsic to the features of the raw materials: (a) complex composition; (b) presence of heteroatoms interfering with the catalytic processes and the quality of the final product; (c) high water content and (d) high tendency to deactivate zeolites by coke deposition. Both acidity and porosity are the key features of zeolites influencing activity, selectivity and deactivation resistance by coke deposition in biomass transformation processes. Higher amounts and stronger acid

sites are usually related to higher activities and selectivities to target products. This beneficial effect is counterbalanced by larger amounts of coke and, hence, faster catalyst deactivation. Regarding the porous properties, zeolites with very small micropore sizes exhibit poor activities. To reduce the coke formation and to increase both the activity and selectivity in reactions involving large molecules, different modifications of zeolites have been attempted. Acidic properties can be modulated by variation of the Si/Al ratio, cation exchange and second phase (metals, metal oxides) dispersion. The accessibility of acidic sites for bulky compounds and transport properties are enhanced by increasing the external surface/particle volume ratio or by introducing secondary mesoporosity. The first approach is mainly provided by nanozeolites and, more recently, by 2D zeolites, whereas secondary mesoporosity is typical of hierarchical zeolites. Nevertheless, to attain real beneficial catalytic effects with these porosity-tailored zeolites in reactions of biomass conversion it is necessary to reach a proper balance with their acidic properties. Thus, high density of strong or Brønsted acid sites on the accessible surface should be avoided as they are associated with coke formation or are even poorly active in some interesting reactions, like glucose dehydration to 5-HMF. In this sense, the preparation of bifunctional catalysts by dispersing active phases on zeolites with enhanced textural properties is a very rational way to overcome the aforementioned limitations. Although they have been just scarcely explored at present, 2D zeolites are especially good candidates, so more intensive research work is expected in this area in the near future.

Although zeolites have currently very strong positions in industrial catalytic applications, there are still many challenges that can be improved with regard to their synthesis and possible future applications. Some of them are mentioned here:

(a) Synthesis of important zeolites without organic structure-directing agents. A lot of successful syntheses without organics have been recently performed but some of the interesting zeolites still need organics to be prepared.

(b) Only very few zeolites can be directly synthesized in the whole range of Si/Al ratios from 1 to infinity. In most cases, we need to apply various post-synthesis methods to adjust the chemical composition.

(c) Location of active sites in zeolite frameworks, inside of the channels *versus* on the external surface, in different pores for zeolites having more than one type of channels, is still a matter of accidental synthesis than a scientific concept.

(d) Less than 20 zeolites have been prepared as two-dimensional analogues; however, we can believe that maybe all the zeolites will be prepared in 2D forms, which could substantially enhance the possibility for their applications.

These four points clearly indicate that despite the very strong position of zeolites in laboratories and industry, there are many possible improvements. Hopefully, this review will help in achieving them soon.

Conflicts of interest

There are no conflicts to declare.

Acknowledgements

J. P. and J. Č. acknowledge the Charles University Centre of Advanced Materials (CUCAM) (OP VVV Excellent Research Teams, project number CZ.02.1.01/0.0/0.0/15_003/0000417) and the Czech Science Foundation (P106/12/G015). J. Č., P. P., and D. S. gratefully acknowledge the financial support from the European Union Seventh Framework Programme (FP7/2007–2013) under grant agreement no. 604307 (CASCATBEL project). P. P. and D. S. also acknowledge the funding received from the Spanish Ministry of Economy and Competitiveness through the CATPLASBIO project (Ref. CTQ2014-602209-R).

References

1 S. Al-Khattaf, S. A. Ali, A. M. Aitani, N. Zilkova, D. Kubicka and J. Cejka, *Catal. Rev.: Sci. Eng.*, 2014, **56**, 333–402.
2 A. Burton, *Catal. Rev.: Sci. Eng.*, 2018, **60**, 132–175.
3 A. Corma, *J. Catal.*, 2003, **216**, 298–312.
4 J. L. Sun, C. Bonneau, A. Cantin, A. Corma, M. J. Diaz-Cabanas, M. Moliner, D. L. Zhang, M. R. Li and X. D. Zou, *Nature*, 2009, **458**, U1154–U1190.
5 J. Perez-Ramirez, C. H. Christensen, K. Egeblad, C. H. Christensen and J. C. Groen, *Chem. Soc. Rev.*, 2008, **37**, 2530–2542.
6 J. Perez-Ramirez, S. Mitchell, D. Verboekend, M. Milina, N. L. Michels, F. Krumeich, N. Marti and M. Erdmann, *ChemCatChem*, 2011, **3**, 1731–1734.
7 L. Gueudre, M. Milina, S. Mitchell and J. Perez-Ramirez, *Adv. Funct. Mater.*, 2014, **24**, 209–219.
8 W. J. Roth and J. Čejka, *Catal. Sci. Technol.*, 2011, **1**, 43–53.
9 W. J. Roth, P. Nachtigall, R. E. Morris and J. Čejka, *Chem. Rev.*, 2014, **114**, 4807–4837.
10 M. V. Opanasenko, W. J. Roth and J. Cejka, *Catal. Sci. Technol.*, 2016, **6**, 2467–2484.
11 F. S. O. Ramos, M. K. De Pietre and H. O. Pastore, *RSC Adv.*, 2013, **3**, 2084–2111.
12 L. Tosheva and V. P. Valtchev, *Chem. Mater.*, 2005, **17**, 2494–2513.
13 S. Maheshwari, C. Martínez, M. Teresa Portilla, F. J. Llopis, A. Corma and M. Tsapatsis, *J. Catal.*, 2010, **272**, 298–308.
14 D. P. Serrano, R. Sanz, P. Pizarro and I. Moreno, *Appl. Catal., A*, 2012, **435-436**, 32–42.
15 C. S. Cundy and P. A. Cox, *Chem. Rev.*, 2003, **103**, 663–702.
16 M. E. Davis and R. F. Lobo, *Chem. Mater.*, 1992, **4**, 756–768.
17 K. G. Strohmaier, in *Zeolites in Catalysis. Properties and Applications* ed. J. Čejka, R. E. Morris and P. Nachtigall, 2017, pp. 73–97.
18 D. P. Serrano and R. van Grieken, *J. Mater. Chem.*, 2001, **11**, 2391–2407.
19 C. S. Cundy and P. A. Cox, *Microporous Mesoporous Mater.*, 2005, **82**, 1–78.
20 Y. Ji, Y. Wang, B. Xie and F.-S. Xiao, *Comments Inorg. Chem.*, 2016, **36**, 1–16.
21 Y. Wang, Q. Wu, X. Meng and F.-S. Xiao, *Engineering*, 2017, **3**, 567–574.

22 X. Meng, Q. Wu, F. Chen and F.-S. Xiao, *Sci. China: Chem.*, 2015, **58**, 6–13.
23 D. P. Serrano, M. A. Uguina, G. Ovejero, R. Van Grieken and M. Camacho, *Chem. Commun.*, 1996, 1097–1098.
24 D. P. Serrano, M. A. Uguina, G. Ovejero, R. Van Grieken and M. Camacho, *Microporous Mater.*, 1996, **7**, 309–321.
25 X. Meng and F.-S. Xiao, *Chem. Rev.*, 2014, **114**, 1521–1543.
26 M. A. Camblor, A. Corma and S. Valencia, *J. Mater. Chem.*, 1998, **8**, 2137–2145.
27 D. P. Serrano, R. Van Grieken, P. Sánchez, R. Sanz and L. Rodríguez, *Microporous Mesoporous Mater.*, 2001, **46**, 35–46.
28 S. I. Zones, R. J. Darton, R. Morris and S.-J. Hwang, *J. Phys. Chem. B*, 2005, **109**, 652–661.
29 Y. Li and W. Yang, *J. Membr. Sci.*, 2008, **316**, 3–17.
30 S. Askari, S. Miar Alipour, R. Halladj and M. H. Davood Abadi Farahani, *J. Porous Mater.*, 2013, **20**, 285–302.
31 P. Eliášová, M. Opanasenko, P. S. Wheatley, M. Shamzhy, M. Mazur, P. Nachtigall, W. J. Roth, R. E. Morris and J. Cejka, *Chem. Soc. Rev.*, 2015, **44**, 7177–7206.
32 R. Pophale, P. A. Cheeseman and M. W. Deem, *Phys. Chem. Chem. Phys.*, 2011, **13**, 12407–12412.
33 R. Millini and G. Bellussi, in *Zeolites in Catalysis: Properties and Applications*, ed. J. Čejka, R. E. Morris and P. Nachtigall, 2017, pp. 1–28.
34 J.-P. Gilson and M. Guisnet, *Zeolites For Cleaner Technologies*, Imperial College Press, 2002.
35 E. G. Derouane, J. C. Védrine, R. R. Pinto, P. M. Borges, L. Costa, M. A. N. D. A. Lemos, F. Lemos and F. R. Ribeiro, *Catal. Rev.*, 2013, **55**, 454–515.
36 L.-E. Sandoval-Díaz, J.-A. González-Amaya and C.-A. Trujillo, *Microporous Mesoporous Mater.*, 2015, **215**, 229–243.
37 D. Barthomeuf, *Catal. Rev.*, 1996, **38**, 521–612.
38 R. J. Davis, *J. Catal.*, 2003, **216**, 396–405.
39 J. Jae, G. A. Tompsett, A. J. Foster, K. D. Hammond, S. M. Auerbach, R. F. Lobo and G. W. Huber, *J. Catal.*, 2011, **279**, 257–268.
40 S. M. Csicsery, *Zeolites*, 1984, **4**, 202–213.
41 P. B. Weisz and V. J. Frilette, *J. Phys. Chem.*, 1960, **64**, 382.
42 N. Van-Den-Begin, L. V. C. Rees, J. Caro and M. Bülow, *Zeolites*, 1989, **9**, 287–292.
43 S. L. Burkett and M. E. Davis, *Chem. Mater.*, 1995, **7**, 920–928.
44 M. A. Camblor, A. Corma and S. Valencia, *Chem. Commun.*, 1996, 2365–2366.
45 G. T. Kerr, *J. Phys. Chem.*, 1969, **73**, 2780–2782.
46 A. Corma, M. Faraldos and A. Mifsud, *Appl. Catal.*, 1989, **47**, 125–133.
47 L. Brabec, M. Jeschke, R. Klik, J. Nováková, L. Kubelková, D. Freude, V. Bosáček and J. Meusinger, *Appl. Catal., A*, 1998, **167**, 309–320.
48 T. Inui, S. Iwamoto, S. Kojo and T. Yoshida, *Catal. Lett.*, 1992, **13**, 87–93.
49 B. Kraushaar and J. H. C. Van Hooff, *Catal. Lett.*, 1988, **1**, 81–84.
50 A. Tuel, S. Moussa-Khouzami, Y. B. Taarit and C. Naccache, *J. Mol. Catal.*, 1991, **68**, 45–52.
51 G. Wu, Y. Wang, L. Wang, W. Feng, H. Shi, Y. Lin, T. Zhang, X. Jin, S. Wang, X. Wu and P. Yao, *Chem. Eng. J.*, 2013, **215-216**, 306–314.
52 H. Y. Luo, J. D. Lewis and Y. Román-Leshkov, *Annu. Rev. Chem. Biomol. Eng.*, 2016, **7**, 663–692.
53 R. Bai, Q. Sun, N. Wang, Y. Zou, G. Guo, S. Iborra, A. Corma and J. Yu, *Chem. Mater.*, 2016, **28**, 6455–6458.
54 W. M. H. Sachtler and Z. Zhang, in *Advances in Catalysis*, ed. D. D. Eley, H. Pines and P. B. Weisz, Academic Press, 1993, vol. 39, pp. 129–220.
55 J. Guzman and B. C. Gates, *Dalton Trans.*, 2003, 3303–3318.
56 P. Mériaudeau and C. Naccache, *Catal. Rev.*, 1997, **39**, 5–48.
57 T. Barakat, J. C. Rooke, H. L. Tidahy, M. Hosseini, R. Cousin, J. F. Lamonier, J. M. Giraudon, G. De Weireld, B. L. Su and S. Siffert, *ChemSusChem*, 2011, **4**, 1420–1430.
58 R. S. Gomez, X. Li, R. L. Yson and H. H. Patterson, *Res. Chem. Intermed.*, 2011, **37**, 729–745.
59 A. Kumbhar, *Top. Curr. Chem.*, 2016, **375**, 2.
60 E. Koohsaryan and M. Anbia, *Chin. J. Catal.*, 2016, **37**, 447–467.
61 V. Valtchev and L. Tosheva, *Chem. Rev.*, 2013, **113**, 6734–6760.
62 T. Tago, H. Konno, Y. Nakasaka and T. Masuda, *Catal. Surv. Asia*, 2012, **16**, 148–163.
63 Y. Yan, X. Guo, Y. Zhang and Y. Tang, *Catal. Sci. Technol.*, 2015, **5**, 772–785.
64 S. Mintova, J. Grand and V. Valtchev, *C. R. Chim*, 2016, **19**, 183–191.
65 N. N. Feoktistova, S. P. Zhdanov, W. Lutz and M. Büllow, *Zeolites*, 1989, **9**, 136–139.
66 S. Mintova, V. Valtchev, E. Vultcheva and S. Veleva, *Zeolites*, 1992, **12**, 210–215.
67 V. P. Valtchev and K. N. Bozhilov, *J. Phys. Chem. B*, 2004, **108**, 15587–15598.
68 Y. Huang, K. Wang, D. Dong, D. Li, M. R. Hill, A. J. Hill and H. Wang, *Microporous Mesoporous Mater.*, 2010, **127**, 167–175.
69 D. Hu, Q. H. Xia, X. H. Lu, X. B. Luo and Z. M. Liu, *Mater. Res. Bull.*, 2008, **43**, 3553–3561.
70 S. N. Azizi, S. Ghasemi and S. Kavian, *Biosens. Bioelectron.*, 2014, **62**, 1–7.
71 S. Kavian, S. N. Azizi and S. Ghasemi, *J. Mol. Liq.*, 2016, **218**, 663–669.
72 E.-P. Ng, H. Awala, K.-H. Tan, F. Adam, R. Retoux and S. Mintova, *Microporous Mesoporous Mater.*, 2015, **204**, 204–209.
73 H. Zhang, H. Zhang, P. Wang, Y. Zhao, Z. Shi, Y. Zhang and Y. Tang, *RSC Adv.*, 2016, **6**, 47623–47631.
74 B. Xie, J. Song, L. Ren, Y. Ji, J. Li and F.-S. Xiao, *Chem. Mater.*, 2008, **20**, 4533–4535.
75 G. Reding, T. Mäurer and B. Kraushaar-Czarnetzki, *Microporous Mesoporous Mater.*, 2003, **57**, 83–92.
76 G. Majano, A. Darwiche, S. Mintova and V. Valtchev, *Ind. Eng. Chem. Res.*, 2009, **48**, 7084–7091.
77 Z. Chen, S. Li and Y. Yan, *Chem. Mater.*, 2005, **17**, 2262–2266.

78 M. Mehdipourghazi, A. Moheb and H. Kazemian, *Microporous Mesoporous Mater.*, 2010, **136**, 18–24.
79 Y. Pan, M. Ju, J. Yao, L. Zhang and N. Xu, *Chem. Commun.*, 2009, 7233–7235.
80 C.-X. Zhao, L. He, S. Z. Qiao and A. P. J. Middelberg, *Chem. Eng. Sci.*, 2011, **66**, 1463–1479.
81 Y. Huang and A. J. Hill, AIChE Annual Meeting, Conference proceedings, 2008.
82 X. Ke, C. Zeng, L. Zhang and N. Xu, *Shiyou Huagong/Petrochemical Technology*, 2005, **34**, 486–490.
83 Z. L. Sun, Y. G. Wang, J. Z. Gui, X. T. Zhang and G. Su, *Shiyou Huagong Gaodeng Xuexiao Xuebao/Journal of Petrochemical Universities*, 2005, **18**, 15–19.
84 A. Charkhi, H. Kazemian and M. Kazemeini, *Powder Technol.*, 2010, **203**, 389–396.
85 A. Nezamzadeh-Ejhieh and S. Khorsandi, *J. Ind. Eng. Chem.*, 2014, **20**, 937–946.
86 T. Kurniawan, O. Muraza, A. S. Hakeem and A. M. Al-Amer, *Cryst. Growth Des.*, 2017, **17**, 3313–3320.
87 H. Wang, L. Huang, Z. Wang, A. Mitra and Y. Yan, *Chem. Commun.*, 2001, 1364–1365.
88 Y. Wang, Y. Tang, A. Dong, X. Wang, N. Ren and Z. Gao, *J. Mater. Chem.*, 2002, **12**, 1812–1818.
89 M. Hartmann, *Angew. Chem., Int. Ed.*, 2004, **43**, 5880–5882.
90 C. Schomburg, D. Wöhrle and G. Schulz-Ekloff, *Zeolites*, 1996, **17**, 232–236.
91 C. J. H. Jacobsen, C. Madsen, J. Houzvicka, I. Schmidt and A. Carlsson, *J. Am. Chem. Soc.*, 2000, **122**, 7116–7117.
92 Y. Wang, L. Ma, N. Zhu, F. Chen and X. Zhan, *Prog. Chem.*, 2009, **21**, 1722–1733.
93 D. P. Serrano, J. Aguado and J. M. Escola, *Catalysis*, 2011, **23**, 253–283.
94 D. Verboekend, S. Mitchell and J. Pérez-Ramírez, *Chimia*, 2013, **67**, 327–332.
95 D. P. Serrano, J. M. Escola and P. Pizarro, *Chem. Soc. Rev.*, 2013, **42**, 4004–4035.
96 Y. Wei, T. E. Parmentier, K. P. De Jong and J. Zečević, *Chem. Soc. Rev.*, 2015, **44**, 7234–7261.
97 W. Schwieger, A. G. Machoke, T. Weissenberger, A. Inayat, T. Selvam, M. Klumpp and A. Inayat, *Chem. Soc. Rev.*, 2016, **45**, 3353–3376.
98 M. Hartmann, A. G. Machoke and W. Schwieger, *Chem. Soc. Rev.*, 2016, **45**, 3313–3330.
99 M. L. Occelli and P. O'Connor, *Stud. Surf. Sci. Catal.*, 2001, **134**, 1.
100 W. J. Roth, O. V. Shvets, M. Shamzhy, P. Chlubná, M. Kubů, P. Nachtigall and J. Čejka, *J. Am. Chem. Soc.*, 2011, **133**, 6130–6133.
101 W. J. Roth, P. Nachtigall, R. E. Morris, P. S. Wheatley, V. R. Seymour, S. E. Ashbrook, P. Chlubna, L. Grajciar, M. Polozij, A. Zukal, O. Shvets and J. Cejka, *Nat. Chem.*, 2013, **5**, 628–633.
102 P. Chlubná, W. J. Roth, H. F. Greer, W. Z. Zhou, O. Shvets, A. Zukal, J. Čejka and R. E. Morris, *Chem. Mater.*, 2013, **25**, 542–547.
103 M. Ogura, S. Y. Shinomiya, J. Tateno, Y. Nara, E. Kikuchi and M. Matsukata, *Chem. Lett.*, 2000, 882–883.
104 J. Peréz-Ramírez, D. Verboekend, A. Bonilla and S. Abelló, *Adv. Funct. Mater.*, 2009, **19**, 3972–3979.
105 D. Verboekend and J. Pérez-Ramírez, *Catal. Sci. Technol.*, 2011, **1**, 879–890.
106 Z. Qin, L. Lakiss, J. P. Gilson, K. Thomas, J. M. Goupil, C. Fernandez and V. Valtchev, *Chem. Mater.*, 2013, **25**, 2759–2766.
107 L. Brabec and M. Kočiřík, *Mater. Chem. Phys.*, 2007, **102**, 67–74.
108 Z. Qin, G. Melinte, J. P. Gilson, M. Jaber, K. Bozhilov, P. Boullay, S. Mintova, O. Ersen and V. Valtchev, *Angew. Chem., Int. Ed.*, 2016, **55**, 15049–15052.
109 I. Schmidt, A. Boisen, E. Gustavsson, K. Ståhl, S. Pehrson, S. Dahl, A. Carlsson and C. J. H. Jacobsen, *Chem. Mater.*, 2001, **13**, 4416–4418.
110 S. S. Kim, J. Shah and T. J. Pinnavaia, *Chem. Mater.*, 2003, **15**, 1664–1668.
111 Z. Yang, Y. Xia and R. Mokaya, *Adv. Mater.*, 2004, **16**, 727–732.
112 M. Y. Kustova, P. Hasselriis and C. H. Christensen, *Catal. Lett.*, 2004, **96**, 205–211.
113 M. Y. Kustova, A. L. Kustov and C. H. Christensen, *Stud. Surf. Sci. Catal.*, 2005, **158A**, 255–262.
114 H. Chen, J. Wydra, X. Zhang, P. S. Lee, Z. Wang, W. Fan and M. Tsapatsis, *J. Am. Chem. Soc.*, 2011, **133**, 12390–12393.
115 H. S. Cho and R. Ryoo, *Microporous Mesoporous Mater.*, 2012, **151**, 107–112.
116 J. B. Koo, N. Jiang, S. Saravanamurugan, M. Bejblova, Z. Musilova, J. Čejka and S. E. Park, *J. Catal.*, 2010, **276**, 327–334.
117 J. Zhou, Z. Hua, X. Cui, Z. Ye, F. Cui and J. Shi, *Chem. Commun.*, 2010, **46**, 4994–4996.
118 C. Li, Y. Wang, B. Shi, J. Ren, X. Liu, Y. Wang, Y. Guo, Y. Guo and G. Lu, *Microporous Mesoporous Mater.*, 2009, **117**, 104–110.
119 M. B. Yue, L. B. Sun, T. T. Zhuang, X. Dong, Y. Chun and J. H. Zhu, *J. Mater. Chem.*, 2008, **18**, 2044–2050.
120 Y. Wang, Y. Tang, X. Wang, W. Shan, A. Dong, N. Ren and Z. Gao, *Chem. Lett.*, 2002, 862–863.
121 H. Yang, Z. Liu, H. Gao and Z. Xie, *Appl. Catal., A*, 2010, **379**, 166–171.
122 F. S. Xiao, L. Wang, C. Yin, K. Lin, Y. Di, J. Li, R. Xu, D. S. Su, R. Schlögl, T. Yokoi and T. Tatsumi, *Angew. Chem., Int. Ed.*, 2006, **45**, 3090–3093.
123 B. T. Holland, L. Abrams and A. Stein, *J. Am. Chem. Soc.*, 1999, **121**, 4308–4309.
124 F. Liu, T. Willhammar, L. Wang, L. Zhu, Q. Sun, X. Meng, W. Carrillo-Cabrera, X. Zou and F. S. Xiao, *J. Am. Chem. Soc.*, 2012, **134**, 4557–4560.
125 J. Zhao, Y. Yin, Y. Li, W. Chen and B. Liu, *Chem. Eng. J.*, 2016, **284**, 405–411.
126 D. P. Serrano, J. Aguado, J. M. Escola, J. M. Rodríguez and A. Peral, *Chem. Mater.*, 2006, **18**, 2462–2464.
127 H. Wang and T. J. Pinnavaia, *Angew. Chem., Int. Ed.*, 2006, **45**, 7603–7606.

128 M. Choi, H. S. Cho, R. Srivastava, C. Venkatesan, D. H. Choi and R. Ryoo, *Nat. Mater.*, 2006, **5**, 718–723.
129 V. N. Shetti, J. Kim, R. Srivastava, M. Choi and R. Ryoo, *J. Catal.*, 2008, **254**, 296–303.
130 D. P. Serrano, J. Aguado, J. M. Escola, J. M. Rodriguez and A. Peral, *J. Mater. Chem.*, 2008, **18**, 4210–4218.
131 J. Aguado, D. P. Serrano and J. M. Rodríguez, *Microporous Mesoporous Mater.*, 2008, **115**, 504–513.
132 D. P. Serrano, J. Aguado, G. Morales, J. M. Rodríguez, A. Peral, M. Thommes, J. P. Epping and B. F. Chmelka, *Chem. Mater.*, 2009, **21**, 641–654.
133 D. P. Serrano, unpublished work.
134 J. García-Martínez, M. Johnson, J. Valla, K. Li and J. Y. Ying, *Catal. Sci. Technol.*, 2012, **2**, 987–994.
135 I. I. Ivanova and E. E. Knyazeva, *Chem. Soc. Rev.*, 2013, **42**, 3671–3688.
136 A. Sachse and J. García-Martínez, *Chem. Mater.*, 2017, **29**, 3827–3853.
137 A. Sachse, A. Grau-Atienza, E. O. Jardim, N. Linares, M. Thommes and J. García-Martínez, *Cryst. Growth Des.*, 2017, **17**, 4289–4305.
138 N. Linares, A. Sachse, E. Serrano, A. Grau-Atienza, E. De Oliveira Jardim, J. Silvestre-Albero, M. A. L. Cordeiro, F. Fauth, G. Beobide, O. Castillo and J. García-Martínez, *Chem. Mater.*, 2016, **28**, 8971–8979.
139 D. Verboekend, R. Caicedo-Realpe, A. Bonilla, M. Santiago and J. Pérez-Ramírez, *Chem. Mater.*, 2010, **22**, 4679–4689.
140 D. Verboekend, T. C. Keller, M. Milina, R. Hauert and J. Pérez-Ramírez, *Chem. Mater.*, 2013, **25**, 1947–1959.
141 D. P. Serrano, R. Sanz, P. Pizarro, I. Moreno and S. Shami, *Microporous Mesoporous Mater.*, 2014, **189**, 71–82.
142 D. P. Serrano, J. M. Escola, R. Sanz, R. A. Garcia, A. Peral, I. Moreno and M. Linares, *New J. Chem.*, 2016, **40**, 4206–4216.
143 J. M. Escola, D. P. Serrano, R. Sanz, R. A. Garcia, A. Peral, I. Moreno and M. Linares, *Catal. Today*, 2018, **304**, 89–96.
144 D. P. Serrano, T. J. Pinnavaia, J. Aguado, J. M. Escola, A. Peral and L. Villalba, *Catal. Today*, 2014, **227**, 15–25.
145 A. Boisen, I. Schmidt, A. Carlsson, S. Dahl, M. Brorson and C. J. H. Jacobsen, *Chem. Commun.*, 2003, 958–959.
146 M. H. F. Kox, E. Stavitski, J. C. Groen, J. Pérez-Ramírez, F. Kapteijn and B. M. Weckhuysen, *Chem. – Eur. J.*, 2008, **14**, 1718–1725.
147 Y. Liu, W. Zhang, Z. Liu, S. Xu, Y. Wang, Z. Xie, X. Han and X. Bao, *J. Phys. Chem. C*, 2008, **112**, 15375–15381.
148 J. Jagiello, M. Sterling, P. Eliasova, M. Opanasenko, A. Zukal, R. E. Morris, M. Navaro, A. Mayoral, P. Crivelli, R. Warringham, S. Mitchell, J. Perez-Ramirez and J. Cejka, *Phys. Chem. Chem. Phys.*, 2016, **18**, 15269–15277.
149 S. Lee, C. Jo and R. Ryoo, *J. Mater. Chem. A*, 2017, **5**, 11086–11093.
150 J. Aguado, D. P. Serrano, J. M. Escola and J. M. Rodríguez, *Microporous Mesoporous Mater.*, 2004, **75**, 41–49.
151 D. P. Serrano, J. M. Escola and P. Pizarro, *Mesoporous Zeolites: Preparation, Characterization and Applications*, 2015, pp. 157–198.
152 C. H. Christensen, K. Johannsen, E. Törnqvist, I. Schmidt, H. Topsøe and C. H. Christensen, *Catal. Today*, 2007, **128**, 117–122.
153 J. C. Groen, W. Zhu, S. Brouwer, S. J. Huynink, F. Kapteijn, J. A. Moulijn and J. Pérez-Ramírez, *J. Am. Chem. Soc.*, 2007, **129**, 355–360.
154 R. Valiullin, J. Kärger, K. Cho, M. Choi and R. Ryoo, *Microporous Mesoporous Mater.*, 2011, **142**, 236–244.
155 H. Zhao, J. Ma, Q. Zhang, Z. Liu and R. Li, *Ind. Eng. Chem. Res.*, 2014, **53**, 13810–13819.
156 M. S. Holm, S. Svelle, F. Joensen, P. Beato, C. H. Christensen, S. Bordiga and M. Bjørgen, *Appl. Catal., A*, 2009, **356**, 23–30.
157 K. Suzuki, Y. Aoyagi, N. Katada, M. Choi, R. Ryoo and M. Niwa, *Catal. Today*, 2008, **132**, 38–45.
158 D. P. Serrano, R. A. Garcia, G. Vicente, M. Linares, D. Prochazkova and J. Cejka, *J. Catal.*, 2011, **279**, 366–380.
159 D. P. Serrano, R. A. García, M. Linares and B. Gil, *Catal. Today*, 2012, **179**, 91–101.
160 F. Thibault-Starzyk, I. Stan, S. Abello, A. Bonilla, K. Thomas, C. Fernandez, J. P. Gilson and J. Perez-Ramirez, *J. Catal.*, 2009, **264**, 11–14.
161 K. Sadowska, K. Góra-Marek and J. Datka, *J. Phys. Chem. C*, 2013, **117**, 9237–9244.
162 R. Srivastava, M. Choi and R. Ryoo, *Chem. Commun.*, 2006, 4489–4491.
163 J. Kim, M. Choi and R. Ryoo, *J. Catal.*, 2010, **269**, 219–228.
164 L. Lakiss, F. Ngoye, C. Canaff, S. Laforge, Y. Pouilloux, Z. Qin, M. Tarighi, K. Thomas, V. Valtchev, A. Vicente, L. Pinard, J. P. Gilson and C. Fernandez, *J. Catal.*, 2015, **328**, 165–172.
165 M. Kustova, K. Egeblad, C. H. Christensen, A. L. Kustov and C. H. Christensen, *Stud. Surf. Sci. Catal.*, 2007, **170**, 267–275.
166 B. Liu, K. Xie, S. C. Oh, D. Sun, Y. Fang and H. Xi, *Chem. Eng. Sci.*, 2016, **153**, 374–381.
167 D. Verboekend, K. Thomas, M. Milina, S. Mitchell, J. Pérez-Ramírez and J. P. Gilson, *Catal. Sci. Technol.*, 2011, **1**, 1331–1335.
168 A. Martínez, M. A. Arribas, M. Derewinski and A. Burkat-Dulak, *Appl. Catal., A*, 2010, **379**, 188–197.
169 J. M. Escola, J. Aguado, D. P. Serrano, L. Briones, J. L. Díaz De Tuesta, R. Calvo and E. Fernandez, *Energy Fuels*, 2012, **26**, 3187–3195.
170 X. Peng, K. Cheng, J. Kang, B. Gu, X. Yu, Q. Zhang and Y. Wang, *Angew. Chem., Int. Ed.*, 2015, **54**, 4553–4556.
171 B. Puértolas, L. García-Andújar, T. García, M. V. Navarro, S. Mitchell and J. Pérez-Ramírez, *Appl. Catal., B*, 2014, **154-155**, 161–170.
172 C. H. Christensen, I. Schmidt, A. Carlsson, K. Johannsen and K. Herbst, *J. Am. Chem. Soc.*, 2005, **127**, 8098–8102.
173 X. Shen, J. Kang, W. Niu, M. Wang, Q. Zhang and Y. Wang, *Catal. Sci. Technol.*, 2017, **7**, 3598–3612.
174 N. Jiang, H. Jin, E. Y. Jeong and S. E. Park, *J. Nanosci. Nanotechnol.*, 2010, **10**, 227–232.
175 W. Fu, L. Zhang, D. Wu, M. Xiang, Q. Zhuo, K. Huang, Z. Tao and T. Tang, *J. Catal.*, 2015, **330**, 423–433.

176 A. Berenguer, J. A. Bennett, J. Hunns, I. Moreno, J. M. Coronado, A. F. Lee, P. Pizarro, K. Wilson and D. P. Serrano, *Catal. Today*, 2018, **304**, 72–79.
177 Y. Zhao, W. Lv, N. Lu, X. Shi, B. Fan and R. Li, *Microporous Mesoporous Mater.*, 2018, **257**, 35–41.
178 X. F. Guo and G. J. Kim, *Top. Catal.*, 2010, **53**, 510–516.
179 K. Zhu, J. Hu, X. She, J. Liu, Z. Nie, Y. Wang, C. H. F. Peden and H. K. Ja, *J. Am. Chem. Soc.*, 2009, **131**, 9715–9721.
180 S. Mitchell and J. Pérez-Ramírez, *Catal. Today*, 2011, **168**, 28–37.
181 L. Zhou, Z. Liu, M. Shi, S. Du, Y. Su, X. Yang and J. Xu, *Carbohydr. Polym.*, 2013, **98**, 146–151.
182 C. J. Heard, J. Čejka, M. Opanasenko, P. Nachtigall, G. Centi and S. Perathoner, *Adv. Mater.*, 2018, 1801712.
183 W. J. Roth, B. Gil, W. Makowski, B. Marszalek and P. Eliasova, *Chem. Soc. Rev.*, 2016, **45**, 3400–3438.
184 B. Marler, Y. Wang, J. Song and H. Gies, *Dalton Trans.*, 2014, **43**, 10396–10416.
185 R. Ravishankar, T. Sen, V. Ramaswamy, H. S. Soni, S. Ganapathy and S. Sivasanker, in *Studies in Surface Science and Catalysis*, ed. J. Weitkamp, H. G. Karge, H. Pfeifer and W. Hölderich, Elsevier, 1994, vol. 84, pp. 331–338.
186 L. Puppe and J. Weisser, *US Pat.*, 4439409, Bayer Aktiengesselschaft, 1984.
187 S. I. Zones, EP0231860, Chevron Research Company, 1987.
188 M. K. Rubin and P. Chu, *US Pat.*, 4954325, ExxonMobil Oil Corp., 1990.
189 R. Millini, G. Perego, W. O. Parker Jr, G. Bellussi and L. Carluccio, *Microporous Mater.*, 1995, **4**, 221–230.
190 M. E. Leonowicz, J. A. Lawton, S. L. Lawton and M. K. Rubin, *Science*, 1994, **264**, 1910–1913.
191 W. J. Roth, C. T. Kresge, J. C. Vartuli, M. E. Leonowicz, A. S. Fung and S. B. McCullen, *Stud. Surf. Sci. Catal.*, 1995, **94**, 301–308.
192 S. L. Lawton, A. S. Fung, G. J. Kennedy, L. B. Alemany, C. D. Chang, G. H. Hatzikos, D. N. Lissy, M. K. Rubin, H.-K. C. Timken, S. Steuernagel and D. E. Woessner, *J. Phys. Chem.*, 1996, **100**, 3788–3798.
193 W. J. Roth, *Stud. Surf. Sci. Catal.*, 2005, **158A and B**, 19–26.
194 L. Xu, X. Ji, S. Li, Z. Zhou, X. Du, J. Sun, F. Deng, S. Che and P. Wu, *Chem. Mater.*, 2016, **28**, 4512–4521.
195 R. P. D. Graham, *Proceedings and transactions of the Royal Society of Canada. Délibérations et mémoires de la Société royale du Canada*, Royal Society of Canada, Ottawa, 1918, vol. 12, ser. 3, pp. 185–190.
196 L. Schreyeck, P. Caullet, J. C. Mougenel, J. L. Guth and B. Marler, *Microporous Mater.*, 1996, **6**, 259–271.
197 T. Ikeda, Y. Akiyama, Y. Oumi, A. Kawai and F. Mizukami, *Angew. Chem., Int. Ed.*, 2004, **43**, 4892–4896.
198 D. L. Dorset and G. J. Kennedy, *J. Phys. Chem. B*, 2004, **108**, 15216–15222.
199 Z. Zhao, W. Zhang, P. Ren, X. Han, U. Müller, B. Yilmaz, M. Feyen, H. Gies, F.-S. Xiao, D. De Vos, T. Tatsumi and X. Bao, *Chem. Mater.*, 2013, **25**, 840–847.
200 W. J. Roth, B. Gil, W. Makowski, A. Sławek, J. Grzybek, M. Kubu and J. Čejka, *Chem. Mater.*, 2016, **28**, 3616–3619.
201 U. Díaz and A. Corma, *Dalton Trans.*, 2014, **43**, 10292–10316.
202 A. W. Burton and S. I. Zones, in *Studies in Surface Science and Catalysis*, ed. J. Čejka, H. van Bekkum, A. Corma and F. Schüth, Elsevier, 2007, vol. 168, pp. 137–179.
203 M. Choi, K. Na, J. Kim, Y. Sakamoto, O. Terasaki and R. Ryoo, *Nature*, 2009, **461**, 828.
204 C. T. Kresge, M. E. Leonowicz, W. J. Roth, J. C. Vartuli and J. S. Beck, *Nature*, 1992, **359**, 710–712.
205 J. S. Beck, J. C. Vartuli, W. J. Roth, M. E. Leonowicz, C. T. Kresge, K. D. Schmitt, C. T. W. Chu, D. H. Olson, E. W. Sheppard, S. B. McCullen, J. B. Higgins and J. L. Schlenker, *J. Am. Chem. Soc.*, 1992, **114**, 10834–10843.
206 L. Meng, B. Mezari, M. G. Goesten and E. J. M. Hensen, *Chem. Mater.*, 2017, **29**, 4091–4096.
207 J.-C. Kim, R. Ryoo, M. V. Opanasenko, M. V. Shamzhy and J. Čejka, *ACS Catal.*, 2015, **5**, 2596–2604.
208 X. Zhang, D. Liu, D. Xu, S. Asahina, K. A. Cychosz, K. V. Agrawal, Y. Al Wahedi, A. Bhan, S. Al Hashimi, O. Terasaki, M. Thommes and M. Tsapatsis, *Science*, 2012, **336**, 1684–1687.
209 W. Park, D. Yu, K. Na, K. E. Jelfs, B. Slater, Y. Sakamoto and R. Ryoo, *Chem. Mater.*, 2011, **23**, 5131–5137.
210 J. G. Wang, L. Xu, K. Zhang, H. G. Peng, H. H. Wu, J. G. Jiang, Y. M. Liu and P. Wu, *J. Catal.*, 2012, **288**, 16–23.
211 K. Na, M. Choi, W. Park, Y. Sakamoto, O. Terasaki and R. Ryoo, *J. Am. Chem. Soc.*, 2010, **132**, 4169–4177.
212 J. Jung, C. Jo, K. Cho and R. Ryoo, *J. Mater. Chem.*, 2012, **22**, 4637–4640.
213 K. Na, C. Jo, J. Kim, K. Cho, J. Jung, Y. Seo, R. J. Messinger, B. F. Chmelka and R. Ryoo, *Science*, 2011, **333**, 328–332.
214 A. G. Machoke, I. Y. Knoke, S. Lopez-Orozco, M. Schmiele, T. Selvam, V. R. R. Marthala, E. Spiecker, T. Unruh, M. Hartmann and W. Schwieger, *Microporous Mesoporous Mater.*, 2014, **190**, 324–333.
215 R. Wei, H. Yang, J. A. Scott, K.-F. Aguey-Zinsou and D. Zhang, *Appl. Mater. Today*, 2018, **11**, 22–33.
216 W. Kim, J.-C. Kim, J. Kim, Y. Seo and R. Ryoo, *ACS Catal.*, 2013, **3**, 192–195.
217 F. Marques Mota, P. Eliasova, J. Jung and R. Ryoo, *Catal. Sci. Technol.*, 2016, **6**, 2653–2662.
218 C. Jo, K. Cho, J. Kim and R. Ryoo, *Chem. Commun.*, 2014, **50**, 4175–4177.
219 S. W. Han, J. Kim and R. Ryoo, *Microporous Mesoporous Mater.*, 2017, **240**, 123–129.
220 C. Jo, Y. Seo, K. Cho, J. Kim, H. S. Shin, M. Lee, J.-C. Kim, S. O. Kim, J. Y. Lee, H. Ihee and R. Ryoo, *Angew. Chem., Int. Ed.*, 2014, **53**, 5117–5121.
221 H. L. Chen, S. W. Li and Y. M. Wang, *J. Mater. Chem. A*, 2015, **3**, 5889–5900.
222 J. Přech, P. Eliášová, D. Aldhayan and M. Kubů, *Catal. Today*, 2015, **243**, 134–140.

223 V. Kasneryk, M. Opanasenko, M. Shamzhy, Z. Musilova, Y. S. Avadhut, M. Hartmann and J. Cejka, *J. Mater. Chem. A*, 2017, **5**, 22576–22587.
224 V. Kasneryk, M. Shamzhy, M. Opanasenko, P. S. Wheatley, S. A. Morris, S. E. Russell, A. Mayoral, M. Trachta, J. Čejka and R. E. Morris, *Angew. Chem., Int. Ed.*, 2017, **56**, 4324–4327.
225 D. S. Firth, S. A. Morris, P. S. Wheatley, S. E. Russell, A. M. Z. Slawin, D. M. Dawson, A. Mayoral, M. Opanasenko, M. Položij, J. Čejka, P. Nachtigall and R. E. Morris, *Chem. Mater.*, 2017, **29**, 5605–5611.
226 J. X. Jiang, J. H. Yu and A. Corma, *Angew. Chem., Int. Ed.*, 2010, **49**, 3120–3145.
227 J. X. Jiang, J. L. Jorda, M. J. Diaz-Cabanas, J. H. Yu and A. Corma, *Angew. Chem., Int. Ed.*, 2010, **49**, 4986–4988.
228 M. Mazur, P. S. Wheatley, M. Navarro, W. J. Roth, M. Položij, A. Mayoral, P. Eliášová, P. Nachtigall, J. Čejka and R. E. Morris, *Nat. Chem.*, 2016, **8**, 58–62.
229 S. A. Morris, G. P. M. Bignami, Y. Tian, M. Navarro, D. S. Firth, J. Čejka, P. S. Wheatley, D. M. Dawson, W. A. Slawinski, D. S. Wragg, R. E. Morris and S. E. Ashbrook, *Nat. Chem.*, 2017, **9**, 1012–1018.
230 R. E. Morris and J. Cejka, *Nat. Chem.*, 2015, **7**, 381–388.
231 E. Verheyen, L. Joos, K. Van Havenbergh, E. Breynaert, N. Kasian, E. Gobechiya, K. Houthoofd, C. Martineau, M. Hinterstein, F. Taulelle, V. Van Speybroeck, M. Waroquier, S. Bals, G. Van Tendeloo, C. E. A. Kirschhock and J. A. Martens, *Nat. Mater.*, 2012, **11**, 1059–1064.
232 M. Mazur, A. Arevalo-Lopez, P. S. Wheatley, G. P. M. Bignami, S. E. Ashbrook, A. Morales-Garcia, P. Nachtigall, J. P. Attfield, J. Cejka and R. E. Morris, *J. Mater. Chem. A*, 2018, **6**, 5255–5259.
233 M. Opanasenko, W. O. N. Parker, M. Shamzhy, E. Montanari, M. Bellettato, M. Mazur, R. Millini and J. Čejka, *J. Am. Chem. Soc.*, 2014, **136**, 2511–2519.
234 X. Li and M. W. Deem, *J. Phys. Chem. C*, 2014, **118**, 15835–15839.
235 M. Mazur, M. Kubu, P. S. Wheatley and P. Eliasova, *Catal. Today*, 2015, **243**, 23–31.
236 M. V. Shamzhy, C. Ochoa-Hernandez, V. I. Kasneryk, M. V. Opanasenko and M. Mazur, *Catal. Today*, 2016, **277**, 37–47.
237 M. V. Shamzhy, P. Eliasova, D. Vitvarova, M. V. Opanasenko, D. S. Firth and R. E. Morris, *Chem. – Eur. J.*, 2016, **22**, 17377–17386.
238 Y. Wang, Y. Liu, L. Wang, H. Wu, X. Li, M. He and P. Wu, *J. Phys. Chem. C*, 2009, **113**, 18753–18760.
239 W. J. Roth and C. T. Kresge, *Microporous Mesoporous Mater.*, 2011, **144**, 158–161.
240 M. Opanasenko, M. Shamzhy, F. Yu, W. Zhou, R. E. Morris and J. Cejka, *Chem. Sci.*, 2016, **7**, 3589–3601.
241 P. Wu, J. F. Ruan, L. L. Wang, L. L. Wu, Y. Wang, Y. M. Liu, W. B. Fan, M. Y. He, O. Terasaki and T. Tatsumi, *J. Am. Chem. Soc.*, 2008, **130**, 8178–8187.
242 M. E. Landis, B. A. Aufdembrink, P. Chu, I. D. Johnson, G. W. Kirker and M. K. Rubin, *J. Am. Chem. Soc.*, 1991, **113**, 3189–3190.
243 M. Kubů, W. J. Roth, H. F. Greer, W. Zhou, R. E. Morris, J. Přech and J. Čejka, *Chem. – Eur. J.*, 2013, **19**, 13937–13945.
244 D. E. W. Vaughan, *Catal. Today*, 1988, **2**, 187–198.
245 J. Přech and J. Čejka, *Catal. Today*, 2016, **277**, 2–8.
246 J. Přech, M. A. Carretero and J. Čejka, *ChemCatChem*, 2017, **9**, 3063–3072.
247 B. Liu, C. Wattanaprayoon, S. C. Oh, L. Emdadi and D. Liu, *Chem. Mater.*, 2015, **27**, 1479–1487.
248 H. Gies, M. Feyen, T. De Baerdemaeker, D. E. De Vos, B. Yilmaz, U. Müller, X. Meng, F.-S. Xiao, W. Zhang, T. Yokoi, T. Tatsumi and X. Bao, *Microporous Mesoporous Mater.*, 2016, **222**, 235–240.
249 L. Liu, U. Díaz, R. Arenal, G. Agostini, P. Concepción and A. Corma, *Nat. Mater.*, 2016, **16**, 132.
250 Z. Zhao, Y. Li, M. Feyen, R. McGuire, U. Müller and W. Zhang, *ChemCatChem*, 2018, **10**, 2254–2259.
251 A. Corma, V. Fornes, S. B. Pergher, T. L. M. Maesen and J. G. Buglass, *Nature*, 1998, **396**, 353–356.
252 J. Přech, unpublished work.
253 A. J. Jacobson, *Mater. Sci. Forum*, 1994, **152-153**, 1–12.
254 R. Ma and T. Sasaki, *Adv. Mater.*, 2010, **22**, 5082–5104.
255 T. Maluangnont, Y. Yamauchi, T. Sasaki, W. J. Roth, J. Čejka and M. Kubů, *Chem. Commun.*, 2014, **50**, 7378–7381.
256 K. Varoon, X. Zhang, B. Elyassi, D. D. Brewer, M. Gettel, S. Kumar, J. A. Lee, S. Maheshwari, A. Mittal, C.-Y. Sung, M. Cococcioni, L. F. Francis, A. V. McCormick, K. A. Mkhoyan and M. Tsapatsis, *Science*, 2011, **334**, 72–75.
257 K. Na, C. Jo, J. Kun, W. S. Ahn and R. Ryoo, *ACS Catal.*, 2011, **1**, 901–907.
258 J. Kim, J. Chun and R. Ryoo, *Chem. Commun.*, 2015, **51**, 13102–13105.
259 C. A. Fyfe, G. C. Gobbi, J. S. Hartman, J. Klinowski and J. M. Thomas, *J. Phys. Chem.*, 1982, **86**, 1247–1250.
260 G. Majano, L. Delmotte, V. Valtchev and S. Mintova, *Chem. Mater.*, 2009, **21**, 4184–4191.
261 Y. Seo, K. Cho, Y. Jung and R. Ryoo, *ACS Catal.*, 2013, **3**, 713–720.
262 A. Lacarriere, F. Luck, D. Świerczyński, F. Fajula and V. Hulea, *Appl. Catal., A*, 2011, **402**, 208–217.
263 J.-P. Gilson, G. C. Edwards, A. W. Peters, K. Rajagopalan, R. F. Wormsbecher, T. G. Roberie and M. P. Shatlock, *J. Chem. Soc., Chem. Commun.*, 1987, 91–92.
264 C. O. Arean, M. R. Delgado, P. Nachtigall, H. V. Thang, M. Rubes, R. Bulanek and P. Chlubna-Eliasova, *Phys. Chem. Chem. Phys.*, 2014, **16**, 10129–10141.
265 K. Góra-Marek, K. Tarach and M. Choi, *J. Phys. Chem. C*, 2014, **118**, 12266–12274.
266 S. Laforge, P. Ayrault, D. Martin and M. Guisnet, *Appl. Catal., A*, 2005, **279**, 79–88.
267 N. S. Nesterenko, F. Thibault-Starzyk, V. Montouilliout, V. V. Yushchenko, C. Fernandez, J.-P. Gilson, F. Fajula and I. I. Ivanova, *Kinet. Catal.*, 2006, **47**, 40–48.

268 C. Jo, R. Ryoo, N. Zilkova, D. Vitvarova and J. Cejka, *Catal. Sci. Technol.*, 2013, **3**, 2119–2129.
269 E. F. Rakiewicz, A. W. Peters, R. F. Wormsbecher, K. J. Sutovich and K. T. Mueller, *J. Phys. Chem. B*, 1998, **102**, 2890–2896.
270 Q. Zhao, W.-H. Chen, S.-J. Huang, Y.-C. Wu, H.-K. Lee and S.-B. Liu, *J. Phys. Chem. B*, 2002, **106**, 4462–4469.
271 W. E. Farneth and R. J. Gorte, *Chem. Rev.*, 1995, **95**, 615–635.
272 M. Niwa and N. Katada, *Chem. Rec.*, 2013, **13**, 432–455.
273 S. Bordiga, C. Lamberti, F. Bonino, A. Travert and F. Thibault-Starzyk, *Chem. Soc. Rev.*, 2015, **44**, 7262–7341.
274 G. Busca, *Chem. Rev.*, 2007, **107**, 5366–5410.
275 N. Katada, *Mol. Catal.*, 2017, DOI: 10.1016/j.mcat.2017.12.024.
276 M. Niwa, K. Suzuki, N. Katada, T. Kanougi and T. Atoguchi, *J. Phys. Chem. B*, 2005, **109**, 18749–18757.
277 L. P. Hammett and A. J. Deyrup, *J. Am. Chem. Soc.*, 1932, **54**, 2721–2739.
278 L. P. Hammett and M. A. Paul, *J. Am. Chem. Soc.*, 1934, **56**, 827–829.
279 M. W. Anderson and J. Klinowski, *Zeolites*, 1986, **6**, 150–153.
280 M. Taramasso, G. Perego and B. Notari, *US Pat.*, 4410501, Snam Pregetti SpA, 1983.
281 P. Ratnasamy, D. Srinivas and H. Knözinger, *Advances in Catalysis*, Academic Press, 2004, vol. 48, pp. 1–169.
282 Q. Guo, K. Sun, Z. Feng, G. Li, M. Guo, F. Fan and C. Li, *Chem. – Eur. J.*, 2012, **18**, 13854–13860.
283 J. Přech, D. Vitvarová, L. Lupínková, M. Kubů and J. Čejka, *Microporous Mesoporous Mater.*, 2015, **212**, 28–34.
284 M. Sasaki, Y. Sato, Y. Tsuboi, S. Inagaki and Y. Kubota, *ACS Catal.*, 2014, **4**, 2653–2657.
285 G. Ricchiardi, A. Damin, S. Bordiga, C. Lamberti, G. Spanò, F. Rivetti and A. Zecchina, *J. Am. Chem. Soc.*, 2001, **123**, 11409–11419.
286 S. Bordiga, F. Bonino, A. Damin and C. Lamberti, *Phys. Chem. Chem. Phys.*, 2007, **9**, 4854–4878.
287 A. Corma, U. Diaz, V. Fornes, J. L. Jorda, M. Domine and F. Rey, *Chem. Commun.*, 1999, 779–780.
288 S. Valencia and A. Corma, *US Pat.*, 09407652, Honeywell UOP LLC, 1999.
289 A. Corma, L. T. Nemeth, M. Renz and S. Valencia, *Nature*, 2001, **412**, 423–425.
290 M. Renz, T. Blasco, A. Corma, V. Fornés, R. Jensen and L. Nemeth, *Chem. – Eur. J.*, 2002, **8**, 4708–4717.
291 A. Al-Nayili, K. Yakabi and C. Hammond, *J. Mater. Chem. A*, 2016, **4**, 1373–1382.
292 R. Bermejo-Deval, R. S. Assary, E. Nikolla, M. Moliner, Y. Román-Leshkov, S.-J. Hwang, A. Palsdottir, D. Silverman, R. F. Lobo, L. A. Curtiss and M. E. Davis, *Proc. Natl. Acad. Sci. U. S. A.*, 2012, **109**, 9727–9732.
293 L. Ren, Q. Guo, P. Kumar, M. Orazov, D. Xu, S. M. Alhassan, K. A. Mkhoyan, M. E. Davis and M. Tsapatsis, *Angew. Chem., Int. Ed.*, 2015, **54**, 10848–10851.
294 J. W. Harris, M. J. Cordon, J. R. Di Iorio, J. C. Vega-Vila, F. H. Ribeiro and R. Gounder, *J. Catal.*, 2016, **335**, 141–154.
295 G. Liu, J.-G. Jiang, B. Yang, X. Fang, H. Xu, H. Peng, L. Xu, Y. Liu and P. Wu, *Microporous Mesoporous Mater.*, 2013, **165**, 210–218.
296 H. Y. Luo, L. Bui, W. R. Gunther, E. Min and Y. Román-Leshkov, *ACS Catal.*, 2012, **2**, 2695–2699.
297 K. Chaudhari, T. K. Das, P. R. Rajmohanan, K. Lazar, S. Sivasanker and A. J. Chandwadkar, *J. Catal.*, 1999, **183**, 281–291.
298 N. K. Mal, V. Ramaswamy, S. Ganapathy and A. V. Ramaswamy, *J. Chem. Soc., Chem. Commun.*, 1994, 1933–1934.
299 N. K. Mal and A. V. Ramaswamy, *J. Mol. Catal. A: Chem.*, 1996, **105**, 149–158.
300 M. Boronat, P. Concepción, A. Corma, M. Renz and S. Valencia, *J. Catal.*, 2005, **234**, 111–118.
301 Z. Zhu, H. Xu, J. Jiang, X. Liu, J. Ding and P. Wu, *Appl. Catal., A*, 2016, **519**, 155–164.
302 P. R. Hari Prasad Rao, A. V. Ramaswamy and P. Ratnasamy, *J. Catal.*, 1992, **137**, 225–231.
303 A. Corma, M. a. T. Navarro and M. Renz, *J. Catal.*, 2003, **219**, 242–246.
304 R. Bermejo-Deval, M. Orazov, R. Gounder, S.-J. Hwang and M. E. Davis, *ACS Catal.*, 2014, **4**, 2288–2297.
305 C. Martínez, D. Verboekend, J. Pérez-Ramírez and A. Corma, *Catal. Sci. Technol.*, 2013, **3**, 972–981.
306 A. Ishihara, K. Kimura, T. Hashimoto and H. Nasu, *J. Jpn. Pet. Inst.*, 2014, **57**, 34–46.
307 A. Ishihara, D. Kawaraya, T. Sonthisawate, K. Kimura, T. Hashimoto and H. Nasu, *J. Mol. Catal. A: Chem.*, 2015, **396**, 310–318.
308 V. P. S. Caldeira, A. Peral, M. Linares, A. S. Araujo, R. A. Garcia-Muñoz and D. P. Serrano, *Appl. Catal., A*, 2017, **531**, 187–196.
309 *The Development of Catalysis: A History of Key Processes and Personas in Catalytic Science and Technology*, ed. A. Zecchina and S. Califano, John Wiley & Sons, 2017.
310 S. F. Abdo and S. T. Wilson, *Zeolites in Catalysis: Properties and Applications*, The Royal Society of Chemistry, 2017, pp. 310–350.
311 F. Di Renzo and F. Fajula, in *Studies in Surface Science and Catalysis*, ed. J. Ĉejka and H. van Bekkum, Elsevier, 2005, vol. 157, pp. 1–12.
312 C. Perego, A. Carati, P. Ingallina, M. A. Mantegazza and G. Bellussi, *Appl. Catal., A*, 2001, **221**, 63–72.
313 M. N. Akhtar, N. Al-Yassir, S. Al-Khattaf and J. Čejka, *Catal. Today*, 2012, **179**, 61–72.
314 C. Fernandez, I. Stan, J. P. Gilson, K. Thomas, A. Vicente, A. Bonilla and J. Pérez-Ramírez, *Chem. – Eur. J.*, 2010, **16**, 6224–6233.
315 R. A. García-Muñoz, D. P. Serrano, G. Vicente, M. Linares, D. Vitvarova and J. Čejka, *Catal. Today*, 2015, **243**, 141–152.

316 M. Linares, C. Vargas, A. Garcia, C. Ochoa-Hernandez, J. Cejka, R. A. Garcia-Munoz and D. P. Serrano, *Catal. Sci. Technol.*, 2017, **7**, 181–190.
317 J. A. Martens, D. Verboekend, K. Thomas, G. Vanbutsele, J. Pérez-Ramírez and J.-P. Gilson, *Catal. Today*, 2013, **218-219**, 135–142.
318 T. Tang, C. Yin, L. Wang, Y. Ji and F.-S. Xiao, *J. Catal.*, 2008, **257**, 125–133.
319 A. P. Vyas, J. L. Verma and N. Subrahmanyam, *Fuel*, 2010, **89**, 1–9.
320 A. Carrero, G. Vicente, R. Rodríguez, M. Linares and G. L. del Peso, *Catal. Today*, 2011, **167**, 148–153.
321 Q. Zhang, W. Ming, J. Ma, J. Zhang, P. Wang and R. Li, *J. Mater. Chem. A*, 2014, **2**, 8712–8718.
322 Y. Sun and R. Prins, *Angew. Chem., Int. Ed.*, 2008, **47**, 8478–8481.
323 Q. Huo, T. Dou, Z. Zhao and H. Pan, *Appl. Catal., A*, 2010, **381**, 101–108.
324 Q. Yu, L. Zhang, R. Guo, J. Sun, W. Fu, T. Tang and T. Tang, *Fuel Process. Technol.*, 2017, **159**, 76–87.
325 M. Y. Kustova, S. B. Rasmussen, A. L. Kustov and C. H. Christensen, *Appl. Catal., B*, 2006, **67**, 60–67.
326 A. L. Kustov, T. W. Hansen, M. Kustova and C. H. Christensen, *Appl. Catal., B*, 2007, **76**, 311–319.
327 A. Śrebowata, K. Tarach, V. Girman and K. Góra-Marek, *Appl. Catal., B*, 2016, **181**, 550–560.
328 K. A. Sashkina, V. S. Labko, N. A. Rudina, V. N. Parmon and E. V. Parkhomchuk, *J. Catal.*, 2013, **299**, 44–52.
329 H.-G. Chen and Y. H. P. Zhang, *Renewable Sustainable Energy Rev.*, 2015, **47**, 117–132.
330 IEA, Internation Energy Agency, 2011.
331 B. Balagurumurthy, R. Singh and T. Bhaskar, *Recent Advances in Thermo-Chemical Conversion of Biomass*, Elsevier, Boston, 2015, pp. 109–132.
332 D. P. Serrano, J. A. Melero, J. M. Coronado, P. Pizarro and G. Morales, *Zeolites in Catalysis: Properties and Applications*, The Royal Society of Chemistry, 2017, pp. 441–480.
333 D. P. Serrano, J. A. Melero, G. Morales, J. Iglesias and P. Pizarro, *Catal. Rev.*, 2018, **60**, 1–70.
334 IEA, Internation Energy Agency, 2008.
335 R. Rinaldi and F. Schuth, *Energy Environ. Sci.*, 2009, **2**, 610–626.
336 J. C. Serrano-Ruiz and J. A. Dumesic, *Energy Environ. Sci.*, 2011, **4**, 83–99.
337 D. Kubička and O. Kikhtyanin, *Catal. Today*, 2015, **243**, 10–22.
338 P. S. Rezaei, H. Shafaghat and W. M. A. W. Daud, *Appl. Catal., A*, 2014, **469**, 490–511.
339 A. V. Bridgwater, *Biomass Bioenergy*, 2012, **38**, 68–94.
340 M. Asadieraghi, W. M. Ashri Wan Daud and H. F. Abbas, *RSC Adv.*, 2015, **5**, 22234–22255.
341 V. Sukumar, V. Manieniyan and S. Sivaprakasam, *Int. J. ChemTech Res.*, 2015, **8**, 196–206.
342 J. Xu, J. Jiang and J. Zhao, *Renewable Sustainable Energy Rev.*, 2016, **58**, 331–340.
343 X. Zhao, L. Wei, S. Cheng and J. Julson, *Catalysts*, 2017, **7**, 83.
344 Y. Li, B. Li, X. Zhang, L. Chen, Q. Zhang, T. Wang and L. Ma, *Energy Convers. Manage.*, 2016, **122**, 1–9.
345 Z. Ma, E. Troussard and J. A. van Bokhoven, *Appl. Catal., A*, 2012, **423-424**, 130–136.
346 S. Kelkar, C. M. Saffron, K. Andreassi, Z. Li, A. Murkute, D. J. Miller, T. J. Pinnavaia and R. M. Kriegel, *Appl. Catal., B*, 2015, **174-175**, 85–95.
347 Y.-K. Park, M. L. Yoo, S. H. Jin and S. H. Park, *Renewable Energy*, 2015, **79**, 20–27.
348 E. L. Schultz, C. A. Mullen and A. A. Boateng, *Energy Technol.*, 2017, **5**, 196–204.
349 S. Wang, Q. Cai, J. Chen, L. Zhang, X. Wang and C. Yu, *Ind. Eng. Chem. Res.*, 2014, **53**, 13935–13944.
350 H. J. Park, K.-H. Park, J.-K. Jeon, J. Kim, R. Ryoo, K.-E. Jeong, S. H. Park and Y.-K. Park, *Fuel*, 2012, **97**, 379–384.
351 X. Ji, B. Liu, W. Ma, G. Chen, B. Yan and Z. Cheng, *J. Anal. Appl. Pyrolysis*, 2017, **123**, 278–283.
352 H. J. Park, J. I. Dong, J.-K. Jeon, K. S. Yoo, J. S. Yim, J. M. Sohn and Y.-K. Park, *J. Ind. Eng. Chem.*, 2007, **13**, 182.
353 M. Asadieraghi and W. M. A. Wan Daud, *Energy Convers. Manage.*, 2015, **101**, 151–163.
354 Z. Wang, R. Ma and W. Song, *J. Anal. Appl. Pyrolysis*, 2016, **122**, 183–190.
355 K. Uemura, S. Appari, S. Kudo, J.-i. Hayashi, H. Einaga and K. Norinaga, *Fuel Process. Technol.*, 2015, **136**, 73–78.
356 Y.-M. Kim, B.-S. Kim, K.-S. Chea, T. S. Jo, S. Kim and Y.-K. Park, *Appl. Chem. Eng.*, 2016, **27**, 407–414.
357 G. T. Neumann and J. C. Hicks, *ACS Catal.*, 2012, **2**, 642–646.
358 D. P. Gamliel, H. J. Cho, W. Fan and J. A. Valla, *Appl. Catal., A*, 2016, **522**, 109–119.
359 L. Y. Jia, M. Raad, S. Hamieh, J. Toufaily, T. Hamieh, M. M. Bettahar, G. Mauviel, M. Tarrighi, L. Pinard and A. Dufour, *Green Chem.*, 2017, **19**, 5442–5459.
360 Y. Wang, Y. Zu and S. Wang, Abstracts of papers of the American Chemical Society, 2014, vol. 247.
361 B. Ma, X. Yi, L. Chen, A. Zheng and C. Zhao, *J. Mater. Chem. A*, 2016, **4**, 11330–11341.
362 H. Hernando, J. Fermoso, C. Ochoa-Hernández, M. Opanasenko, P. Pizarro, J. M. Coronado, J. Čejka and D. P. Serrano, *Catal. Today*, 2018, **304**, 30–38.
363 H. W. Lee, S. H. Park, J.-K. Jeon, R. Ryoo, W. Kim, D. J. Suh and Y.-K. Park, *Catal. Today*, 2014, **232**, 119–126.
364 S. R. Naqvi, Y. Uemura, S. Yusup, Y. Sugiur, N. Nishiyama and M. Naqvi, *Energy Procedia*, 2015, **75**, 793–800.
365 S. R. Naqvi, Y. Uemura, S. Yusup, N. Nishiyama and M. Naqvi, *Energy Procedia*, 2017, **105**, 557–561.
366 S. R. Naqvi, Y. Uemura, S. Yusup, Y. Sugiura and N. Nishiyama, *J. Anal. Appl. Pyrolysis*, 2015, **114**, 32–39.
367 S. R. Naqvi and M. Naqvi, *Int. J. Energy Res.*, 2018, **42**, 1352–1362.
368 J. Fermoso, H. Hernando, P. Jana, I. Moreno, J. Přech, C. Ochoa-Hernández, P. Pizarro, J. M. Coronado, J. Čejka and D. P. Serrano, *Catal. Today*, 2016, **277**, 171–181.
369 J. Fermoso, P. Pizarro, J. M. Coronado and D. P. Serrano, in *Encyclopedia of Sustainability Science and Technology*,

ed. R. A. Meyers, Springer New York, New York, NY, 2017, pp. 1–33.
370 Y. Zhu, Z. Hua, J. Zhou, L. Wang, J. Zhao, Y. Gong, W. Wu, M. Ruan and J. Shi, *Chem. – Eur. J.*, 2011, **17**, 14618–14627.
371 A. Veses, B. Puértolas, J. M. López, M. S. Callén, B. Solsona and T. García, *ACS Sustainable Chem. Eng.*, 2016, **4**, 1653–1660.
372 C. J. Barrett, J. N. Chheda, G. W. Huber and J. A. Dumesic, *Appl. Catal., B*, 2006, **66**, 111–118.
373 R. M. West, Z. Y. Liu, M. Peter, C. A. Gärtner and J. A. Dumesic, *J. Mol. Catal. A: Chem.*, 2008, **296**, 18–27.
374 R. Xing, A. V. Subrahmanyam, H. Olcay, W. Qi, G. P. van Walsum, H. Pendse and G. W. Huber, *Green Chem.*, 2010, **12**, 1933–1946.
375 E. Dumitriu, V. Hulea, I. Fechete, A. Auroux, J.-F. Lacaze and C. Guimon, *Microporous Mesoporous Mater.*, 2001, **43**, 341–359.
376 T. Komatsu, M. Mitsuhashi and T. Yashima, in *Studies in Surface Science and Catalysis*, ed. R. Aiello, G. Giordano and F. Testa, Elsevier, 2002, vol. 142, pp. 667–674.
377 A. Ungureanu, S. Royer, T. V. Hoang, D. Trong On, E. Dumitriu and S. Kaliaguine, *Microporous Mesoporous Mater.*, 2005, **84**, 283–296.
378 O. Kikhtyanin, V. Kelbichová, D. Vitvarová, M. Kubů and D. Kubička, *Catal. Today*, 2014, **227**, 154–162.
379 B. Puértolas, T. C. Keller, S. Mitchell and J. Pérez-Ramírez, *Appl. Catal., B*, 2016, **184**, 77–86.
380 O. Kikhtyanin, P. Chlubna, T. Jindrova and D. Kubicka, *Dalton Trans.*, 2014, **43**, 10628–10641.
381 M. Moliner, Y. Román-Leshkov and M. E. Davis, *Proc. Natl. Acad. Sci. U. S. A.*, 2010, **107**, 6164–6168.
382 C. Moreau, R. Durand, A. Roux and D. Tichit, *Appl. Catal., A*, 2000, **193**, 257–264.
383 M. Moliner, *Dalton Trans.*, 2014, **43**, 4197–4208.
384 Y. Román-Leshkov, M. Moliner, J. A. Labinger and M. E. Davis, *Angew. Chem., Int. Ed.*, 2010, **49**, 8954–8957.
385 C. M. Lew, N. Rajabbeigi and M. Tsapatsis, *Microporous Mesoporous Mater.*, 2012, **153**, 55–58.
386 S. Caratzoulas, M. E. Davis, R. J. Gorte, R. Gounder, R. F. Lobo, V. Nikolakis, S. I. Sandler, M. A. Snyder, M. Tsapatsis and D. G. Vlachos, *J. Phys. Chem. C*, 2014, **118**, 22815–22833.
387 S. Saravanamurugan, M. Paniagua, J. A. Melero and A. Riisager, *J. Am. Chem. Soc.*, 2013, **135**, 5246–5249.
388 V. Choudhary, A. B. Pinar, S. I. Sandler, D. G. Vlachos and R. F. Lobo, *ACS Catal.*, 2011, **1**, 1724–1728.
389 M. Paniagua, S. Saravanamurugan, M. Melian-Rodriguez, J. A. Melero and A. Riisager, *ChemSusChem*, 2015, **8**, 1088–1094.
390 I. Graça, M. C. Bacariza and D. Chadwick, *Microporous Mesoporous Mater.*, 2018, **255**, 130–139.
391 G. Li, E. A. Pidko and E. J. M. Hensen, *Catal. Sci. Technol.*, 2014, **4**, 2241–2250.
392 P. Y. Dapsens, C. Mondelli, J. Jagielski, R. Hauert and J. Perez-Ramirez, *Catal. Sci. Technol.*, 2014, **4**, 2302–2311.
393 J. Zhang, L. Wang, G. Wang, F. Chen, J. Zhu, C. Wang, C. Bian, S. Pan and F.-S. Xiao, *ACS Sustainable Chem. Eng.*, 2017, **5**, 3123–3131.
394 K. Y. Nandiwale, A. M. Pande and V. V. Bokade, *RSC Adv.*, 2015, **5**, 79224–79231.
395 A. Feliczak-Guzik, M. Sprynskyy, I. Nowak, M. Jaroniec and B. Buszewski, *J. Colloid Interface Sci.*, 2018, **516**, 379–383.
396 L. Ren, Q. Guo, M. Orazov, D. Xu, D. Politi, P. Kumar, S. M. Alhassan, K. A. Mkhoyan, D. Sidiras, M. E. Davis and M. Tsapatsis, *ChemCatChem*, 2016, **8**, 1274–1278.
397 X. Ma, D. Zhou, X. Chu, D. Li, J. Wang, W. Song and Q. Xia, *Microporous Mesoporous Mater.*, 2017, **237**, 180–188.
398 E. Nikolla, Y. Román-Leshkov, M. Moliner and M. E. Davis, *ACS Catal.*, 2011, **1**, 408–410.
399 J. M. R. Gallo, D. M. Alonso, M. A. Mellmer and J. A. Dumesic, *Green Chem.*, 2013, **15**, 85–90.
400 S. Lima, M. Pillinger and A. A. Valente, *Catal. Commun.*, 2008, **9**, 2144–2148.
401 R. O'Neill, M. N. Ahmad, L. Vanoye and F. Aiouache, *Ind. Eng. Chem. Res.*, 2009, **48**, 4300–4306.
402 P. L. Dhepe and R. Sahu, *Green Chem.*, 2010, **12**, 2153–2156.
403 E. I. Gürbüz, J. M. R. Gallo, D. M. Alonso, S. G. Wettstein, W. Y. Lim and J. A. Dumesic, *Angew. Chem., Int. Ed.*, 2013, **52**, 1270–1274.
404 J. Iglesias, J. A. Melero, G. Morales, M. Paniagua and B. Hernández, *ChemCatChem*, 2016, **8**, 2089–2099.
405 O. A. Abdelrahman, D. S. Park, K. P. Vinter, C. S. Spanjers, L. Ren, H. J. Cho, D. G. Vlachos, W. Fan, M. Tsapatsis and P. J. Dauenhauer, *ACS Sustainable Chem. Eng.*, 2017, **5**, 3732–3736.
406 M. V. Rodrigues, C. Vignatti, T. Garetto, S. H. Pulcinelli, C. V. Santilli and L. Martins, *Appl. Catal., A*, 2015, **495**, 84–91.
407 C. S. Carriço, F. T. Cruz, M. B. dos Santos, D. S. Oliveira, H. O. Pastore, H. M. C. Andrade and A. J. S. Mascarenhas, *J. Catal.*, 2016, **334**, 34–41.
408 J. S. Yoon, T. Lee, J.-W. Choi, D. J. Suh, K. Lee, J.-M. Ha and J. Choi, *Catal. Today*, 2017, **293-294**, 142–150.
409 W. Xu, S. J. Miller, P. K. Agrawal and C. W. Jones, *Appl. Catal., A*, 2013, **459**, 114–120.
410 K. S. Arias, M. J. Climent, A. Corma and S. Iborra, *Energy Environ. Sci.*, 2015, **8**, 317–331.
411 M. Osman, S. Al-Khattaf, U. Diaz, C. Martinez and A. Corma, *Catal. Sci. Technol.*, 2016, **6**, 3166–3181.
412 C. Xing, W. Shen, G. Yang, R. Yang, P. Lu, J. Sun, Y. Yoneyama and N. Tsubaki, *Catal. Commun.*, 2014, **55**, 53–56.
413 C. Xing, G. Yang, M. Wu, R. Yang, L. Tan, P. Zhu, Q. Wei, J. Li, J. Mao, Y. Yoneyama and N. Tsubaki, *Fuel*, 2015, **148**, 48–57.
414 J. Kang, X. Wang, X. Peng, Y. Yang, K. Cheng, Q. Zhang and Y. Wang, *Ind. Eng. Chem. Res.*, 2016, **55**, 13008–13019.

415 Q.-Q. Hao, C.-Y. Lei, Y.-H. Song, Z.-T. Liu and Z.-W. Liu, *Catal. Today*, 2016, **274**, 109–115.
416 J.-C. Kim, S. Lee, K. Cho, K. Na, C. Lee and R. Ryoo, *ACS Catal.*, 2014, **4**, 3919–3927.
417 Global and China Ethylene Oxide (EO) Industry Report, 2017–2021, ReportBuyer Ltd., 2017.
418 Eni, Titanium Silicalite (TS-1) zeolite based proprietary catalyst, https://www.scribd.com/document/208913719/TS1-Flyer-Lug09, accessed 13.5.2017.
419 Eni, Cyclohexanone Oxime Ammoximation of Cyclohexanone with Titanium Silicalite (TS-1) proprietary catalyst, https://www.versalis.eni.com/irj/go/km/docs/versalis/Contenuti%20Versalis/EN/Documenti/La%20nostra%20offerta/Licensing/Catalizzatori/ESE_Tecniche_Cyclohexanone_180214.pdf, accessed 13.5.2017.
420 F. S. Xiao, B. Xie, H. Y. Zhang, L. Wang, X. J. Meng, W. P. Zhang, X. H. Bao, B. Yilmaz, U. Muller, H. Gies, H. Imai, T. Tatsumi and D. De Vos, *ChemCatChem*, 2011, **3**, 1442–1446.
421 Z. Deng, Y. Yang, X. Lu, J. Ding, M. He and P. Wu, *Catal. Sci. Technol.*, 2016, **6**, 2605–2615.
422 P. Wu, T. Tatsumi, T. Komatsu and T. Yashima, *Chem. Lett.*, 2000, 774–775.
423 P. Wu, T. Tatsumi, T. Komatsu and T. Yashima, *J. Phys. Chem. B*, 2001, **105**, 2897–2905.
424 J. Přech, *Catal. Rev.*, 2018, **60**, 71–131.
425 L. L. Wang, Y. Wang, Y. M. Liu, H. H. Wu, X. H. Li, M. Y. He and P. Wu, *J. Mater. Chem.*, 2009, **19**, 8594–8602.
426 H. Xu, L. Fu, J.-G. Jiang, M. He and P. Wu, *Microporous Mesoporous Mater.*, 2014, **189**, 41–48.
427 C.-G. Li, Y. Lu, H. Wu, P. Wu and M. He, *Chem. Commun.*, 2015, **51**, 14905–14908.
428 X. Fang, Q. Wang, A. Zheng, Y. Liu, Y. Wang, X. Deng, H. Wu, F. Deng, M. He and P. Wu, *Catal. Sci. Technol.*, 2012, **2**, 2433–2435.
429 M. B. Yue, M. N. Sun, F. Xie and D. D. Ren, *Microporous Mesoporous Mater.*, 2014, **183**, 177–184.
430 D. P. Serrano, R. Sanz, P. Pizarro and I. Moreno, *Top. Catal.*, 2010, **53**, 1319–1329.
431 M. Yoshioka, T. Yokoi and T. Tatsumi, *Microporous Mesoporous Mater.*, 2014, **200**, 11–18.
432 M. Moliner and A. Corma, *Chem. Mater.*, 2012, **24**, 4371–4375.
433 D. Serrano, R. Sanz, P. Pizarro and I. Moreno, *Chem. Commun.*, 2009, 1407–1409.
434 F. Jin, C.-C. Chang, C.-W. Yang, J.-F. Lee, L.-Y. Jang and S. Cheng, *J. Mater. Chem. A*, 2015, **3**, 8715–8724.
435 A. Kumar and D. Srinivas, *Catal. Today*, 2012, **198**, 59–68.
436 N. Tsunoji, M. Opanasenko, M. Kubů, J. Čejka, H. Nishida, S. Hayakawa, Y. Ide, M. Sadakane and T. Sano, *ChemCatChem*, 2018, **10**, 2536–2540.
437 A. Baeyer and V. Villiger, *Chem. Ber.*, 1899, **32**, 3625–3633.
438 J. Fischer and W. F. Hölderich, *Appl. Catal., A*, 1999, **180**, 435–443.
439 R. Llamas, C. Jiménez-Sanchidrián and J. R. Ruiz, *Tetrahedron*, 2007, **63**, 1435–1439.
440 A. Bhaumik, P. Kumar and R. Kumar, *Catal. Lett.*, 1996, **40**, 47–50.
441 H. Xu, J. Jiang, B. Yang, H. Wu and P. Wu, *Catal. Commun.*, 2014, **55**, 83–86.
442 S. Conrad, P. Wolf, P. Müller, H. Orsted and I. Hermans, *ChemCatChem*, 2017, **9**, 175–182.
443 M. Boronat, P. Concepción, A. Corma and M. Renz, *Catal. Today*, 2007, **121**, 39–44.
444 X. Ouyang, Y.-J. Wanglee, S.-J. Hwang, D. Xie, T. Rea, S. I. Zones and A. Katz, *Dalton Trans.*, 2014, **43**, 10417–10429.
445 B. Yang and Q. Zou, *Chem. Lett.*, 2017, **46**, 1781–1784.
446 X. Liu, H. Xu, L. Zhang, L. Han, J. Jiang, P. Oleynikov, L. Chen and P. Wu, *ACS Catal.*, 2016, **6**, 8420–8431.
447 W. Ponndorf, *Angew. Chem.*, 1926, **39**, 138–143.
448 H. Meerwein and R. Schmidt, *Justus Liebigs Ann. Chem.*, 1925, **444**, 221–238.
449 A. Verley, *Bull. Soc. Chim. Fr.*, 1925, **37**, 537–542.
450 R. V. Oppenauer, *Recl. Trav. Chim. Pays-Bas*, 1937, **56**, 137–144.
451 P. J. Kunkeler, B. J. Zuurdeeg, J. C. van der Waal, J. A. van Bokhoven, D. C. Koningsberger and H. van Bekkum, *J. Catal.*, 1998, **180**, 234–244.
452 E. J. Creyghton, S. D. Ganeshie, R. S. Downing and H. van Bekkum, *J. Chem. Soc., Chem. Commun.*, 1995, 1859–1860.
453 J. C. van der Waal, K. Tan and H. van Bekkum, *Catal. Lett.*, 1996, **41**, 63–67.
454 A. Corma, M. E. Domine, L. Nemeth and S. Valencia, *J. Am. Chem. Soc.*, 2002, **124**, 3194–3195.
455 A. Corma and M. Renz, *Angew. Chem., Int. Ed.*, 2007, **46**, 298–300.
456 J. Wang, K. Okumura, S. Jaenicke and G.-K. Chuah, *Appl. Catal., A*, 2015, **493**, 112–120.
457 A. Corma, M. E. Domine and S. Valencia, *J. Catal.*, 2003, **215**, 294–304.
458 Y. Matsunaga, H. Yamazaki, H. Imai, T. Yokoi, T. Tatsumi and J. N. Kondo, *Microporous Mesoporous Mater.*, 2015, **206**, 86–94.
459 Y. Zhu, Z. Hua, X. Zhou, Y. Song, Y. Gong, J. Zhou, J. Zhao and J. Shi, *RSC Adv.*, 2013, **3**, 4193–4198.
460 D. P. Serrano, R. Sanz, P. Pizarro, I. Moreno and S. Medina, *Appl. Catal., B*, 2014, **146**, 35–42.
461 J. Přech, R. E. Morris and J. Čejka, *Catal. Sci. Technol.*, 2016, **6**, 2775–2786.
462 H. van Bekkum and H. W. Kouwenhoven, *Zeolite Manual for the Organic Chemist*, Mijnbestseller.nl, Delft, 2015.
463 S. V. d. Vyver and Y. Román-Leshkov, *Angew. Chem., Int. Ed.*, 2015, **54**, 12554–12561.
464 Y. Sun and R. Prins, *Appl. Catal., A*, 2008, **336**, 11–16.
465 K. Y. Nandiwale, P. Thakur and V. V. Bokade, *Appl. Petrochem. Res.*, 2015, **5**, 113–119.
466 D. Wang, X. Li, Z. Liu, Y. Zhang, Z. Xie and Y. Tang, *J. Colloid Interface Sci.*, 2010, **350**, 290–294.
467 J. Čejka, G. A. Kapustin and B. Wichterlová, *Appl. Catal., A*, 1994, **108**, 187–204.

468 J. i. Čejka, A. Vondrová, B. Wichterlová, G. Vorbeck and R. Fricke, *Zeolites*, 1994, **14**, 147–153.
469 J.-C. Kim, K. Cho and R. Ryoo, *Appl. Catal., A*, 2014, **470**, 420–426.
470 L. Emdadi, S. C. Oh, Y. Wu, S. N. Oliaee, Y. Diao, G. Zhu and D. Liu, *J. Catal.*, 2016, **335**, 165–174.
471 M. V. Opanasenko, M. V. Shamzhy, C. Jo, R. Ryoo and J. Cejka, *ChemCatChem*, 2014, **6**, 1919–1927.
472 B. Yang, H. Wu and P. Wu, *J. Phys. Chem. C*, 2014, **118**, 24662–24669.
473 X. Ouyang, S.-J. Hwang, R. C. Runnebaum, D. Xie, Y.-J. Wanglee, T. Rea, S. I. Zones and A. Katz, *J. Am. Chem. Soc.*, 2014, **136**, 1449–1461.
474 L. Červený, K. Mikulcová and J. Čejka, *Appl. Catal., A*, 2002, **223**, 65–72.
475 P. J. Harrington and E. Lodewijk, *Org. Process Res. Dev.*, 1997, **1**, 72–76.
476 C.-G. Li, L. Xu, P. Wu, H. Wu and M. He, *Chem. Commun.*, 2014, **50**, 15764–15767.

